ELECTROCHROMIC, ELECTROFLUOROCHROMIC, AND PHOTOACTIVE PROPERTIES OF THIAZOLOTHIAZOLE-BASED, MULTIFUNCTIONAL MATERIALS

by

Tyler Joseph Adams

A dissertation submitted to the faculty of
The University of North Carolina at Charlotte
in partial fulfillment of the requirements
for the degree of Doctor of Philosophy in
Nanoscale Science

Charlotte

2023

Approved by:

_____
Dr. Michael G. Walter

_____
Dr. Christopher Bejger

_____
Dr. Tom Schmedake

_____
Dr. Jordan C. Poler

_____
Dr. Mona Azarbayjani

©2023
Tyler J. Adams
All Rights Reserved

ABSTRACT

TYLER JOSEPH ADAMS. Electrochromic, Electrofluorochromic, and Photoactive Properties of Thiazolothiazole-based Multifunctional Materials. (Under the direction of DR. MICHAEL G. WALTER)

There have been an increasing number of materials developed that show multifunctional chromogenic properties (such as electrochromism, electrofluorochromism, or photochromism), but to date, few materials have shown all three properties. Materials that are electrochemically and optically active are attractive for a diverse set of applications that include smart-windows, lighting, sensing, energy production, and conservation. Achieving systems made from organic, cost-effective, readily synthesized materials would make them easy to utilize in a variety of fields. Multifunctional chromogenic dipyridinium thiazolo(5,4-d)thiazole (TTz) show promise in achieving these needs as they offer high contrast color change, high fluorescent quantum yields above 90%, and water processability while made from inexpensive starting materials. The planar, rigid, heterocyclic TTz core improves stability and reversibility as the TTz reduces from yellow TTz^{2+} to purple $TTz^{\bullet+}$ to blue TTz^{0} compared to other viologen systems.

When implemented in a low-cost poly(vinyl alcohol) (PVA)/borax hydrogel device using conductive glass electrodes, the TTz can change color and fluorescence intensity with applied voltage or light exposure. The electrochromism offers 75% transmittance contrast that is stable for 250 on/off cycles and electrofluorochromism with >90% contrast. By adjusting gel components and coating/drying the hydrogel, a variety of photochromic thin films were produced. Remarkably, the TTz-embedded films retain

their high contrast chromogenic properties showing photochromism (yellow TTz^{2+} to blue TTz^{0} color change) and photofluorochromism after only one minute of light exposure. After turning blue, the oxidation back to yellow occurs through interactions with oxygen. This is potentially an effective way to optically detect the presence of oxygen which is useful for a variety smart packaging applications for food, pharmaceuticals, and electronics. The color change speed and contrast can be tuned by adjusting borax and TTz concentrations. Because the TTz's show multifunctional capabilities, photo-charging battery devices were designed and tested demonstrating the ability to simultaneously generate and store electrical charge under illumination. When paired with the appropriate catholyte and anion exchange membrane, TTz shows evidence of photocharging in hydrogel and thin film devices. Comparing charge discharge curves of the battery devices, illumination can increase voltages by 0.2 V and improve charging capacity. This work shows the remarkable multifunctional electroactive and photoactive properties of dipyridinium thiazolothiazole materials. In addition, applications were developed that highlight their multifunctional nature yielding reversible, high contrast electrochromism, electrofluorochromism, photochromism, photofluorochromism, and light-responsive charging capabilities.

ACKNOWLEDGEMENTS

First, I would like to thank my advisor, Dr. Michael G. Walter for his guidance, explanations, and contagious excitement for research. It's been exciting to explore the many applications of all things TTz! Also, thank you to my committee for the insight and asking difficult but helpful questions. For all the times I was searching for specialty glassware or nitrogen gas line connectors, thank you Dr. Adam Fessler. Thank you to the collaborators I've worked with, it was refreshing to work on different projects that still share common ground and learn from you about other viewpoints and applications. Thank you to my fellow graduate students for training on instruments and straight forward explanations as well as the comradery. To the undergraduate researchers of the Walter lab, thank you for replicating and verifying results as well as listening to my explanations that often uncovered further research questions and discoveries. Thank you to the whole chemistry department for the common quick conversations in the hallways that make the department feel like home.

Thank you to my family, particularly my Mom and Dad for their continued love, encouragement, and support during this journey. Also, thank you Mom, Dad, and Aunt Tammie for making the trek here for so many holidays. I would like to thank my friends that are always there to share complaints about non-ideal results and share so many memories together.

Table of Contents

LIST OF FIGURES

LIST OF ABBREVIATIONS

ΔE_p	change in potential between forward and reverse peaks
ΔT	change in transmittance
ε	molar extinction coefficient
λ	wavelength
$\lambda_{max\ abs}$	maximum absorbance wavelength
$\lambda_{max\ em}$	maximum emission wavelength
λ_{em}	emission wavelength
λ_{ex}	excitation wavelength
Φ_F	fluorescence quantum yield
^{1}H-NMR	proton nuclear magnetic resonance
^{13}C-NMR	carbon-13 nuclear magnetic resonance
A	electrode area
AEM	anion exchange membrane
A_{on}/A_{off}	contrast ratio: initial area of fluorescence/final area of fluorescence
AORFB	aqueous organic redox flow battery
Bz_2TTz^{2+}	N,N'-dibenzyl 2,5-bis(4-pyridinium)thiazolo[5,4-d] thiazole
C_0	concentration
C_p	capacity
$CDCl_3$	deuterated chloroform
CD_3CN	deuterated acetonitrile
CG	chromogenic
CGD	chromogenic device

COF	covalent organic framework
CV	cyclic voltammetry
D_0	diffusion coefficient
D_2O	deuterated water
DI	deionized
DMF	dimethylformamide
DMSO	dimethyl sulfoxide
E_{red}	reduction energy
E_{ox}	oxidation energy
EFC	electrofluorochromic
$Fc(CH_2OH)_2$	1,1'-ferrocenedimethanol
FTO	fluorine doped tin oxide
I_{on}/I_{off}	contrast ratio: initial intensity/final intensity
i_p	peak current
MALDI-TOF MS	matrix-assisted laser desorption ionization time-of-flight mass spectrometry
Me_2TTz^{2+}	N,N'-dimethyl 2,5-Bis(4-pyridinium)thiazolo[5,4-d]thiazole
MOF	metal organic framework
MV^{2+}	methyl viologen
N	number of electrons
NHE	normal hydrogen electrode
NIR	near-infrared
NMR	nuclear magnetic resonance

$(NPr)_2TTz^{4+}$	N,N'-di(trimethylaminopropyl)-2,5-Bis(4-pyridinium)thiazolo[5,4-d]thiazole
OFET	organic field effect transistor
OH-TEMPO	4-hydroxy-2,2,6,6-tetramethylpiperidin-1-oxyl
OLED	organic light emitting diode
OPV	organic photovoltaic
PC	photochromic
PEDOT:PSS	poly(3,4-ethylenedioxythiophene) polystyrene sulfonate
PEEK	polyetheretherketone
PET	polyethyleneterephthalate
PMMA	poly(methyl methacrylate-co-methacrylic acid)
Py_2TTz	2,5-di(pyridin-4-yl)thiazolo[5,4-d]thiazole
PVA	poly(vinyl alcohol)
RFB	redox flow battery
SCE	saturated calomel electrode
SOC	state of charge
$(SPr)_2TTz$	3,3'-(thiazolo[5,4-d]thiazole-2,5-diylbis(pyridine-1-ium-4,1-diyl))bis(propane-1-sulfonate)
SRFB	solar redox flow battery
$TBAPF_6$	tetrabutylammonium hexafluorophosphate
TEMPO	(2,2,6,6-Tetramethylpiperidin-1-yl)oxyl
TMS	tetramethylsilane
TTz	thiazolo[5,4-d]thiazole

UV-vis	ultraviolet-visible
v	scan rate
V	volume
% w/w	percent weight per weight
$\#e^-$	number of electrons

Chapter 1: Introduction

1.1 Electrochromism, Electrofluorochromism, and Photochromism

Electrochromism occurs when there is a color change induced by an applied voltage, which can be useful for tinting eyeglasses,[1] auto-darkening mirrors,[2] displays,[3] and smart windows. Organic electrochromic devices are made of earth-abundant materials, can be tuned for specific colors, and are usually flexible.[1, 4] Additionally, organic materials possess high contrast,[5] fast response,[5] cost efficiency,[6] and easy processability.[6-7] Viologens, including extended viologens, both symmetric and asymmetric, are commonly used for electrochromism.[5-6, 8-16] Many groups focus on electrochromic polymers that show high contrast and a wide range of colors.[1, 4, 17-19]

Many materials are also electrofluorochromic, which indicates a change in fluorescence color or intensity when exposed to a voltage. Electrofluorochromism can occur if a material is highly fluorescent in its neutral state but becomes non-emissive with the formation of a radical under electrical bias.[20-21] Other molecules are non-emissive and become fluorescent with the addition of a radical[22] or other electrofluorochromic pathways.[3] The electrofluorochromism can be helpful for applications like lighting, displays, or sensors.[23-24] Some materials have difficulty with high contrast and fast switching.

Materials that change color upon light exposure are photochromic,[25] which can be used for smart windows,[26] erasable memory devices,[27] displays,[17-18] and sensors.[3, 17-18] Their use in smart windows is particularly useful for reducing solar heat gain, reducing building energy usage. Materials that are mechanically flexible are advantageous because

they can be easily applied to nearly any surface and can be used for windows, wearable devices, and smart packaging.

Very few materials exhibit all three properties (electrochromism, electrofluorochromism, and photochromism). The limitations of electrochromic, electrofluorochromic, and photochromic materials are price and stability. The use of organic materials greatly reduces cost compared to implanting inorganic metal oxide compounds and are highly stable/reversible for hundreds of cycles but begin to lose contrast after thousands of cycles. The loss of stability is often caused by unstable intermediates and reactions with ambient oxygen.

1.2 Thiazolothiazoles

Thiazolo[5,4-d]thiazole (TTz) is a bicyclic, conjugated heterocycle containing two fused thiazole rings, and surprisingly, only recently has been researched and explored compared to similar heterocycles.[28] Since TTz was first reported by Johnson and Ketcham in 1960,[29] it has been used in a variety of applications, as a bridge for donor/acceptor asymmetric push-pull molecules,[30-31] metal organic frameworks,[32] polymer backbones,[17-19, 33] and extended dipyridinium viologens.[15-16, 34] The highly conjugated electron-deficient TTz core promotes planarity, rigidity, stability, and fluorescence when included between conjugated side groups. When included as an extended viologen, the TTz yields high fluorescence quantum yields, often above 85%.[15-16] The TTz core has been used in applications like voltage sensitive cell imaging,[30] organic photovoltaics,[35] organic field-effect transistors,[36-38] organic light emitting diodes,[39] redox flow batteries,[34] organic vapor sensing,[31] and mercury sensing.[32]

Previously, methyl viologen (MV^{2+}) and other 4,4'-bipyridinium viologen derivatives have been widely researched for applications such as redox flow batteries[40-41] and electrochromism.[6, 10] Methyl viologen has two single electron reductions with the second reduction becoming more irreversible. However, including an extended conjugated bridge in between the pyridinium rings (like TTz), an increase stability and reversibility is observed.[34] The two single electron reductions of dipyridinium TTz^{2+} are shown in **figure 1.1**. The dipyridinium TTz's have reduction potentials (-0.52 and -0.58 V vs SCE Me_2TTz^{2+} in DMSO),[15] which makes it easier to reduce than methyl viologen (-0.804 and -1.224 V vs SCE in acetonitrile).[42] Because of these low reduction potentials, the dipyridinium TTz's can also easily photo-oxidize various compounds, like amines and give a visible color change, due to a high photoexcited-state oxidation potential. This is one reason for their use in sensors and photo-redox catalysis.

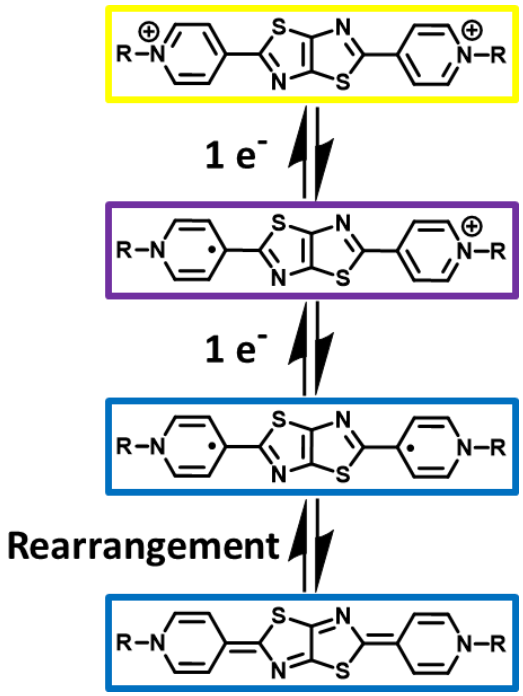

Figure 1.1: The two single electron reductions of dipyridinium TTz.

1.3 Oxygen Sensors

When the fully reduced TTz^0 is in contact with oxygen, it oxidizes back to the TTz^{2+} form. Therefore, a TTz photochromic film could be used as an oxygen sensor. There is a constant need to keep track of the quality and safety of common goods. Oxygen is often the cause for oxidation of metals, degradation of materials, and food spoilage. Oxygen sensing is advantageous for smart packaging of perishable items[43-44] or monitoring oxygen levels in confined work spaces.[45] Food is commonly packaged under nitrogen or carbon dioxide to reduce oxygen content to 0.5 to 2%, which decreases spoilage.[44] Oxygen induced spoilage occurs from aerobic microorganism growth, oxidation of oils or lipids, or enzymatic reactions that cause fruit/vegetable browning.[43-44] Packaging under inert atmospheres is also important for electronics, medical equipment, and pharmaceuticals to prohibit oxidation. Decataldo et al. used agarose hydrogel based organic electrochemical sensors made of PEDOT:PSS for flexible, wearable sensing in the tight range of 13-21% oxygen levels.[45] Quantitative color changes have been reported using platinum porphyrin and CdTe quantum dots.[46] Viologen containing MOF's have also been used for high contrast photochromism and oxygen sensing.[47] A functional material that not only senses the presence of oxygen, but also indicates the direction or location of a leak is advantageous to eliminate leaks or failure points.

1.4 Redox Flow Batteries

With the increasing need for renewable energy solutions, there also needs to be effective energy storage. This is particularly important for solar or wind energy

production, where they are weather dependent and have inconsistent output.[40-41, 48] Lithium ion batteries are difficult to scale up for grid use because of expense and limited earth abundance.[48] Redox flow batteries (RFBs) store charge in the electrolyte solution tanks, rather than the electrodes like traditional batteries.[48] Power can be tuned based upon size of the electrodes and number of cells in the stack, and storage capacity is dictated by concentration and volume of the electrolyte, which also makes modular design available.[48] RFBs consist of two storage tanks that separately contain the two redox couples with electrolyte which are connected to an electrode chamber, consisting of the anode and cathode, with flowing solution and a semi-permeable membrane for supporting electrolyte to transfer between solutions (**Figure 1.2**).[48-49] When charging, the catholyte oxidizes, while the anolyte reduces, causing a change in charges and moving electrolyte ions. When discharged, the opposite occurs, causing ions to move and create electrical current.

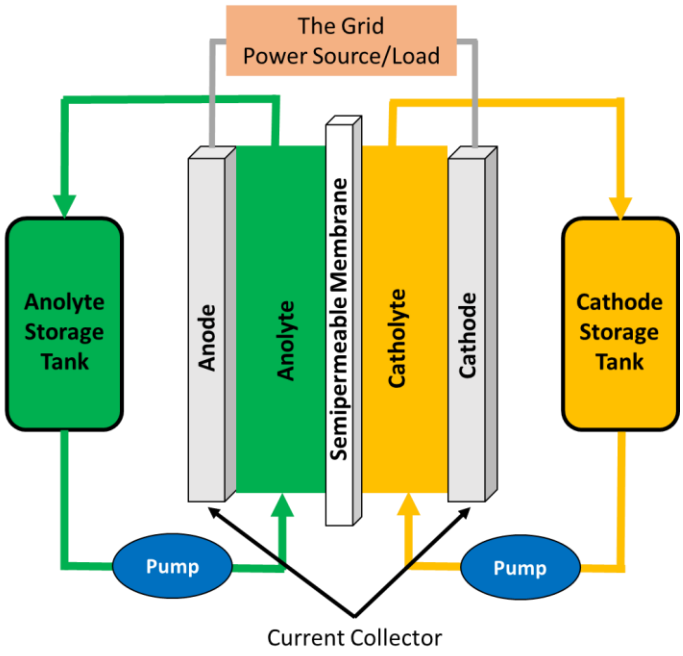

Figure 1.2: Schematic of redox flow batteries.

Vanadium RFBs have been implemented at large scale, up to 6 MWh at wind farms, however, sulfuric acid is used as an electrolyte.[48] Vanadium RFBs take advantage of vanadium's four oxidation states, using VO_2^+ to VO^{2+} as the catholyte and V^{2+} to V^{3+} for the anolyte to afford a cell voltage of 1.26 V when discharging.[48] At the necessary high concentrations, the vanadium and sulfuric acid solution is toxic and corrosive. Traditional RFBs, like those employing vanadium or Zn – Br_2, that use transition metals are highly reported, but have difficulty with large scale implementation due to low energy density, low materials abundance, mining practices, high cost, and corrosive electrolytes.[50-51] To reduce costs, organic materials have been increasingly researched as well as water-based systems to reduce toxicity.[50]

1.5 Dissertation Summary

Although viologen compounds have been researched extensively for electrochromism, electrofluorochromism, and photofluorochromism applications, few have been able to create systems that show multifunctional chromogenic properties.[16] Previously, Woodward et al. used dipyridinium TTz in organic solvents to achieve one color change and electrofluorochromism that was only able to cycle a few times.[15] Herein, this dissertation investigates dipyridinium TTz's that are highly water soluble, multifunctional, and used for numerous applications while having enhanced reversibility and unlocking additional color changes.

Multifunctional chromogenic hydrogel devices that show reversible electrochromism, electrofluorochromism, and photochromism are discussed in chapter 2. The water-based devices employ an inexpensive PVA/Borax gel that enhances solubility

of the redox components and reversibility. The electrochromic, electrofluorochromic, and photochromic properties of four dipyridinium TTz's are reported, including their activation voltages, reversibility, and contrast.

By mixing the dipyridinium TTz with a polymer matrix and coating it into a dried film, flexible photochromic, photofluorochromic, and oxygen sensing films can be utilized. Different formulations and their effects on color contrast and color change speed are explored in chapter 3. These films also have the ability to sense oxygen, which may be useful in smart packaging and due to their flexibility, they can be easily implemented.

As shown in chapter 2, the hydrogel devices are both electroactive and photoactive, which may make it possible to use these materials for energy production. Chapter 4 discusses how these two properties of the [$((NPr)_2TTz^{4+})4Br^-$] are interconnected and how they can be used for solar redox flow batteries and battery devices. Solution phase H-cells are tested as well as hydrogel and film battery devices which show photovoltages and photocurrents as well as traditional charge discharge capabilities.

Chapter 2: Chromogenic Hydrogel Devices

Adapted with permission from Adv. Funct. Mater. 2021, 2103408. Copyright (2021) John Wiley and Sons.

2.1 Introduction

Electrochromic devices (ECDs) have gained interest for use in tinting eyeglasses,[1] auto-darkening mirrors,[2] wearable electronics,[52] glucose detection biosensors,[17-18] energy storage,[52] and tinting windows in buildings, cars, or airplanes. Similarly, photochromic systems are often sought after for tinting eyeglasses and windows, whereas electrofluorochromics (EFCs) are applicable for displays, biosensors, or chemical sensors.[3] Although inorganic materials possess some of these qualities, there is currently a larger focus on organic materials because of high contrast,[5] fast response,[5] processability,[6-7] and cost efficiency.[6] Previously researched EC organic molecules include benzonitriles,[53] symmetric and asymmetric viologens,[5-6, 8-14] thioxathone viologens,[54] and the heterocycle in this study, thiazolothiazoles (TTz's).[15] There has also been a large interest in EC polymers, including those utilizing thiazolothiazole,[17-19] thiophene,[55] and benzothiadiazole moieties.[55] Some materials, like phthalates,[20] poly(4-cyanotriphenylamine),[21] thienoviologen ionic liquid crystals,[22] and a variety of liquid crystal materials[56] are also electrofluorochromic. Arylamines have also been used as a redox site with extended conjugation substituents to yield highly reversible high contrast electrochromic and electrofluorochromic devices.[23, 57] Thienoviologen extended viologens also show high fluorescence quantum yields and extreme contrast ratios of up to 337.[58] Some compounds, like the TTz's in this work, are fluorescent in the neutral state, but become non-emissive with the formation of a radical from the applied

voltage.[20-21] Other molecules become more fluorescent with the addition of a radical,[22] or other electrofluorochromic switching mechanisms.[3] There exists a wide variety of organic photochromic materials that change their absorbance when switching between dark and light intensive environments,[25] or switching between UV and visible wavelengths.[59] Some compounds like diarylethene containing triphenylamine,[59] pentaarylbiimidazole,[60] phenoxyl-imidazolyl radical complex,[60] and rhodamine B salicylaldehyde hydrazone metal complexes[25] show strong photochromic color change properties. The development of organic materials that could exhibit all three properties (electrochromic, electrofluorochromic, and photochromic) is an attractive pursuit for a wide variety of applications. For instance, a multifunctional material could be designed for a window to be electrochromic and/or photochromic during the day to reduce/modulate solar heat gain while remaining electrofluorochromic at night for displays or lighting.[24] The challenge for realizing this conceptual design is to find a stable organic dye platform that shows the reversible, high contrast, multichromic, and long-term stability seen with the viologens and polymeric materials while also exhibiting the photochromism and high fluorescence quantum efficiency.

Thiazolothiazole (TTz) viologens are good candidates for such demanding multifunctional applications. We previously reported TTz dye systems that have very high fluorescence quantum yields and good electrochromic properties.[15] In addition, environmentally sensitive asymmetric TTz derivatives can serve as molecular probes for cell imaging and cell membrane voltage sensing.[30] The excellent electronic and optical properties of TTz-based materials have enabled them to be studied in a variety of molecular electronic applications such as OPVs,[35] OFETs,[36-38] OLEDs,[39] MOF/COF

materials,[32, 61-63] and redox flow batteries.[34] Herein, multifunctional chromogenic devices (electrochromic, electrofluorochromic, and photochromic) are demonstrated using extended TTz viologens developed for low cost, non-toxic, water-based hydrogel devices. The chromogenic devices (CGDs) are highly reversible and stable, have fast-switching times, and exhibit stable, multichromic properties. Various TTz derivatives (**Figure 1**) were examined to study how various alkyl groups on the dipyridyl TTz core affect the solubility, device contrast, reversibility, and fluorescence when included in a polyvinyl alcohol (PVA)/borax polyelectrolyte gel CGD. The TTz dyes have two distinct single electron reductions which cause high contrast, visually apparent polyelectrochromic color changes from colorless/light yellow (TTz^{2+}) to purple ($TTz^{\bullet+}$) to blue (TTz^{0}). The CGDs also show fast on/off switching of the fluorescence intensity. We explore the full range of electrochromic, electrofluorochromic, and photochromic characteristics of these devices and analyze their performance when modulating color changes and fluorescence initiated electrochemically and/or photochemically.

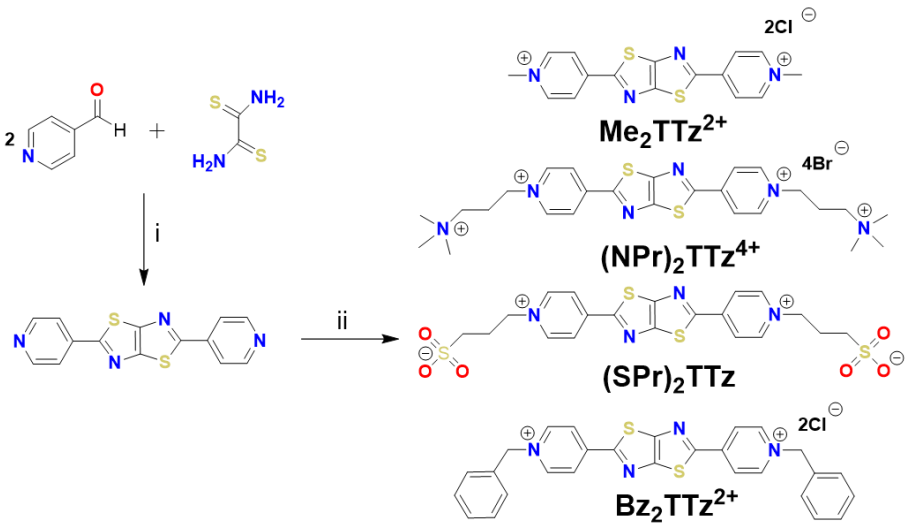

Figure 2.1: Syntheses of the four studied dipyridinium TTz derivatives: [a](i) 150°C in DMF, 6h (ii) heat with $(CH_3)_3N(CH_2)_2Br$ in DMF, or neat with $CH_3C_6H_4SO_3CH_3$, $(CH_2)_3SO_3$, or C_7H_7Br.

2.2 Experimental

Materials and Instrumentation

Dithiooxamide, 4-pyridinecarboxaldehyde, benzyl bromide, 1,3-propanesultone, (3-bromopropyl)-trimethylammonium bromide, poly(vinyl alcohol) (PVA) M_w 11000 – 31000, methyl p-tosylate, toluene, dimethyl sulfoxide (DMSO), methanol, hexanes, Dowex Marathon A OH form anion resin (now called AmberLite), hydrochloric acid, and dimethyl formamide (DMF) were all purchased from Sigma-Aldrich and Baker Scientific while the borax used was 20 Mule Team brand. The Tec-15 FTO (fluorine doped tin oxide) glass used was purchased from Pilkington Glass. ^{1}H-NMR measurements were taken using a JEOL 500 MHz NMR and a JEOL 300 MHz NMR. Mass spectrometry measurements were obtained with a Perceptive Biosystems Voyager MALDI-TOF mass

spectrometer with 1, 8, 9-trihydroxyanthracene. Spectroelectrochemical measurements of reduced TTz^{+2} species were obtained using an EG&G Princeton Applied Research Model 173 potentiostat/galvanostat and a spectroelectrochemical cell with a 1.0 mm path, a printed platinum honeycomb working/counter electrode, and Ag/AgCl reference electrode. Potentials were applied for 15 s before UV-vis spectra were acquired using an Agilent 8453 Spectrophotometer equipped with a photo diode array detector.

A Keithley 236 Source Measure Unit potentiostat, Gamry Reference 600 potentiostat, Cary 300 UV-Vis spectrophotometer, Shimadzu RF-5301PC spectrofluorophotometer and a Jobin Yvon-Spex Fluorolog spectrofluorometer were used for device spectra collection, quantum yield, and molar extinction coefficient determination. Phototochromism/photo-assisted electrochromism was measured using a Newport 67005 lamp with Newport 69911 Power Supply and an Ocean Optics QE65000 spectrometer.

Synthesis

Corresponding ^{1}H-NMR and MALDI-TOF MS spectra are in Appendix II: Supplementary Material.

Synthesis of 2,5-di(pyridin-4-yl)thiazolo[5,4-d]thiazole ***(Py_2TTz)***. Dithiooxamide (0.9962 g, 8.298 mmol) and 4-pyridinecarboxaldehyde (2.2 mL, 23.35 mmol) were refluxed in 40 mL of DMF at 153 ^{o}C for 8 h in an aerated environment. The reaction mixture was cooled to room temperature, and the obtained tan precipitate was filtered via vacuum. The solid was then washed with water and dried under vacuum to give a tan solid in 72.5% yield (1.7830 g). Molecular characterization data quantitatively matched

previously reported values.[15, 34] ^{1}H-NMR (300 MHz, $CDCl_3$,), 8.78 (dd, J = 1.6, 4.6 Hz, 4H), 7.89 (dd, J = 1.6, 4.6 Hz, 4H) ppm.

Synthesis of N,N'-Dimethyl 2,5-Bis(4-pyridinium)thiazolo[5,4-d]thiazole Dichloride ***[(Me_2TTz^{2+})Cl_2]***. Py_2TTz (0.5185 g, 1.75 mmol) and was warmed to 30 ^oC for 48 h in 16.3 mL of methyl p-tosylate. The precipitate was collected, washed with hexanes, and dried to yield 0.6720 g (57.4% yield) of a bright yellow solid.[15] This solid was then treated with Dowex Marathon A anion exchange resin (Cl form). ^{1}H-NMR (300 MHz, CD_3CN, TMS, δ): 8.75 (d, J = 6.87 Hz, 4H), 8.54 (d, J = 6.87 Hz, 4H), 4.34 (s, 6H).

Synthesis of N,N'-di(trimethylaminopropyl)-2,5-Bis(4-pyridinium)thiazolo[5,4-d]thiazole ***[($(NPr)_2TTz^{+4}$)Br_4]***. Py_2TTz (0.2486 g, 0.8388 mmol) was refluxed with (3-bromopropyl) trimethylammonium bromide (0.5521 g, 2.1153 mmol) in DMF under nitrogen at 100 ^oC for 72 h. The precipitate obtained was vacuum filtered and rinsed with DMF and acetonitrile, then dried in the oven to give a yellow solid (0.5110 g, 74.4% yield).[34] ^{1}H-NMR (D_2O, 500 MHz): δ (ppm), 2.53 (m, 4H), 3.09 (s, 18H), 3.46 (t, J = 8.0 Hz, 4H), 4.67 (t, J = 6.5Hz, 4H), 8.60 (d, J = 5.5 Hz, 4H), 8.96 (d, J = 5.5 Hz, 4H)

Synthesis of 3,3'-(thiazolo[5,4-d]thiazole-2,5-diylbis(pyridine-1-ium-4,1-diyl))bis(propane-1-sulfonate) ***[$(SPr)_2TTz$]***. Briefly, Py_2TTz (115 mg) was refluxed in 1,3-propanesultone (1.25 g) at 60 °C for 6 h in air, then cooled to room temperature, yielding a solid yellow mixture. The excess sultone was removed from the solid by sonicating the reaction mixture in 3 x 20 mL of toluene and collecting the remaining solid via vacuum filtration. The resulting yellow solid was dissolved in H_2O and passed through a gravity filtration set-up to remove unreacted Py_2TTz. The filtrate was

centrifuged for 30 min, then the liquid phase was decanted and the remaining solid was discarded. The water was then removed from the decanted solution under reduced pressure, yielding a yellow solid that was further washed with 3 x 25 mL of DMSO. The resulting yellow product was obtained in 33% yield (69 mg). ^{1}H-NMR (300 MHz, D_2O), δ 8.94 (d, J = 7.2 Hz, 4H), 8.56 (d, J = 7.0 Hz, 4H), 4.73 (t, J = 7.4 Hz 4H), 2.94 (t, J = 7.3 Hz, 4H), 2.42 (quint, J = 7.4 Hz, 4H) ppm. ^{13}C NMR (500 MHz, D_2O), δ 165.4, 155.6, 147.5, 145.5, 124.7, 59.9, 47.1, 26.2 ppm. MS [HR-ESI (H_2O)]: m/z calculated for $C_{20}H_{20}N_4O_6S_4$ 540.0266, found 540.0602.

Synthesis of N,N'-dibenzyl 2,5-bis(4-pyridinium)thiazolo[5,4-d] thiazole ***[(Bz_2TTz^{2+})Cl]****:* PyTTz (0.11g, 0.37 mmol) was added to benzyl bromide (3 mL, 25 mmol) and heated at 140 °C for 6 h. The resulting solution was cooled and dissolved in 100 mL of CH_3OH, then washed with hexanes. CH_3OH was then removed to afford 0.10 g (38%) of a yellow solid, and then treated with Dowex Marathon A anion exchange resin to generate the Cl form. Molecular characterization data quantitatively matched previously reported values. ^{1}H-NMR (300 MHz, CD_3CN, TMS, δ): 8.89 (d, *J* = 6.87 Hz, 4H), 8.54 (d, *J* = 6.9 Hz, 4H), 5,78 (s, 4H), 7.52 (m, 10H).

Anion exchange: Dowex Marathon A (OH form) was treated with excess concentrated hydrochloric acid to exchange the OH anions with Cl anions, then washed with DI water. The appropriate TTz molecule was added to approximately 100 mL of H_2O and dissolved thoroughly. Dowex Marathon A, Cl form, was added to the solution in excess 2:1 mole ratio and stirred for 30 min. The resulting mixture was filtered using gravity filtration and washed with DI water. Excess water was removed through rotary evaporation.

Spectroelectrochemistry

The blank and sample solutions were degassed with N_2 for 5 and 15 min, respectively, while in a quartz cuvette with the Ag/AgCl reference and platinum honeycomb electrode. Both forward and reverse spectra were obtained using 0.12 mM $(NPr)_2TTz^{4+}$ and 0.15 mM $(SPr)_2TTz$ in 0.1M Na_2SO_4 solutions. The spectra were obtained from 0 V to -0.9 V and -0.9 V to 0 V in 50 mV increments.

Cyclic Voltammetry

Cyclic Voltammetry (CV). All experiments were carried out in N_2 purged, aqueous 0.5 M Na_2SO_4 supporting electrolyte solutions using a Gamry Reference 600 potentiostat and a three-electrode setup. A 3 mm, PEEK-encased, glassy carbon or Pt disk electrode was used as the working electrode. A strip of platinum foil was used as the counter electrode. The reference electrode consisted of a SCE suspended in saturated KCl solution. The solution of the reference electrode was separated from the analyte solution by a vicor frit. Diffusion coefficients were extracted using a linear regression on plots of peak current (i_p) vs the square root of scan rate. The linear regression was fit accordingly to the Randles-Sevcik equation (Equation 1 for room temperature conditions),[64]

$$i_p = (2.69 \times 10^5) n^{3/2} A D_0^{1/2} C_0 v^{1/2} \qquad (1)$$

where i_p is peak current (A), n = 1 for single electron processes, A is electrode surface area (0.0709 cm^2), D_0 represents the diffusion coefficient, C_0 is concentration (5 x 10^{-6} mol/cm^3), and v is scan rate (V/s).

Chromogenic device assembly

A PVA/borax-based CG gel was obtained following a similar procedure as previously reported.[6] The TTz PVA/borax gel was prepared using 5 mM TTz derivative (Me_2TTz^{2+}, $(NPr)_2TTz^{4+}$, $(SPr)_2TTz$, Bz_2TTz^{2+}) added to a 0.6 mL aqueous PVA solution (4% by mass) and varying concentrations of 1,1'-ferrocenedimethanol ($Fc(CH_2OH)_2$) (0, 5, and 10 mM). After the solution was homogeneous via sonication or vortex, 0.1 mL of borax aqueous solution (4% by mass) was added and mixed vigorously with a spatula until the gel formed.

The prepared CG gel was coated onto one FTO glass and another FTO-coated glass was quickly placed on top of the gel, giving FTO/CG gel/FTO device configuration. The FTO glass was cleaned via sonication with water, acetone, and isopropyl alcohol in 15-min iterations and dried with N_2. Double sided scotch tape was used as a spacer (60 μm) with the FTO glass giving the active CG gel an area of 3 to 4 cm^2.

Electrochromic testing

Transmittance measurements of the CGDs were obtained between 200 nm and 800 nm while voltage was applied at 0 V, 1 V, 1.5 V, 2 V, and 2.5 V. After the wavelength with the highest transmittance contrast was identified, it was monitored as voltage was applied from 0 V to 2.5 V at 20 mVs^{-1} with 100 mV steps to further understand transmittance's voltage dependence. The lowest voltage that gave high transmittance contrast and blue color was used as the "optimal voltage" for other tests since higher voltages, like 2.5 V, slightly degraded the gel. Device cyclability of the transmittance was measured as the optimal voltage was applied on and off every 20 s for

25 cycles. The optimal voltage was applied to the CGD after 3 min and was turned “off” after 63 min to determine their long-term “on”-state durability. The pH of aqueous gels was measured using pH paper test strips before and after long term electrochemical cycling. The pH was found to have changed from pH 8 before, to pH 7 after the electrochemical cycling indicating that device performance degradation was unlikely to be related to increased acidity in the polymer hydrogel.

Electrofluorochromic (EFC) testing

EFC device fluorescence was measured using the max excitation wavelength for each TTz derivative at 0 V, 1 V, 1.5 V, 2 V, and 2.5 V while keeping the device at a 45° angle relative to the source and detector in a Shimadzu RF-5301PC spectrofluorometer. Fluorescence cyclability of CGDs was measured front facing with the CGD 90° to the source and detector in the Jobin Yvon-Spex Fluorolog as the optimal voltage was applied on/off every 20 s for 25 cycles. The max excitation and emission wavelengths for each respective TTz were used to monitor fluorescence switching.

Photochromic (PC) testing

PC properties of the CGDs were observed while placed underneath an AM 1.5 lamp for 30 min. The spectrophotometer was blanked with a PVA/Borax device with no chromogenic compounds. To identify voltage assisted photochromism, the transmittance of the CGD was then measured as a function of applied maximum voltage at which electrochromism does not occur.

2.3 Results and Discussion

The simple CGDs were constructed by sandwiching a TTz containing PVA/borax conductive hydrogel between two pieces of clean FTO glass, while employing double sided tape (60 μm thick) as a spacer (**Fig. 2.2**), similar to recent viologen containing hydrogels.[6] The concentration of TTz derivatives (5 mM Me_2TTz^{2+}, $(NPr)_2TTz^{4+}$, $(SPr)_2TTz$, or Bz_2TTz^{2+}) was kept constant with all tests; however, the concentration of the redox complementary component, 1,1'-ferrocene dimethanol - $Fc(CH_2OH)_2$, was varied, yielding 1:0, 1:1, and 1:2 molar ratios to study its effect on driving voltage, reversibility, and response time. For tests lasting over 15 min, the CGDs were sealed around the edges with hot glue to minimize evaporation of water.

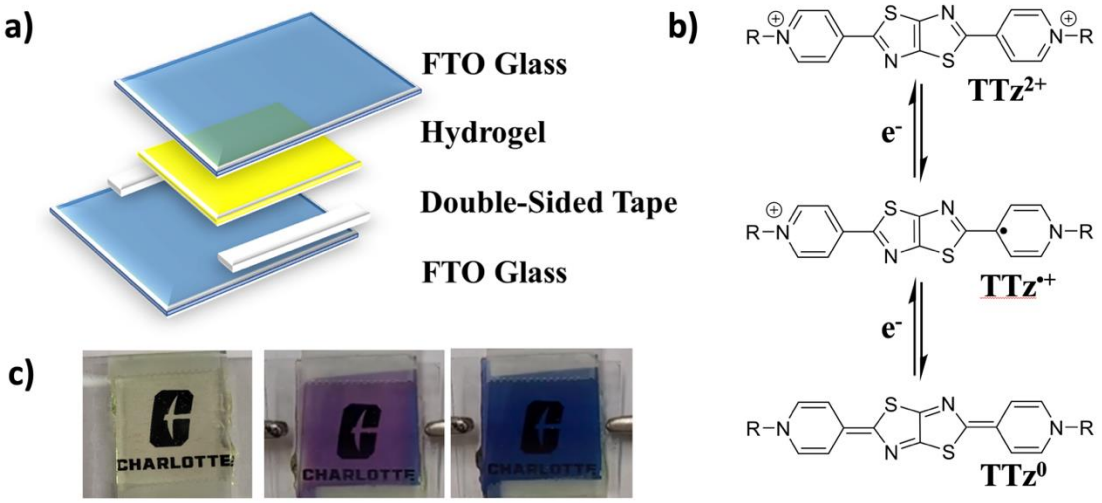

Fig. 2.2: a) Device assembly schematic of CGDs, **b)** the two single electron reductions of TTz, **c)** pictures of a CGD at (left to right) colorless/light yellow dication (TTz^{2+}) state, purple radical cation ($TTz^{\bullet+}$) state, and blue neutral (TTz^0) state.

Prior to testing CGD devices, spectroelectrochemical measurements were made for $(NPr)_2TTz^{4+}$ and $(SPr)_2TTz$ in an aqueous 0.1 M Na_2SO_4 solution (**Supplementary Figs. 1, 2**). Both $(NPr)_2TTz^{4+}$ and $(SPr)_2TTz$ showed a large absorbance peak around 400 nm representing the TTz^{2+} state. Upon electrochemical reduction at -0.65 V and -0.7 V (vs AgCl) for $(NPr)_2TTz^{4+}$ and $(SPr)_2TTz$, respectively, the absorbance at 400 nm decreased, while increasing at 604 nm and 540 nm, indicative of the purple, $TTz^{\bullet+}$ state (**Fig. 2.2 c**). At an applied voltage of -0.9 V, the absorbance at 400 nm further decreased and a second absorption peak at 705 nm and 650 nm ($(NPr)_2TTz^{4+}$ and $(SPr)_2TTz$, respectively) increased, signifying the visually blue, TTz^0 state. The spectroelectrochemical data indicates that both TTz materials have excellent electrochromic reversibility. The intensity of prominent absorbance peaks (400 nm) is readily recovered after electrochemical cycling and returning the TTz^{2+} state. The two single electron reductions are easily distinguishable, similar to spectroelectrochemical results of Bz_2TTz^{2+} and Me_2TTz^{2+} obtained previously by our group.[15] Interestingly, the two single electrochemcial reduction peaks are closely spaced for Bz_2TTz^{2+} and Me_2TTz^{2+} when run in organic solvents (DMSO and CH_3CN), as previously reported,[57] and therefore exhibited only the TTz^{2+} to blue TTz^0 visible electrochromic transition. Using the water-soluble derivatives $(SPr)_2TTz$ and $(NPr)_2TTz^{4+}$ with aqueous electrochemical conditions, the reductions show the purple ($TTz^{\bullet+}$) singly-reduced species as well. The cyclic voltammetry of $(SPr)_2TTz$ and $(NPr)_2TTz^{4+}$ in 0.5 M $Na_2SO_{4\,(aq)}$ solution confirms this observation with more separated reversible reductions at -0.54 V and -0.790 V for $(SPr)_2TTz$ and -0.58 and -0.70 V vs. SCE for $(NPr)_2TTz^{4+}$ (**Supplementary Fig. 3**). The cycling stability was also measured showing aqueous

solutions of $(NPr)_2TTz^{4+}$ that could be cycled for 100 cycles on two consecutive days with minimal loss of electrochemical activity.

2.3.1 Electrochromism

The CGDs' transmittance spectra were collected with the four different TTz derivatives and varying concentrations of $Fc(CH_2OH)_2$ while voltages (0 V, 1 V, 1.5 V, 2 V, 2.5 V) were applied (**Supplementary Figs. 4-7**). Although each TTz derivative showed absorbance intensity variations, they all followed similar trends observed in the spectroelectrochemical data, with a large absorbance around 400 nm and high transparency between 450 – 800 nm at 0 V represented the TTz^{2+} dication. As the applied voltage increases, a single electron reduction occurs, making the CGDs absorb more of the 500 – 650 nm light, corresponding to the purple, radical cation ($TTz^{\bullet+}$) state. When applied voltage is increased further, a second reduction occurs, causing further light absorption at 500 – 800 nm, which appears as the visually dark blue neutral state (TTz^0). The addition of $Fc(CH_2OH)_2$ lowered the amount of applied device voltage necessary for the two single electron reductions to occur by approximately 1 V.

The 1:2 TTz:$Fc(CH_2OH)_2$ CGD transmittance spectra for the four derivatives show each TTz gives a diverse transmittance contrast and they absorb light slightly differently, depending on their side group (**Fig. 2.3**) yielding different shades of the colorless/light yellow, purple, and blue colored neutral and reduced states. The Bz_2TTz^{2+} CGD yields the greatest contrast ratio $\Delta T = 75\%$, while $(SPr)_2TTz$ showed the lowest contrast ratio of 15%. To further understand the CGDs' applied voltage dependence, the max contrast wavelength was monitored as voltage was ramped at 20 mV s^{-1} for the individual TTz's and the various $Fc(CH_2OH)_2$ concentrations (**Supplementary Fig. 8**).

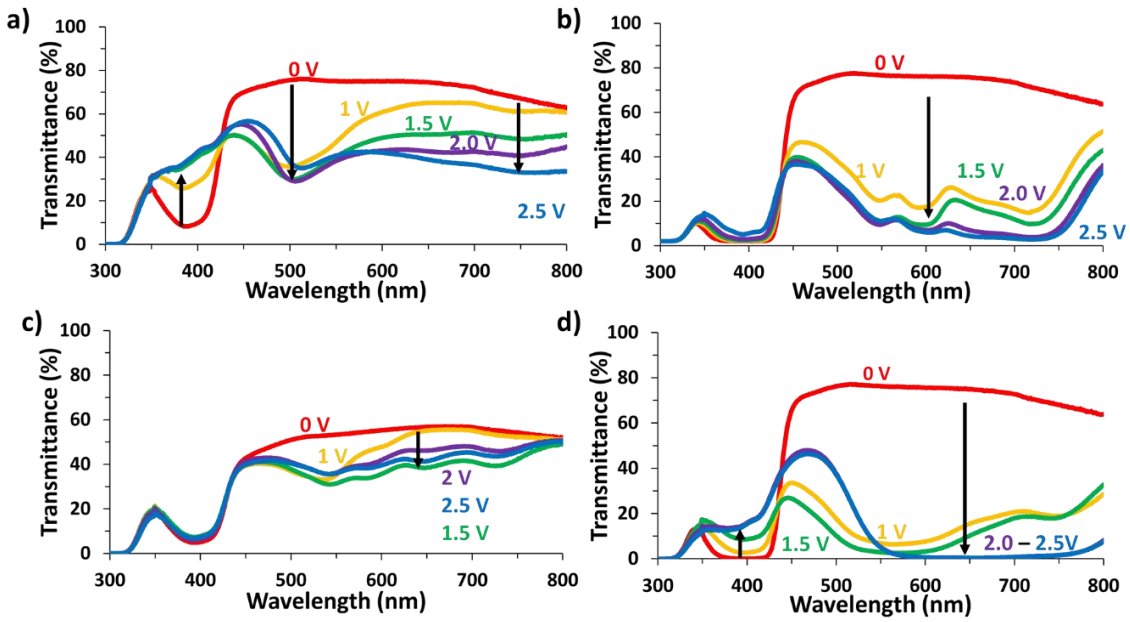

Fig. 2.3: Transmittance spectra of 1:2 TTz:$Fc(CH_2OH)_2$ CGDs with 0 – 2.5 V applied for **a)** Me_2TTz^{2+}, **b)** $(NPr)_2TTz^{4+}$, **c)** $(SPr)_2TTz$, **d)** Bz_2TTz^{2+}.

From the device spectra, the two single electron reductions can be seen. The addition of $Fc(CH_2OH)_2$ lowers the necessary voltage for color change, as expected, while maintaining or increasing transmittance contrast. These scans were also used to determine an "optimal voltage" for the devices, which was the lowest voltage necessary for the full contrast to the visually blue TTz^0 state, since higher voltages of 2.5 V to 3 V slightly degraded the hydrogel.

The reversibility and cyclability of the TTz CGDs were tested by cycling the optimal voltage on/off every 20 s for 25 cycles with different ratios of TTz:$Fc(CH_2OH)_2$ to fully understand the complementary redox component's role in reversibility. **Supplementary Fig. 9** shows the differences in cyclability and reversibility that including $Fc(CH_2OH)_2$ affords. The Me_2TTz^{2+}, $(NPr)_2TTz^{4+}$, and Bz_2TTz^{2+} devices show little cyclability without the $Fc(CH_2OH)_2$, as the TTz remains in the reduced, visually

blue (off) state after several cycles. As the concentration of $Fc(CH_2OH)_2$ is increased, the devices become more reversible and cyclable with faster color changes, noted by the square wave characteristic with 1:2 TTz:$Fc(CH_2OH)_2$ devices. The 1:2 ratio was expected to yield the best results because of the balance of electron stoichiometry between the TTz and the $Fc(CH_2OH)_2$. Therefore, 1:2 TTz:$Fc(CH_2OH)_2$ hydrogels were used for the remainder of device characterization. All the TTz derivatives demonstrated high reversibility in these hydrogel CGDs and had fast coloration times of 12 s, 2 s, 3 s, and 7 s for Me_2TTz^{2+}, $(NPr)_2TTz^{4+}$, $(SPr)_2TTz$, and Bz_2TTz^{2+}, respectively (**Fig 2.4**).

When cycling the Me_2TTz^{2+} CGD on/off, it had an initial contrast ratio of 58% and after 25 cycles, decreased to $\Delta T = 44\%$. $(NPr)_2TTz^{4+}$ had an initial contrast ratio of 57% and after 25 cycles had a contrast of 60% (**Fig. 2.4 a**). The excellent reversibility observed with the $(NPr)_2TTz^{4+}$ led us to examine 250 cycles in an aqueous gel device. Remarkably, the max contrast only decreased by 6% from the max after 250 cycles (**Fig 2.4 a**). The lowest performing derivative, $(SPr)_2TTz$ has an initial contrast ratio of 17% and after 25 cycles, $\Delta T = 10\%$, but then reverses above the initial transmittance (**Supplementary Fig. 10**). The $(SPr)_2TTz$ derivative was the least soluble derivative in the PVA/borax gel, which likely contributed to the observed low contrast cycling. The Bz_2TTz^{2+} CGD had an initial contrast ratio of 47%, which increased to 52% after 25 cycles. Previous reports demonstrated > 65% contrast ratio using 20 mmol L^{-1} ethyl viologen in a PVA/borax hydrogel device that was 200 μm thick. TTz devices such as $(NPr)_2TTz^{4+}$ accomplished comparable contrast with a quarter of the concentration and a quarter of the thickness (60 μm).[6] For large scale applications, thinner devices would require less material and weigh less, while lower concentrations mean cheaper

production. This contrast ratio is also higher than a variety of previously reported viologens[5, 9, 12, 14] and polymers.[2, 17, 19, 55]

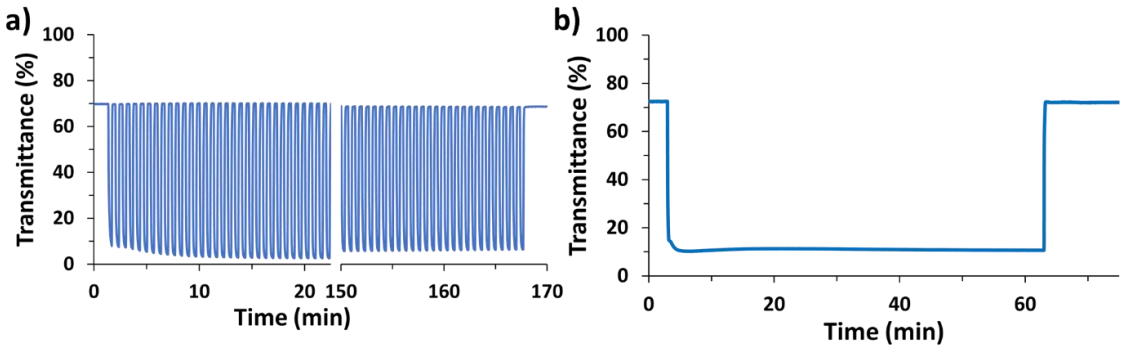

c)

TTz	Applied voltage (V)	Max contrast (ΔT, λ nm)	Contrast difference after 25 cycles	Coloration time* (s)	Bleaching time* (s)
Me_2TTz^{2+}	2.4	58% (700)	- 14%	12	4.8
$(NPr)_2TTz^{4+}$	1.8	67% (710)	+ 3%	2	1.2
$(SPr)_2TTz$	2.0	17% (600)	- 7%	3	0.8
Bz_2TTz^{2+}	1.8	52% (700)	+ 5%	7	2.8

Fig. 2.4: 1:2 $(NPr)_2TTz^{4+}$:$Fc(CH_2OH)_2$ CGD transmittance spectra when devices were **a)** cycled on/off 0 V/1.8 V (20 s on/off) for 250 cycles (710 nm) **b)** turned on (1.8 V) for 60 min (710 nm) **c)** table of EC properties calculated from cycling graphs *time required to obtain 90% full contrast.

To measure durability of CGDs with long term applied voltages, their optimal voltage was applied for 60 min to study degradation losses in contrast and reversibility (**Supplementary Fig. 11**). The Me_2TTz^{2+} CGD has a max contrast ratio of 62% with the lowest transmittance of 9% after 11 min. The transmittance slowly increases to 13% after 60 min and the device has low reversibility. $(NPr)_2TTz^{4+}$ has a contrast ratio of 62%, which is maintained for the 60 min and reverses completely to the ground state transmittance when the voltage is no longer applied (**Fig 2.4 b**). $(SPr)_2TTz$ has an initial

contrast ratio of 14% and slowly loses contrast during the 60 min. When the bias is removed, the transmittance does appear to recover with a slight increase from the initial transmittance. Interestingly, the Bz_2TTz^{2+} device's contrast ratio increased over the 60 min applied bias period, but when the bias was removed, it only partially recovered (**Supplementary Fig. 11d**). The observed reduction in reversibility for several of the derivatives is possibly due to dimerization, which has been observed with similar to 4,4'-dipyridinium viologens.[3, 9] The Me_2TTz^{2+} may be more prone to this dimerization mechanism due to the sterically small methyl on the pyridinium groups. We have also observed slight gel discoloration of the TTz PVA/Borax hydrogels after being left at ambient conditions for more than 24 hours. However, electrochromic devices using $(NPr)_2TTz^{4+}$:$Fc(CH_2OH)_2$ showed nearly identical spectra between a freshly-made device and one tested up to 4 days later (**Supplementary Fig. 12**). The discoloration can be avoided by storing the gel under N_2 or Ar inert conditions.

2.3.2 Electrofluorochromism

Electrofluorochromic properties of the CGDs were probed by exposing the devices to their max excitation wavelengths and applying voltages of 0 V, 1 V, 1.5 V, 2 V, and 2.5 V. All CGDs were highly fluorescent at 0 V and responsive to applied voltage with large fluorescence contrast (**Supplementary Fig. 13**). Although the $(SPr)_2TTz$ CGD showed a 63% drop in fluorescence intensity between 0 V and 2.5 V, the fluorescence of the other CGDs exhibited over 90% change in emission contrast (**Fig 2.5 a - Bz_2TTz^{2+}**). An important figure of merit for EFC's is the contrast ratio, which can be determined by comparing the max intensities or the overall fluorescence (total area) of the highly fluorescent, off (0 V) and the minimally fluorescent on (2.5 V) states (**Fig 2.5 c**).[3]

Emission intensity contrast ratios were 31.4, 11.1, 2.7, and 143.0 for Me_2TTz^{2+}, $(NPr)_2TTz^{4+}$, $(SPr)_2TTz$, and Bz_2TTz^{2+}, respectively. These emission contrast ratios are similar to previously reported small molecule EFC devices; however, Bz_2TTz^{2+} has a much larger contrast, which is ideal for sensors and fluorescent displays.[3]

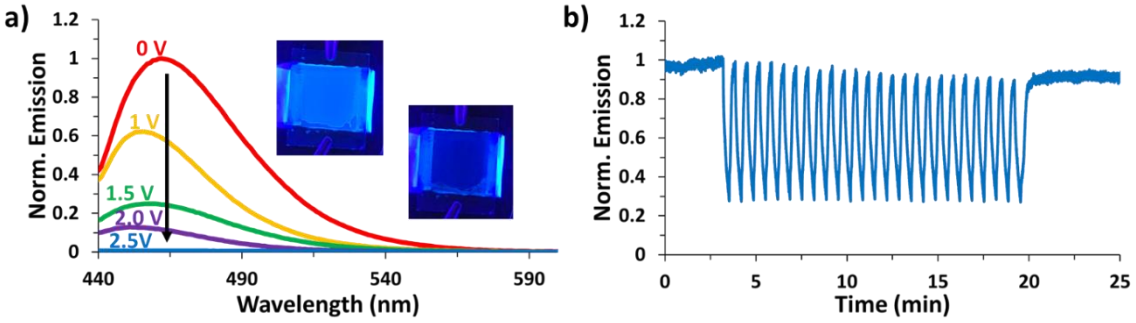

c)

TTz	Contrast ratio[a] (I_{on}/I_{off})	Contrast ratio[a] (A_{on}/A_{off})	Fluorescence decrease time[b*] (s)	Fluorescence increase time[b*] (s)	Max contrast (ΔT)[b]	Contrast difference after 25 cycles[b]
Me_2TTz^{2+}	31.4	9.9	15	4.1	74%	- 8%
$(NPr)_2TTz^{4+}$	11.1	8.5	11	3.3	41%	+ 8%
$(SPr)_2TTz$	2.7	3.1	9	1.3	47%	- 13%
Bz_2TTz^{2+}	143.0	100.5	15	9.7	69%	- 4%

Fig. 2.5: Fluorescence of 1:2 Bz_2TTz^{2+}:$Fc(CH_2OH)_2$ CGDs **a)** at 0 V, 1 V, 1.5 V, 2 V, 2.5 V (λ_{ex}= 419 nm) **b)** cycled (20 s on/off 0 V/1.8 V) 25 cycles (λ_{ex}= 419 nm, λ_{em}= 463 nm) **c)** table of electrofluorochromic performances calculated[a] from 0 V and 2.5 V spectra, calculated[b] from fluorescence cycling data [*]time required to obtain 90% full contrast.

To understand the switching time, reversibility, and consistency of fluorescence switching from the "on" (0 V) and "off" (voltage applied) states, cyclability tests were performed (**Supplementary Fig. 14**). The applied voltage and on/off timing were the same as previously used for electrochromic cyclability. The Me_2TTz^{2+} CGD initially had

a 74% contrast ratio, but over the 25 cycles, lost 8% contrast, whereas $(NPr)_2TTz^{4+}$ had a 33% contrast ratio on the first cycle and gained contrast over the 25 cycles to $\Delta T = 41\%$. The first cycle of the $(SPr)_2TTz$ CGD had 47% fluorescence contrast ratio but decreased to 34% contrast ratio during the 25 cycles. The Bz_2TTz^{2+} CGD had a contrast ratio of 69% initially and maintained most contrast after 25 cycles, $\Delta T = 65\%$ (**Fig 2.5 b**). The switch time to obtain 90% full contrast for the devices was fast, 15 s, 11 s, 9 s, and 15 s for Me_2TTz^{2+}, $(NPr)_2TTz^{4+}$, $(SPr)_2TTz$, and Bz_2TTz^{2+}, respectively. All the CGDs had a slight reduction in baseline emission over time due to photochromism.

2.3.3 Photochromism

Photochromism of the CGDs was studied by the exposing TTz devices to full spectrum (one Sun) lamp illumination (approximately 100 mW cm^{-2}) for 30 min with no applied bias, and intermittently measuring transmittance of light (see **Supplemental Experimental**). Similar to the coloration sequence of the electrochromism studies of the CGDs, the color of the TTz device start in a colorless/light-yellow state and over time undergo photo-induced reductions to produce a final, blue-colored state. For all derivatives, a change in transmittance is caused after 5 or 10 min of light exposure (**Fig. 2.6 a, Supplementary Fig. 15**). All four CGDs initially showed nearly 100% transparence in the 450-800 nm range, while absorbing > 60% of light around 400 nm. As illumination time progressed, the devices absorbed less light at 400 nm and had less transmittance in the 500-700 nm range (**Fig. 2.6**). The Me_2TTz^{2+} CGD had a 35% drop in transmittance at 550 nm after 15 min and only dropped an additional 3% after 30 min of light exposure, while at 395 nm the transmittance was 14% and increased to 35% after 30 min. The $(NPr)_2TTz^{4+}$ CGD dropped in transmittance after 15 min at 602 nm (from 99%

to 41%) with absorption broadening upon continued light exposure (**Fig. 2.6 a**). The transmittance at 400 nm steadily increased from 13% to 35% over 30 min. The $(SPr)_2TTz$-containing device took the longest to reach the full color change, and had a 44% transmittance contrast at 574 nm and increased by 6% at 387 nm after 30 min. The Bz_2TTz^{2+} CGD had the fastest coloration time, which transitioned from 95% transmittance to 54% at 605 nm after only 5 min of illumination. The blue-colored state persisted between 1-2 h after illumination, however, the colorless state could be restored immediately by cycling the electrochromism of the device on and off using +1.5 V of applied bias (**Fig. 2.6 c**).

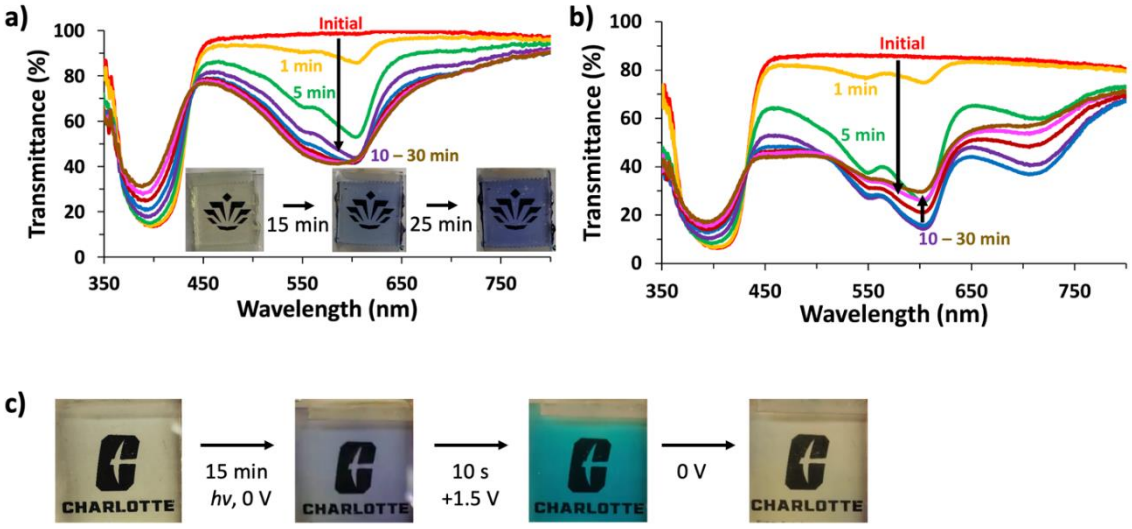

Fig. 2.6: Photochromism spectra of 1:2 $(NPr)_2TTz^{4+}$:$Fc(CH_2OH)_2$ with 1-30 minutes of 100 mW cm^{-2} illumination **a)** without applied voltage (inset images of TTz gel device illuminated for 15 and 25 min) **b)** with 0.8 V applied, and **c)** photochromism engaged and then turned off by electrochromic cycling of the device.

Photochromism was also examined while simultaneously applying a voltage (0.5 – 0.8 V) to examine whether an applied bias could assist the photochromic device color change (**Fig. 2.6 b, Supplementary Fig 16**). These voltages were chosen because they are the highest bias that can be applied without engaging the electrochromism of the CGDs and changing their transmittance. Compared to photochromism without applied voltage, the CGDs change color 50% faster with the low voltage application. The Me_2TTz^{2+} CGD had an 85% transmittance at 524 nm and dropped to 44% after only 5 min, but it then increased again to 55% after 30 min. The device containing $(NPr)_2TTz^{4+}$ showed a larger transmittance contrast at 602 nm when voltage was applied than without an applied voltage: 71% after 10 min instead of 57% after 15 min (**Fig 2.6 b**). After 5 min of light exposure, the $(SPr)_2TTz$ CGD had a transmittance of 52%, after it was initially 89% at 541 nm. The Bz_2TTz^{2+} device had a similar transmittance drop (from 99% to 55% at 574 nm after 10 min) to the photochromism without applied voltage. Consistent with the photochromism and the electrochromism, the transmittance of the CGDs around 400 nm increased over time. The voltage sped up the photochromic color change and provided a higher contrast than devices without an applied voltage. The enhancement is likely due to a lowering of the required applied potential to reduce the TTz dyes in their excited state. Coupling this with the simultaneously occurring photochromic affect results in the observed increase in coloration speed. The voltage-assisted photochromism showed that the devices can obtain a comparable contrast to electrochromism using less power. This indicates that aqueous PVA/borax TTz CGDs can be made tunable by leveraging light illumination with simultaneously applied voltage, further increasing the electrochromic device efficiency.

2.4 Conclusion

Water-based, hydrogel chromogenic devices (CGDs) were developed that show high electrochromic and electrofluorochromic contrast/reversibility while also exhibiting photochromic activity. A simple FTO/hydrogel/FTO device configuration using water-soluble dipyridinium thiazolothiazole (TTz) derivatives and a PVA/borax polyelectrolyte hydrogel yielded a multifunctional chromogenic device. Several of the devices were able to achieve 75% transmittance contrast with a driving voltage of 2 V or a contrast of 50%, just with only exposure to light. The cyclability and reversibility of the TTz CGDs is excellent losing only 6% transmittance contrast after 250 on/off cycles or 1% transmittance loss in contrast after an hour of applied voltage. In addition, it is notable that these devices operate under ambient, aqueous conditions. In the case of electrofluorochromism, > 90% of the fluorescence can be turned off with the application of 2.5 V. These characteristics make the TTz CGDs promising candidates for applications in auto-darkening glass, sensors, fluorescent displays, and most suitable for windows, where the CGDs can darken on command with an applied voltage, with light exposure, or a combination of both.

2.5 Appendix I: Supplementary Information

Solution Photophysical Properties

	$\lambda_{max\ abs.}$ (nm)	$\lambda_{ex.}$ (nm)	$\lambda_{max\ em.}$ (nm)	ε ($M^{-1}\ cm^{-1}$)	ϕ_F
Me_2TTz^{2+}	390	384	454	23,000	> 0.98
$(NPr)_2TTz^{4+}$	397	397	461	28,000	0.98
$(SPr)_2TTz$	396	410	459	42,000	> 0.98
Bz_2TTz^{2+}	397	410	460	18,000	0.86

Supplementary Table 1: Photophysical properties of the 4 TTz derivatives in water.

Spectroelectrochemistry of $(NPr)_2TTz^{4+}$ and $(SPr)_2TTz$

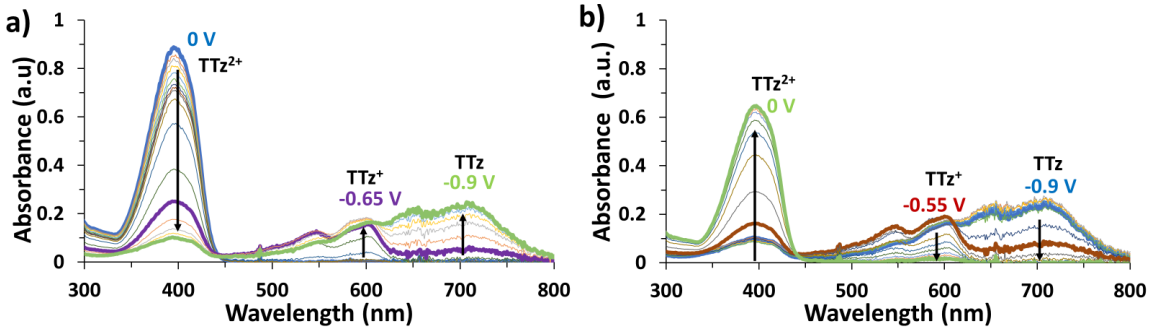

Supplementary Fig. 1: $(NPr)_2TTz^{4+}$ spectroelectrochemistry **a)** forward scan (0 to -0.9 V) **b)** reverse scan (-0.9 V to 0 V).

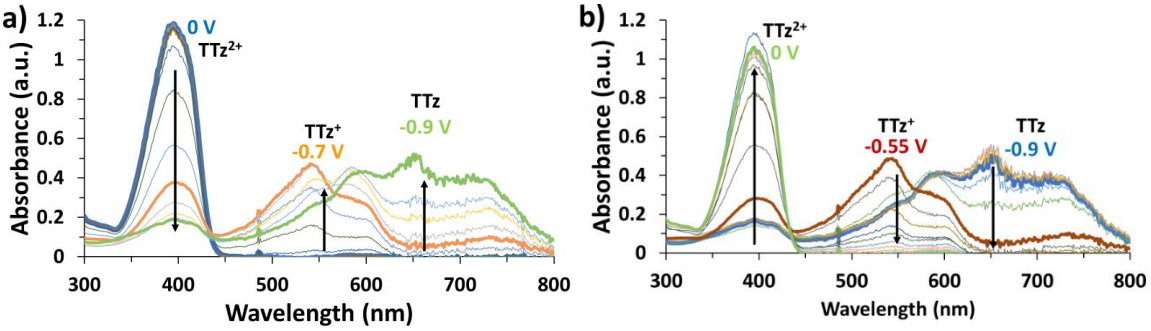

Supplementary Fig. 2: $(SPr)_2TTz$ spectroelectrochemistry **a)** forward scan (0 to -0.9 V) **b)** reverse scan (-0.9 V to 0 V).

Cyclic Voltammetry of $(SPr)_2TTz$ and $(NPr)_2TTz^{4+}$

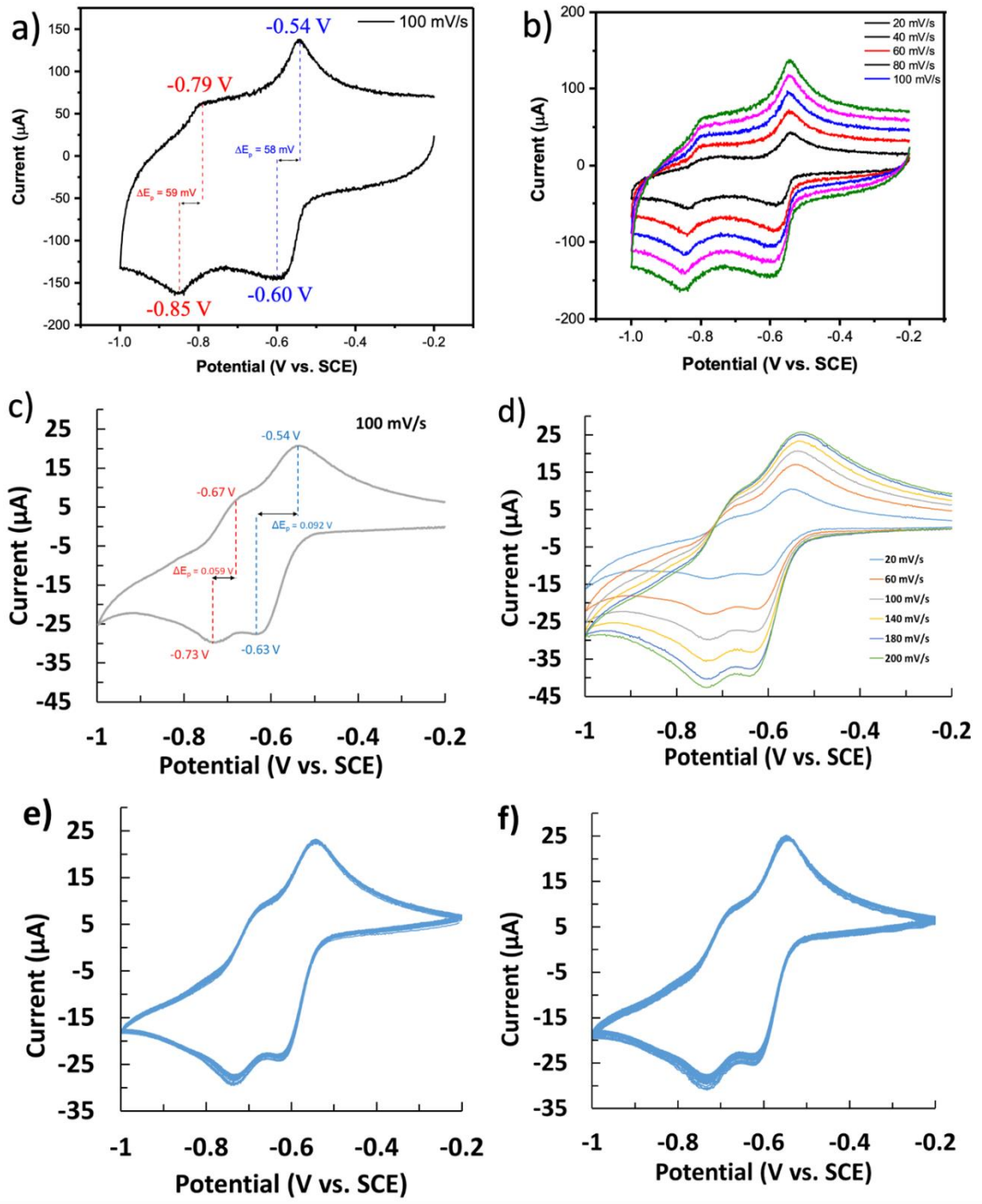

Supplementary Fig. 3: Cyclic voltammetry of (a,b) $(SPr)_2TTz$ in aqueous 0.5 M Na_2SO_4 solution and (c,d) $(NPr)_2TTz^{4+}$, and 50 CV cycles of $(NPr)_2TTz^{4+}$ (e) day 1 and (f) day 2.

Electrochromism

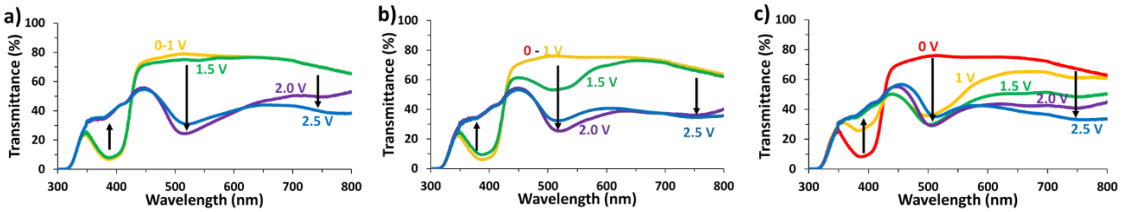

Supplementary Fig. 4: Me_2TTz^{2+}:$Fc(CH_2OH)_2$ Device spectra obtained at 0 V, 1 V, 1.5 V, 2 V and 2.5 V, Progression is shown with the arrows. **a)** 1:0 **b)** 1:1 **c)** 1:2

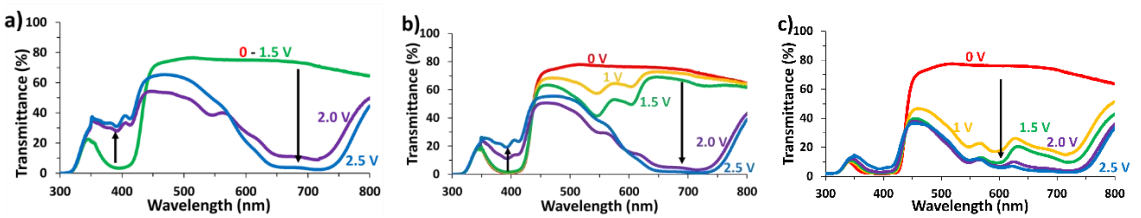

Supplementary Fig. 5: ($NPr)_2TTz^{4+}$:$Fc(CH_2OH)_2$ Device spectra obtained at 0 V, 1 V, 1.5V, 2 V and 2.5 V, Progression is shown with arrows. **a)** 1:0 **b)** 1:1 **c)** 1:2

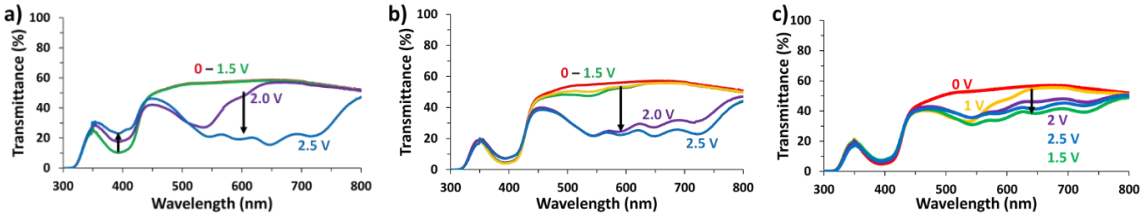

Supplementary Fig. 6: ($SPr)_2TTz$:$Fc(CH_2OH)_2$, Device spectra obtained at 0 V, 1 V, 1.5 V, 2 V and 2.5 V, Progression is shown with the arrows. **a)** 1:0 **b)** 1:1 **c)** 1:2

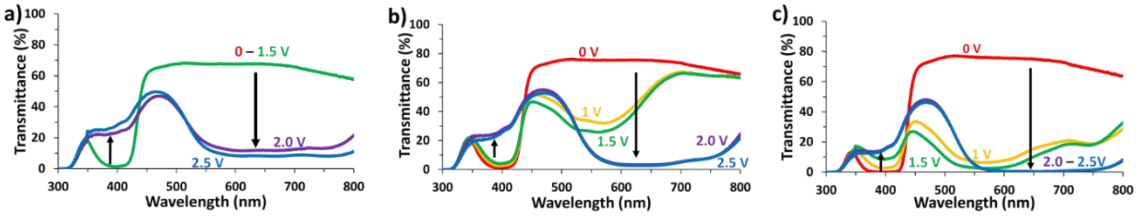

Supplementary Fig. 7: Bz_2TTz^{2+}:$Fc(CH_2OH)_2$, Device spectra obtained at 0 V, 1 V, 1.5 V, 2 V and 2.5 V, Progression is shown with the arrows. **a)** 1:0 **b)** 1:1 **c)** 1:2

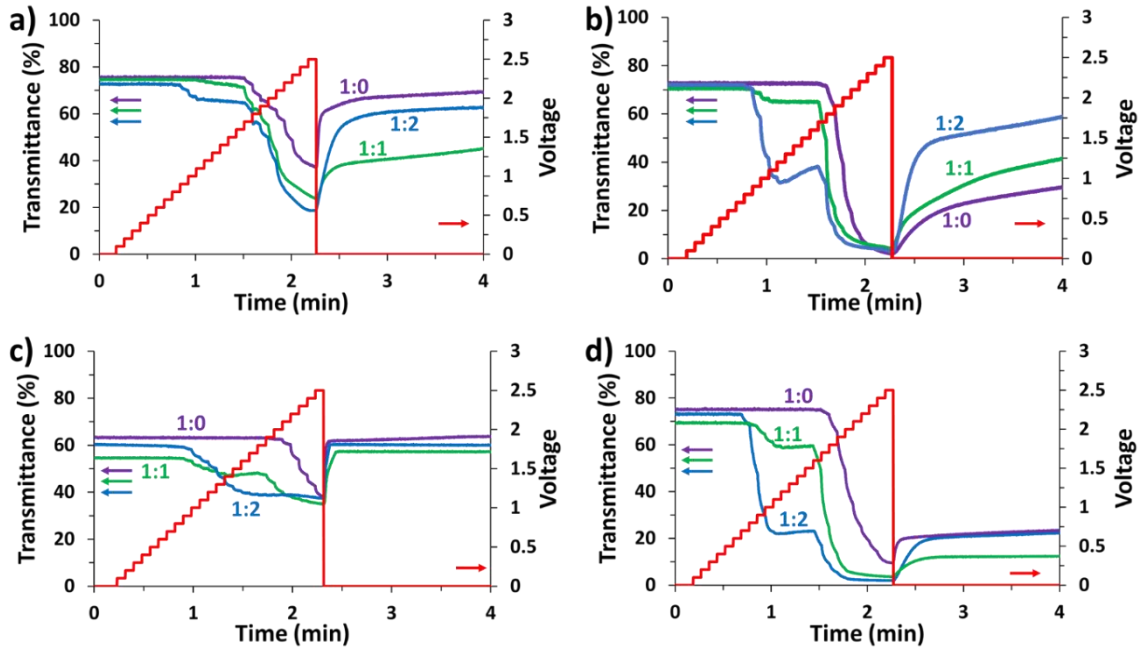

Supplementary Fig. 8: Different ratios of TTz:Fc$(CH_2OH)_2$ CGDs, scanned from 0-2.5 V (20 mV s^{-1}, 100 mV step) **a)** Me_2TTz^{2+} monitored at 700 nm **b)** $(NPr)_2TTz^{4+}$ monitored at 710 nm **c)** $(SPr)_2TTz$ monitored at 650nm for 1:0 and 600 nm for 1:1 and 1:2 **d)** Bz_2TTz^{2+} monitored at 700 nm.

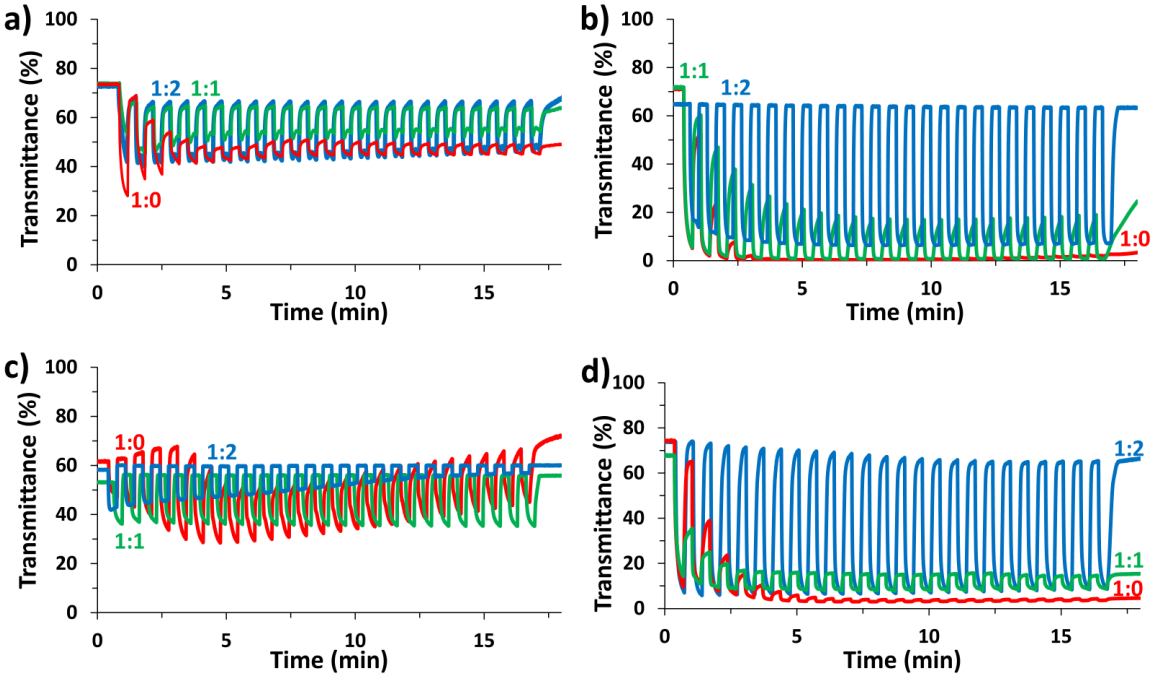

Supplementary Fig. 9: Unsealed CGD cyclability 25 cycles (20 s on/off) with increasing ratios of TTz:Fc$(CH_2OH)_2$ **a)** Me_2TTz^{2+}: 1:0 (515 nm, 2.5 V), 1:1 (519 nm, 1.8 V) and

1:2 (506 nm, 1.8V) **b)** $(NPr)_2TTz^{4+}$: 1:0 (710 nm, 2.4 V), 1:1 (710 nm, 1.8 V) and 1:2 (710 nm,1.8 V) **c)** $(SPr)_2TTz$: 1:0 (650 nm, 2.5 V), 1:1 (600 nm, 2.0 V), 1:2 (600 nm, 1.7 V) **d)** Bz_2TTz^{2+}: 1:0 (700 nm, 2.3 V), 1:1 (700 nm, 1.7 V) and 1:2 (700 nm, 1.7 V).

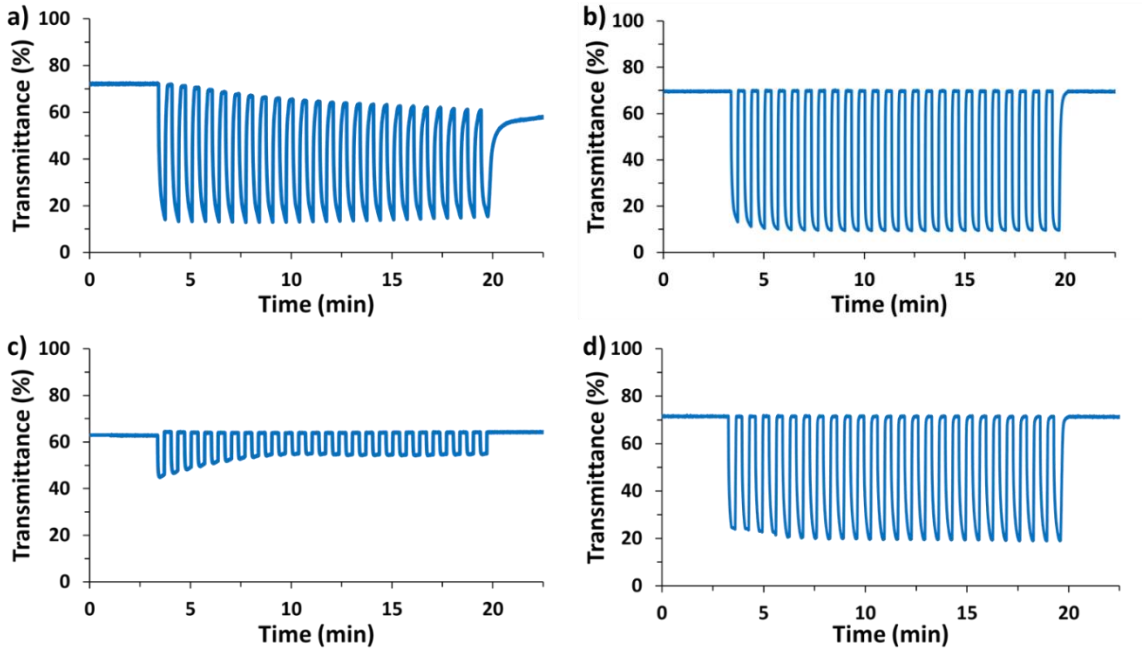

Supplementary Fig. 10: Sealed 1:2 TTz:$Fc(CH_2OH)_2$ CGD cyclability, 20 s on/off for 25 cycles **a)** Me_2TTz^{2+} monitored at 700 nm, 2.4 V applied **b)** $(NPr)_2TTz^{4+}$ monitored at 710 nm, 1.8 V applied **c)** $(SPr)_2TTz$ monitored at 600 nm, 2 V applied **d)** Bz_2TTz^{2+} monitored at 700 nm, 1.8 V applied.

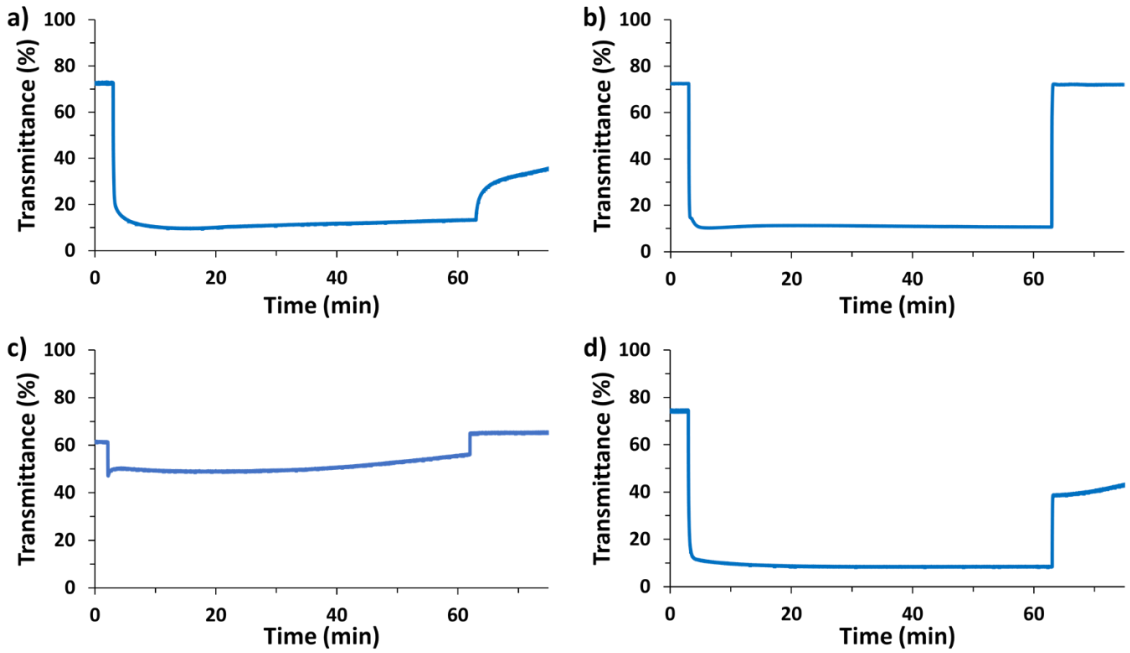

Supplementary Fig. 11: Sealed 1:2 TTz:Fc$(CH_2OH)_2$ CGD durability as the respective optimal voltage is on for 60 min **a)** Me_2TTz^{2+} @ 700 nm, 2.4 V, **b)** $(NPr)_2TTz^{4+}$ @ 710 nm, 1.8 V, **c)** $(SPr)_2TTz$ @ 600 nm, 2 V, **d)** Bz_2TTz^{2+} @ 700 nm, 1.8 V.

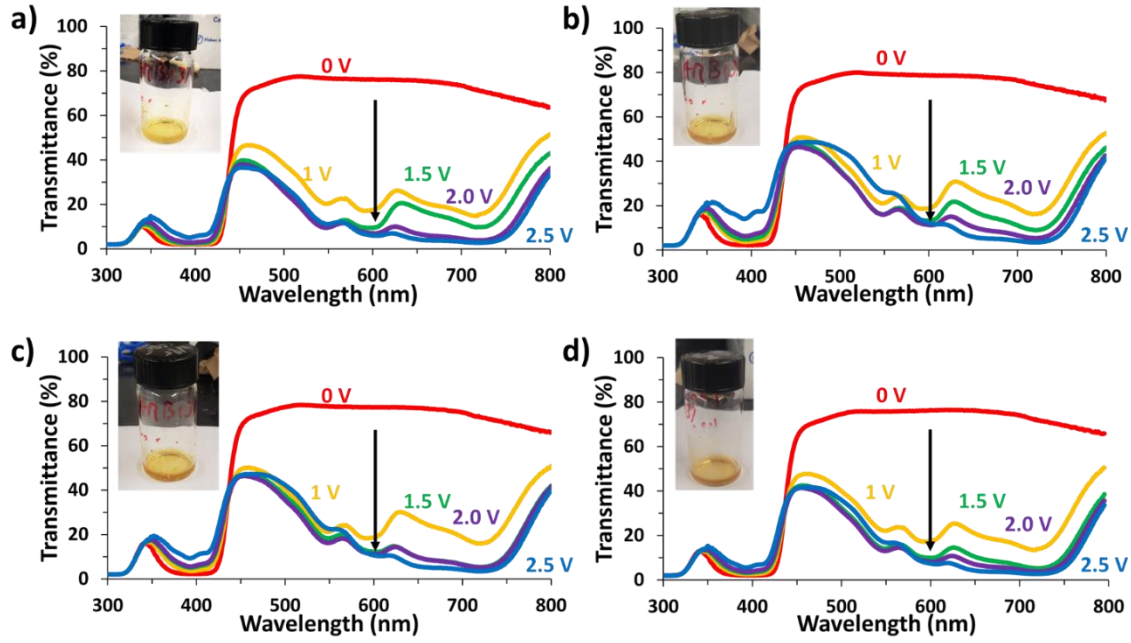

Supplementary Fig. 12: 1:2 **(**$(NPr)_2TTz^{4+}$:Fc$(CH_2OH)_2$ device spectra obtained at 0 V, 1 V, 1.5V, 2 V and 2.5 V, (progression shown with arrows). The same gel was used for devices **a)** on the same day, **b)** one day later, **c)** two days later, **d)** three days later while at ambient conditions.

Electrofluorochromism:

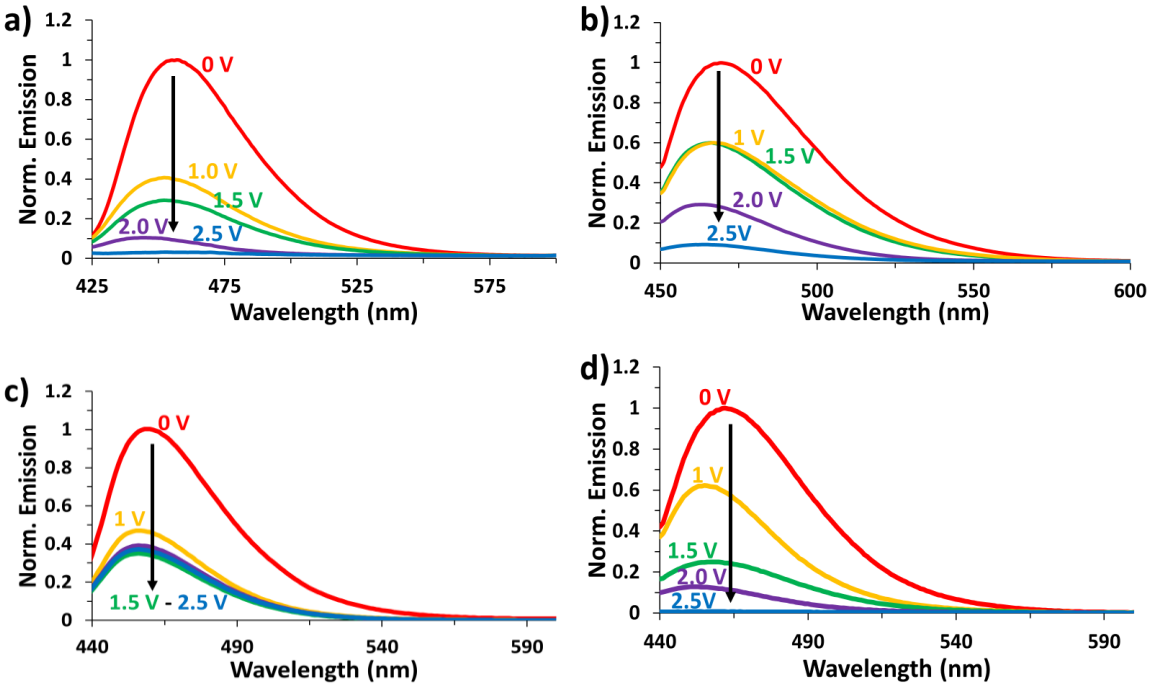

Supplementary Fig. 13: 1:2 ratios **a)** Me_2TTz^{2+} λ_{ex} = 400 nm, **b)** $(NPr)_2TTz^{4+}$ λ_{ex} = 410 nm, **c)** $(SPr)_2TTz$ λ_{ex} = 410 nm, **d)** Bz_2TTz^{2+} λ_{ex} = 419 nm at 0 V, 1 V, 1.5 V, 2 V, 2.5 V.

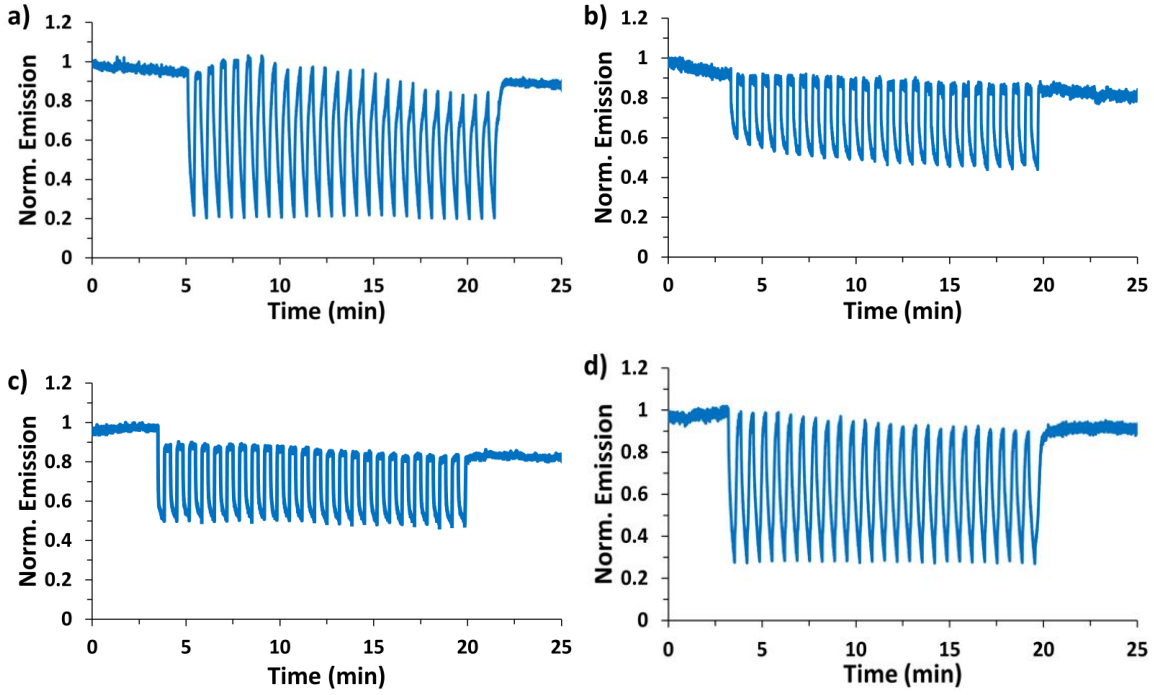

Supplementary Fig. 14: Sealed Fluorescence Cyclability 1:2 ratios, (20 s on/off), 25 cycles **a)** Me_2TTz^{2+} (λ_{ex} = 410 nm, λ_{em} = 452 nm, 2.4 V) **b)** $(NPr)_2TTz^{4+}$ (λ_{ex} = 410 nm,

λ_{em} = 470 nm, 1.8 V) **c)** $(SPr)_2TTz$ (λ_{ex} = 410 nm, λ_{em} = 458 nm, 2 V) **d)** Bz_2TTz^{2+} (λ_{ex} = 419 nm, λ_{em} = 463 nm 1.8 V)

Photochromism

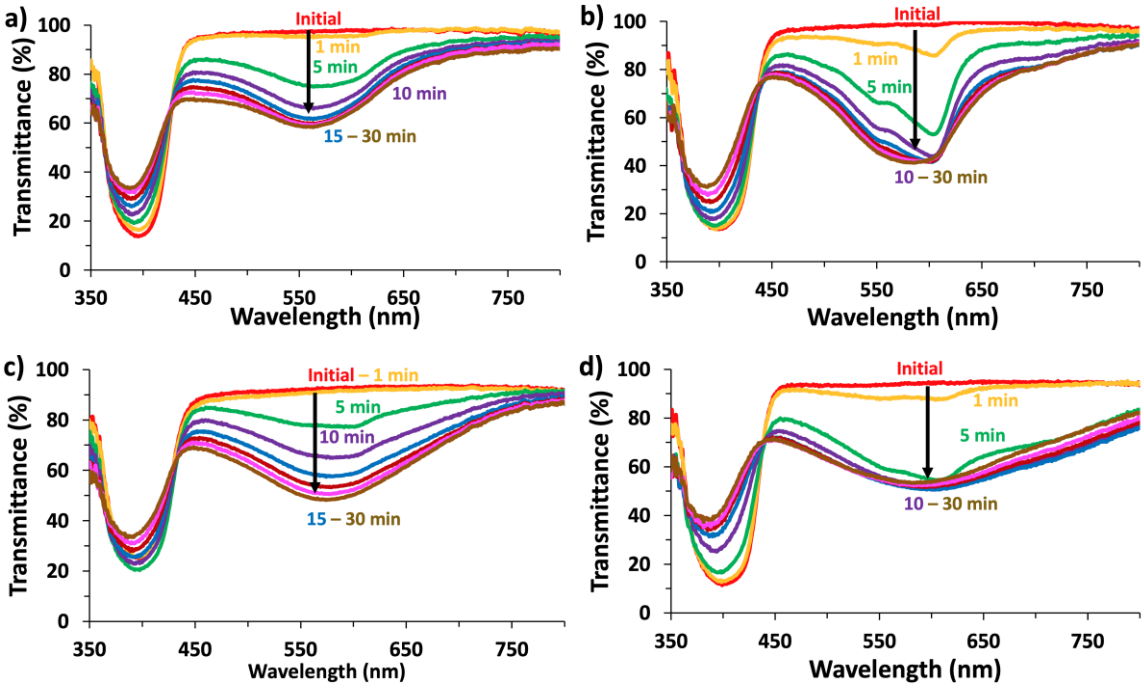

Supplementary Fig. 15: Photochromism of **a)** Me_2TTz^{2+} **b)** $(NPr)_2TTz^{4+}$ **c)** $(SPr)_2TTz$ **d)** Bz_2TTz^{2+} under illumination for 30 min.

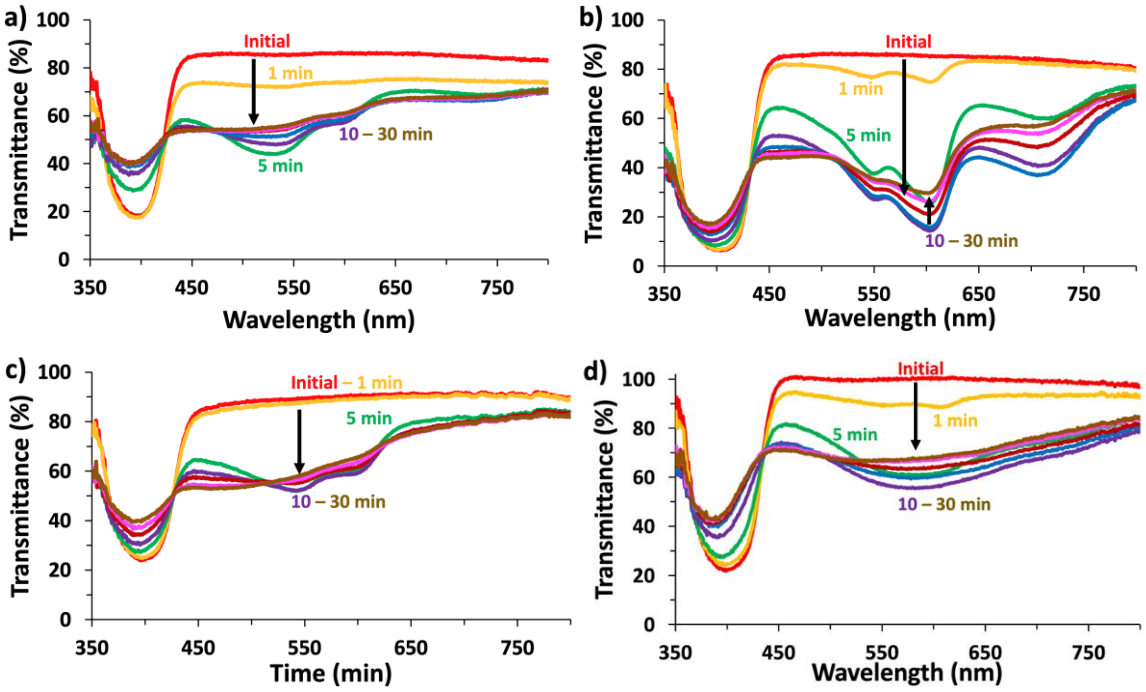

Supplementary Fig. 16: Voltage-assisted photochromism of **a)** Me_2TTz^{2+} at 0.7 V **b)** $(NPr)_2TTz^{4+}$ at 0.8 V **c)** $(SPr)_2TTz$ at 0.8 V **d)** Bz_2TTz^{2+} at 0.5 V under illumination for 30 min.

Characterization of Synthesized TTz's

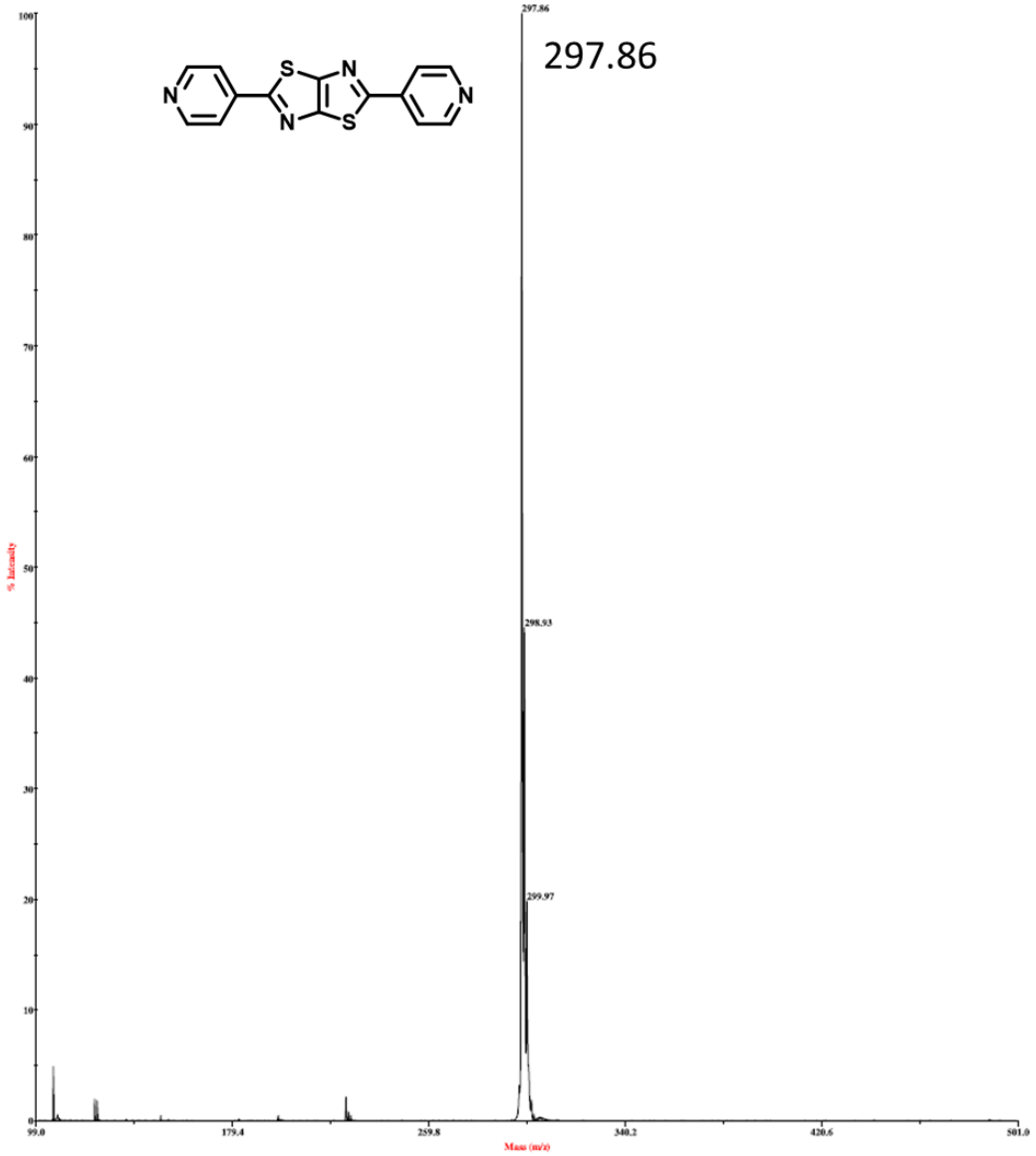

Supplementary Fig 17: MALDI-TOF MS of Py_2TTz. Calculated $(M+H)^+$ = 297.37 m/z, found 297.86 m/z.

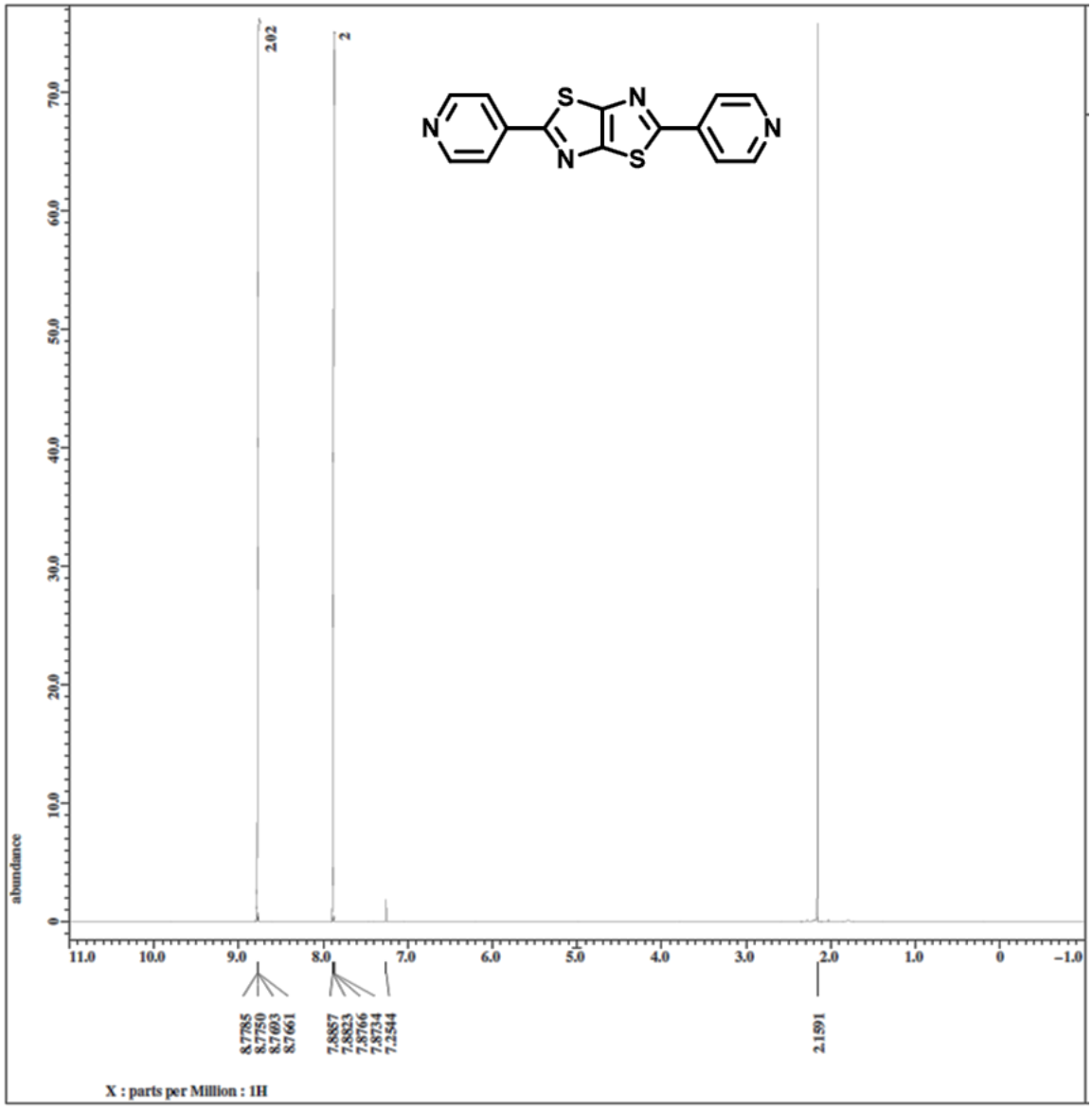
2.02
2
S
N
N
S
N
N
abundance
0
10.0
20.0
30.0
40.0
50.0
60.0
70.0
11.0
10.0
9.0
8.0
7.0
6.0
5.0
4.0
3.0
2.0
1.0
0
−1.0
8.7785
8.7750
8.7693
8.7661
7.8857
7.8823
7.8766
7.8734
7.2544
2.1591
X : parts per Million : 1H

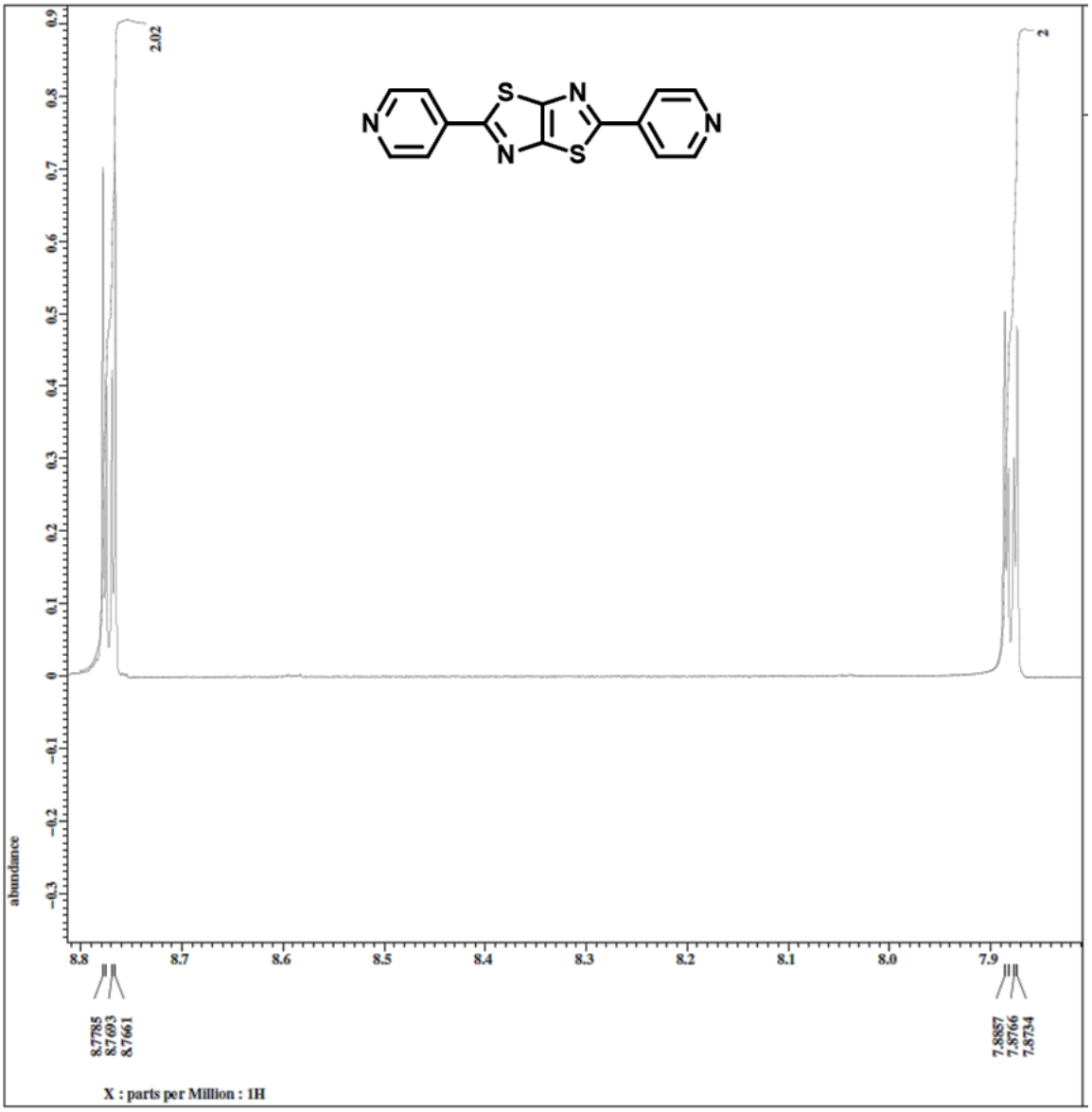

Supplementary Fig 18: ^{1}HNMR of Py_2TTz in $CDCl_3$ and aromatic region. The wide peak at 2 ppm is residual water.

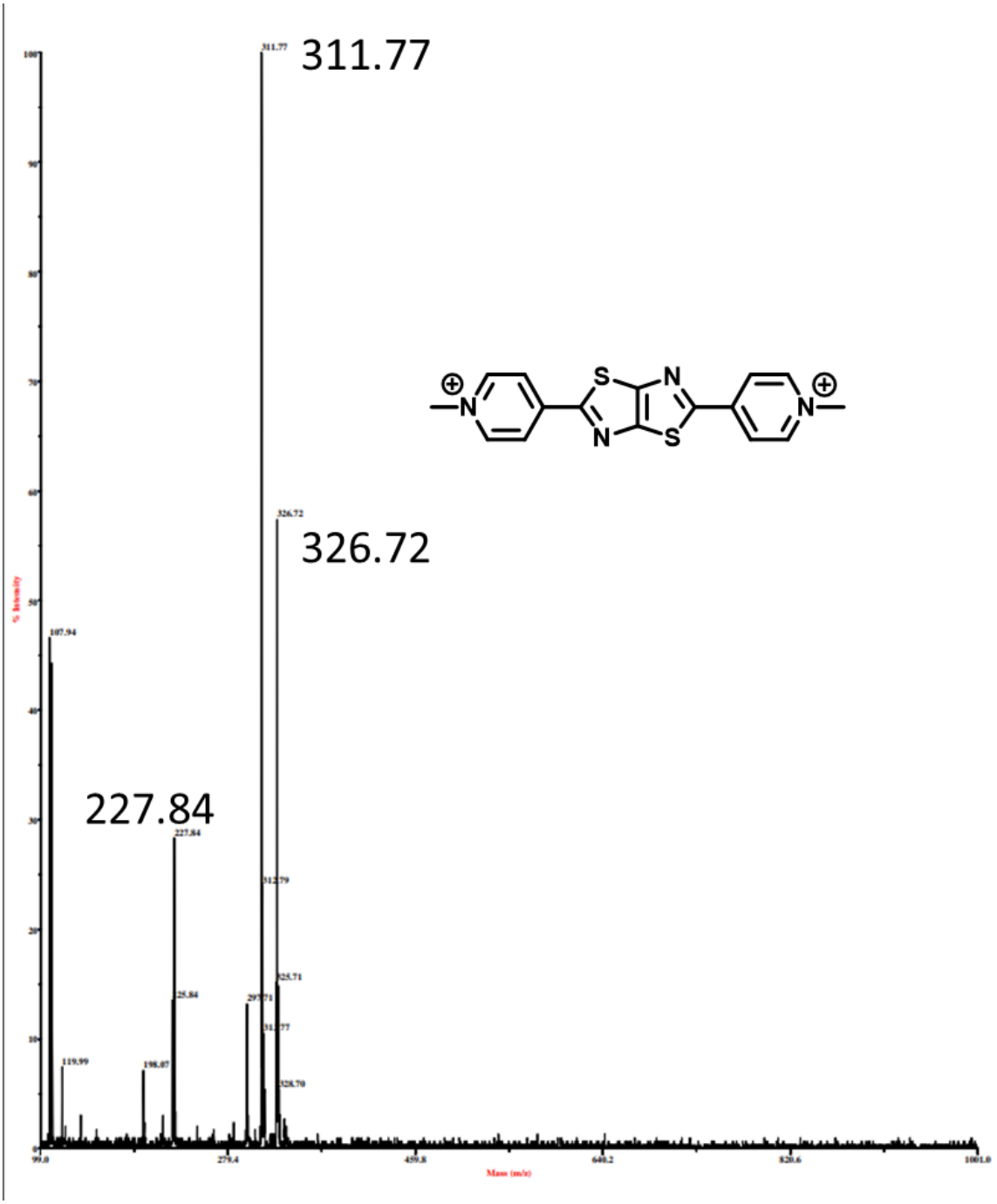

Supplementary Fig 19: MALDI-TOF MS of Me_2TTz. Calculated $(M)^+$ = 326.43 m/z, found 326.72 m/z.

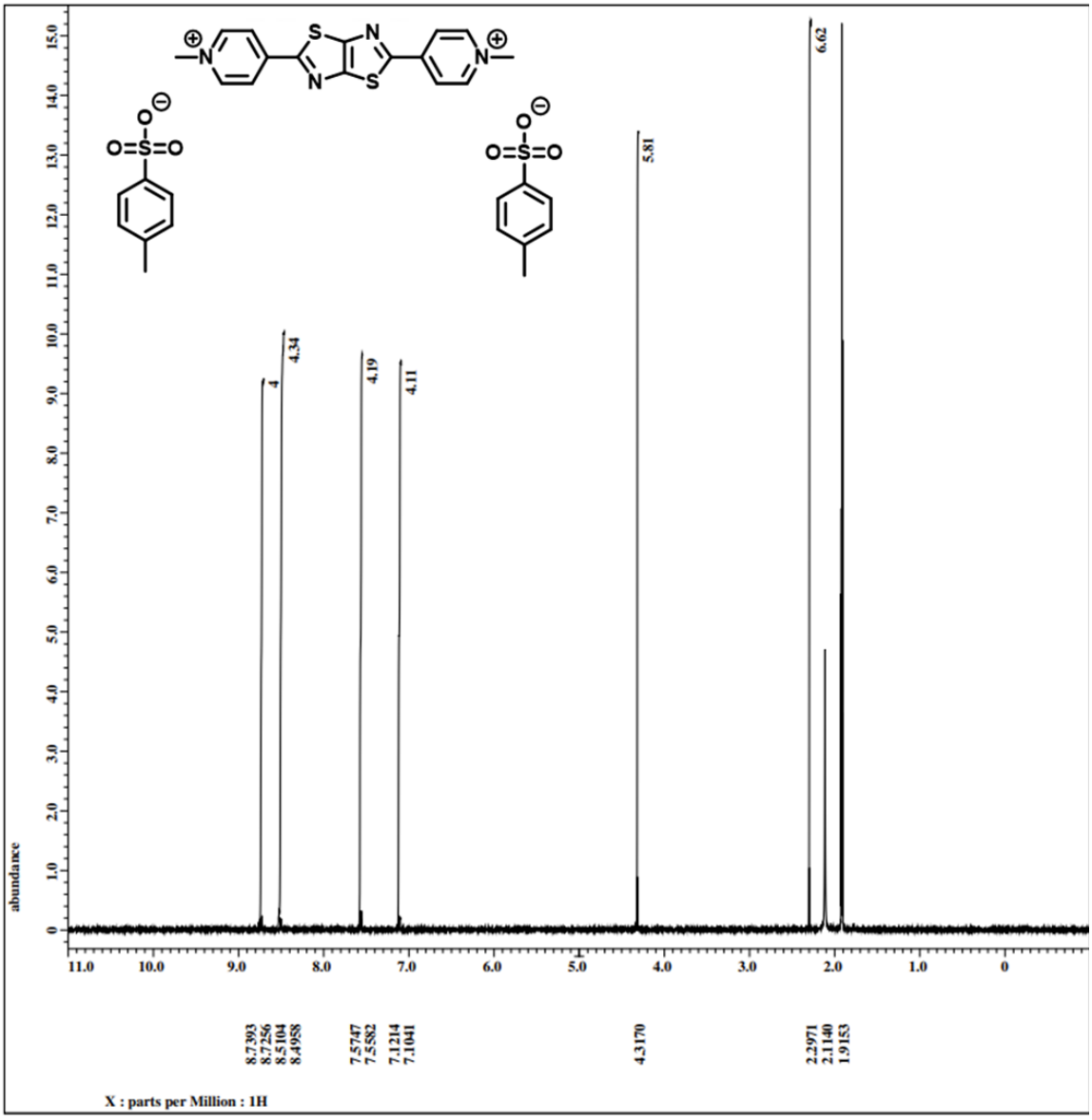
abundance
X : parts per Million : 1H
8.7393
8.7256
8.5104
8.4958
7.5747
7.5582
7.1214
7.1041
4.3170
2.2971
2.1140
1.9153
4
4.34
4.19
4.11
5.81
6.62

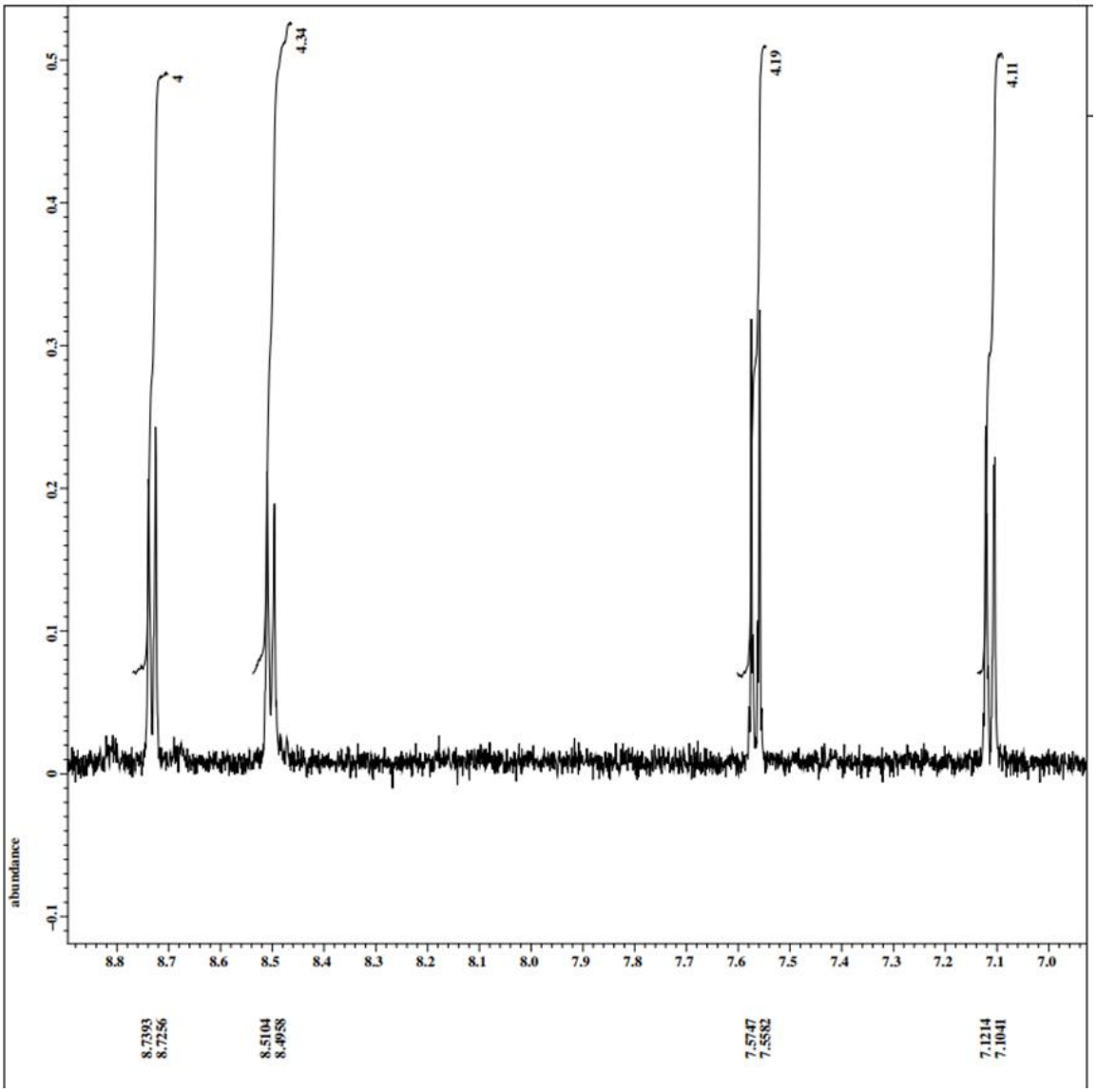

Supplementary Fig 20: ^{1}H-NMR of Me_2TTz in CDCN and aromatic region.

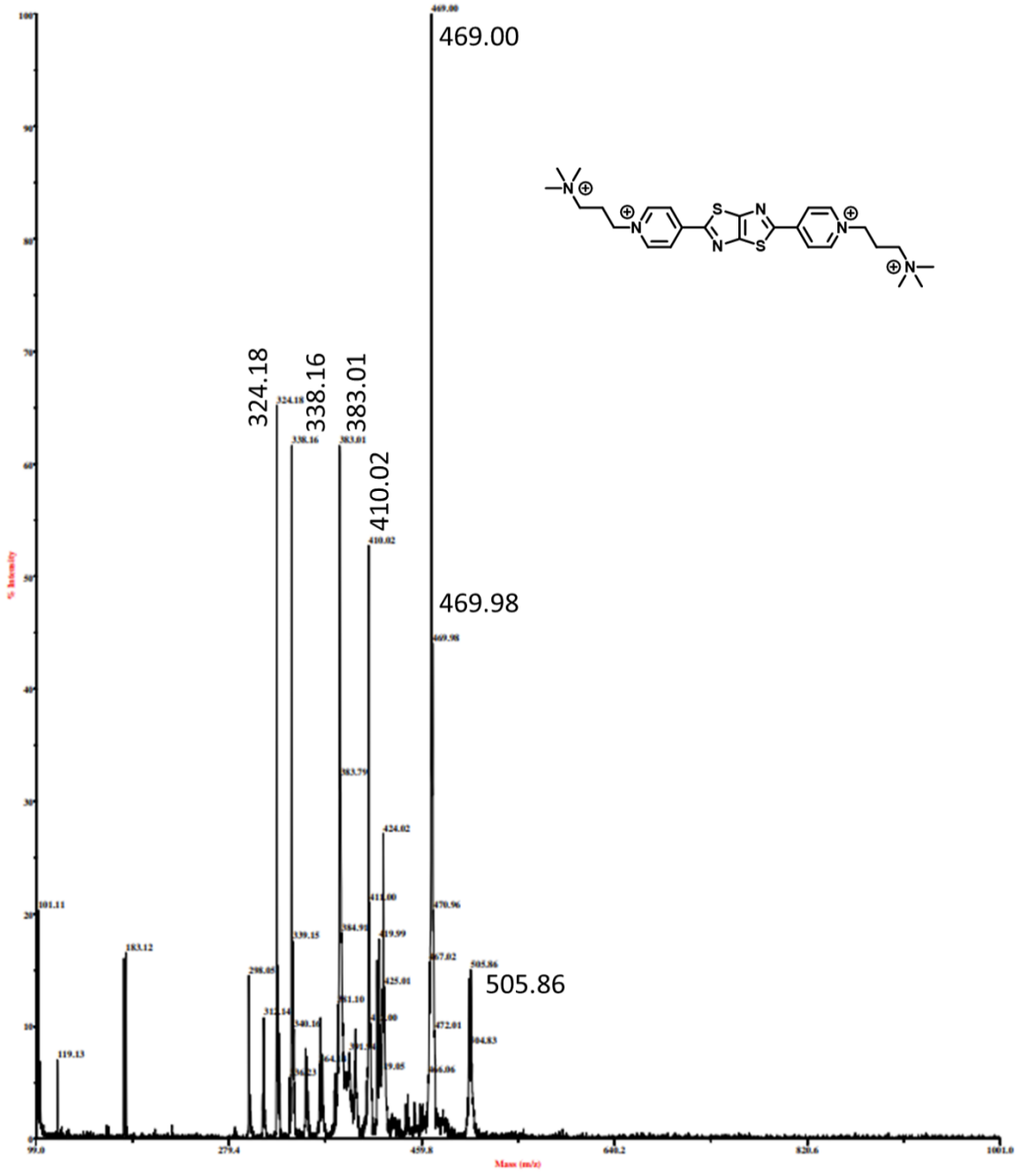

Supplementary Fig 21: MALDI-TOF MS of $(NPr)_2TTz^{4+}$. Calculated $(M)^+$ = 498.776 m/z, found 505.86 m/z.

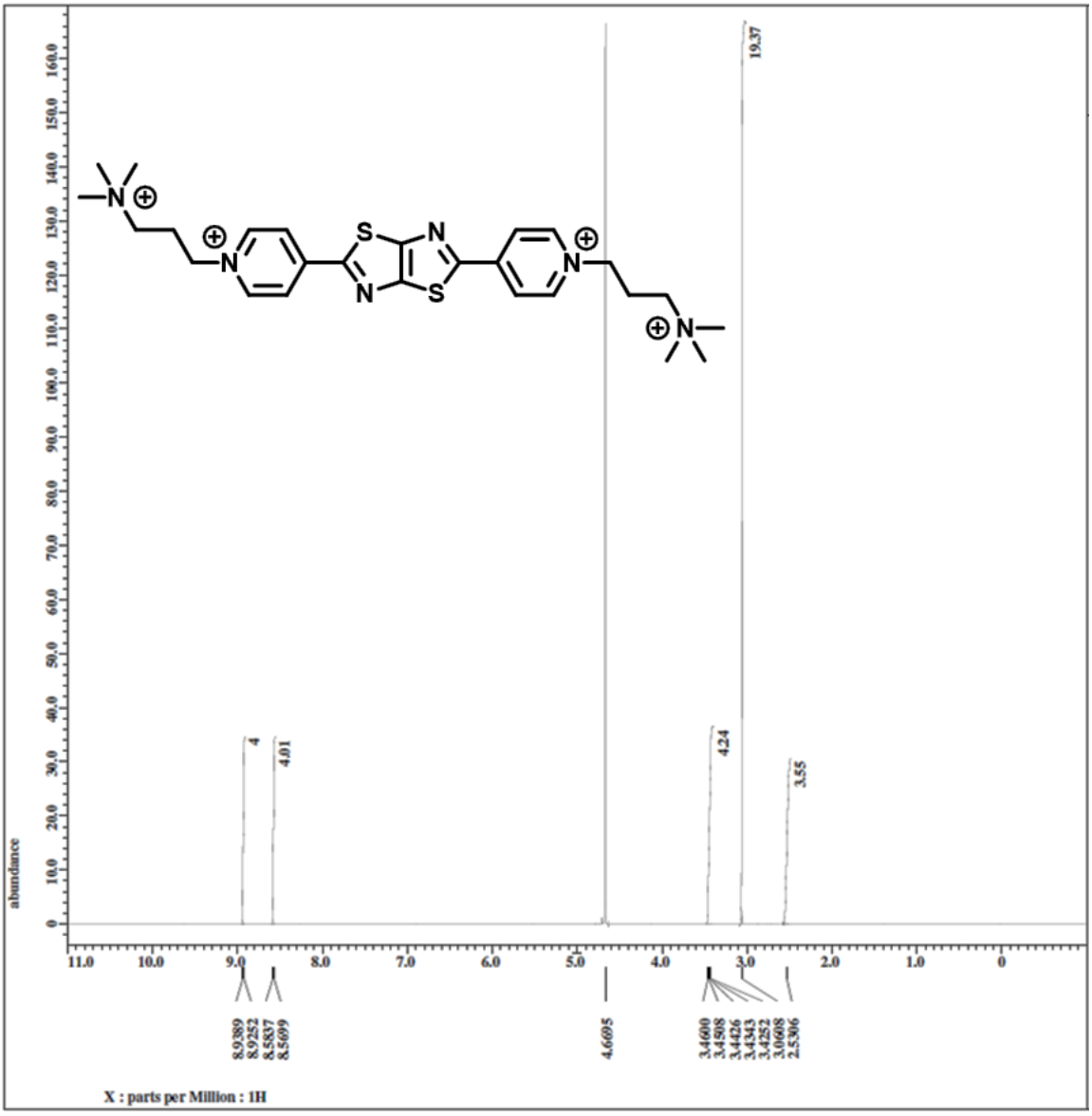
abundance
19.37
4
4.01
4.24
3.55
8.9389
8.9252
8.5837
8.5699
4.6695
3.4600
3.4508
3.4426
3.4343
3.4252
3.0608
2.5306
X : parts per Million : 1H

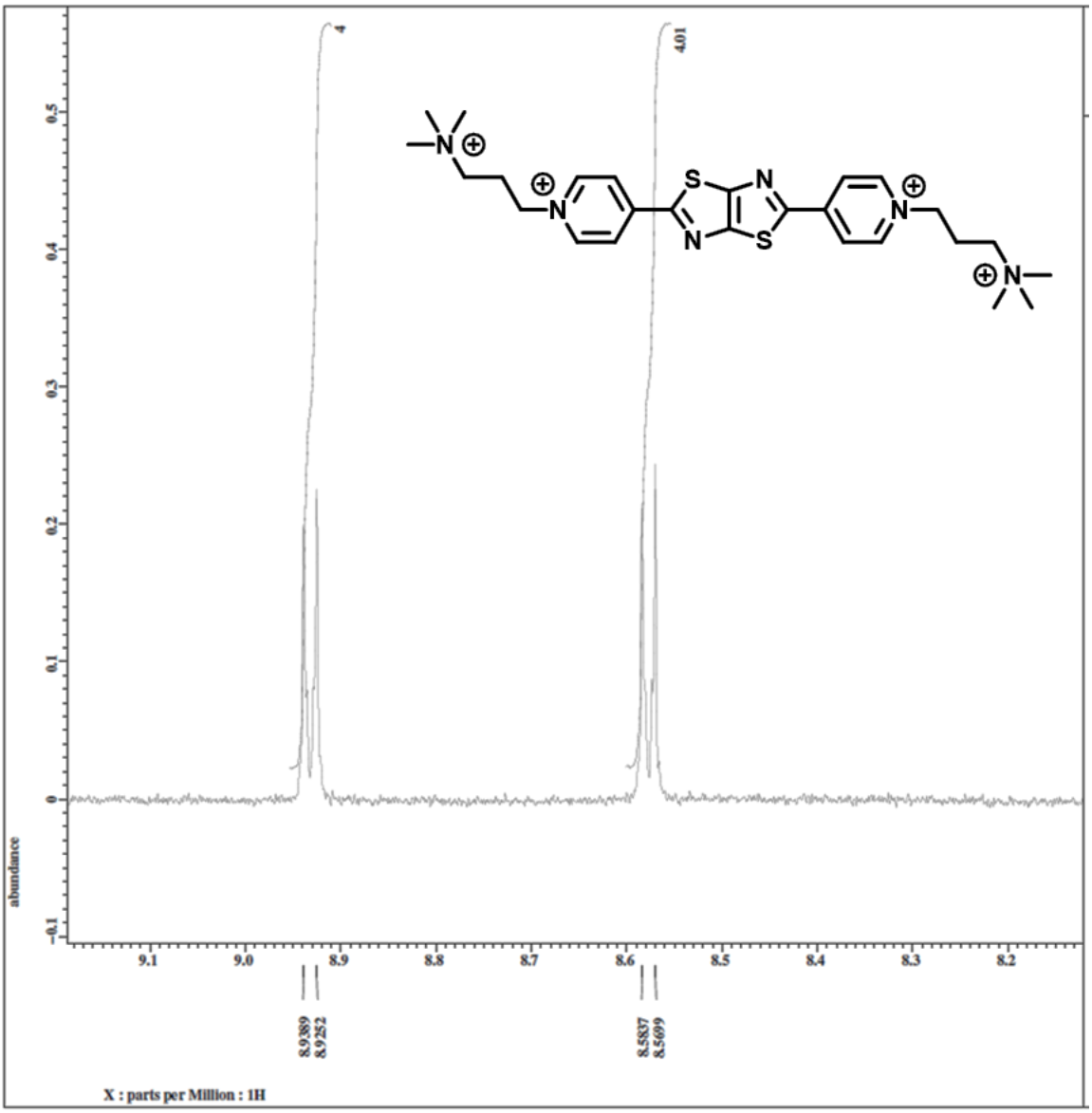

Supplementary Fig 22: ^{1}H-NMR of $(NPr)_2TTz^{4+}$ in D_2O and aromatic region.

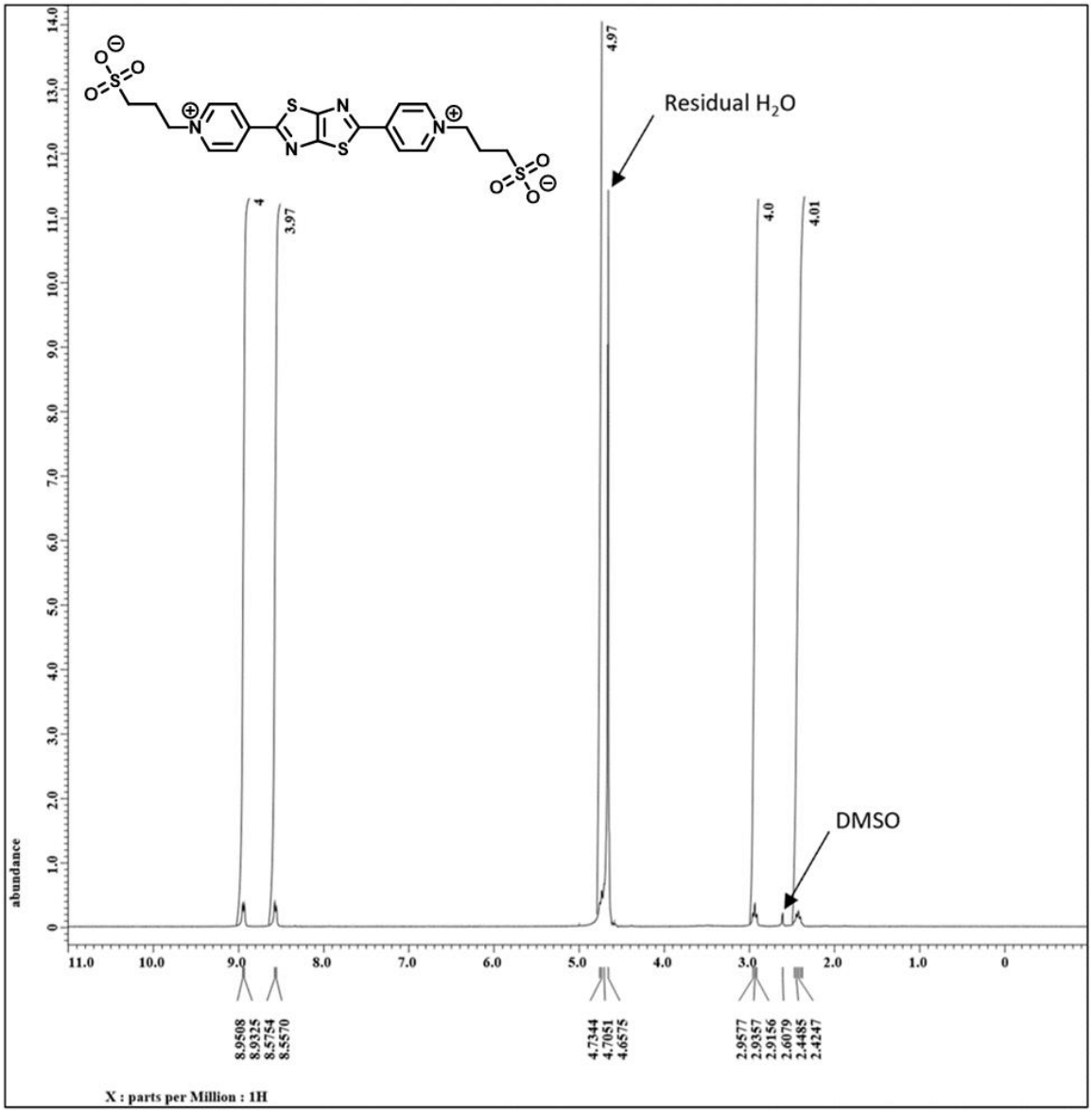

Supplementary Fig 24: ^{1}H-NMR of SPr_2TTz in D_2O.

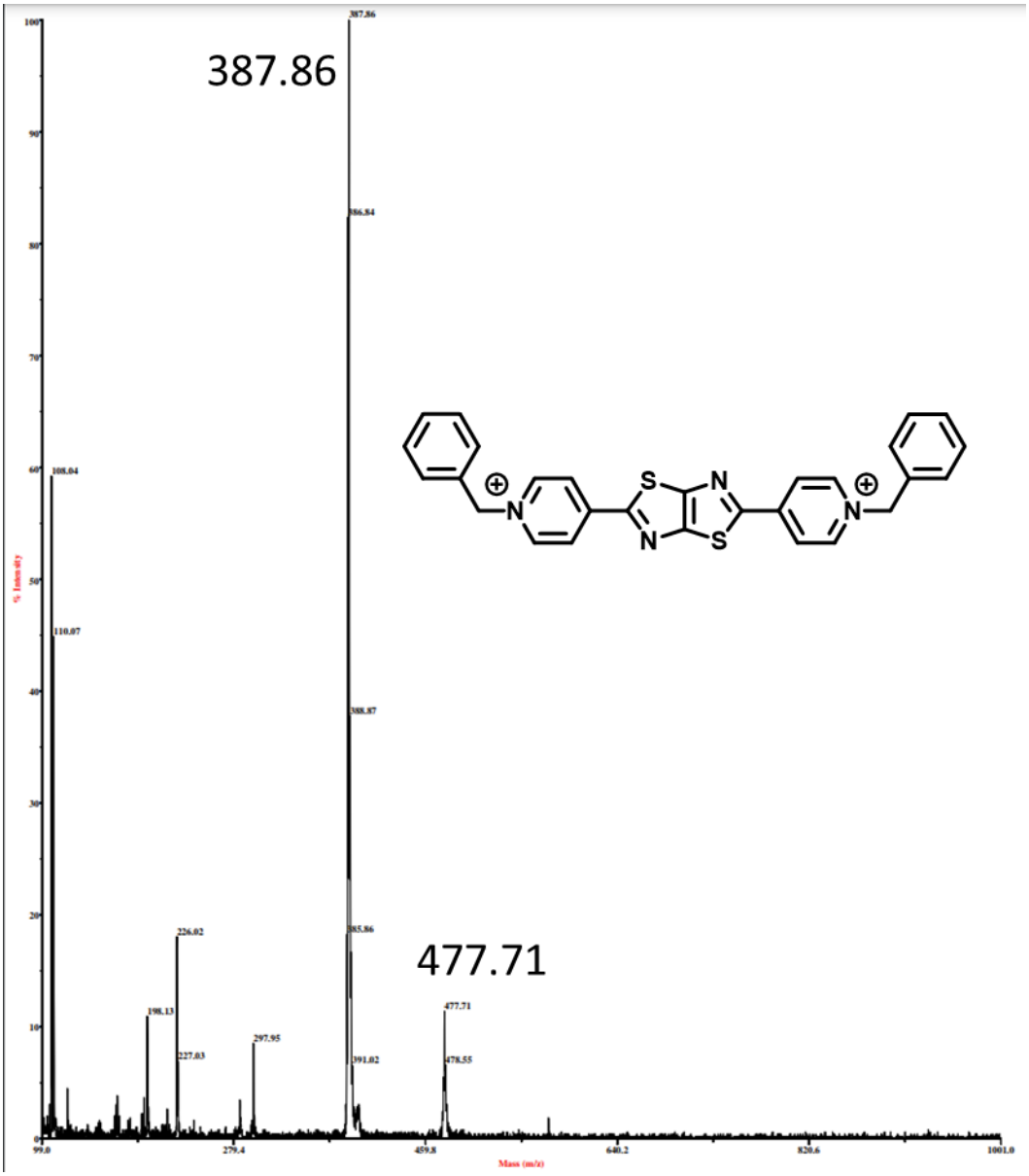

Supplementary Fig 25: MALDI-TOF MS of Bz_2TTz^{2+}. Calculated $(M)^+$ = 478.63 m/z, found 477.71 m/z.

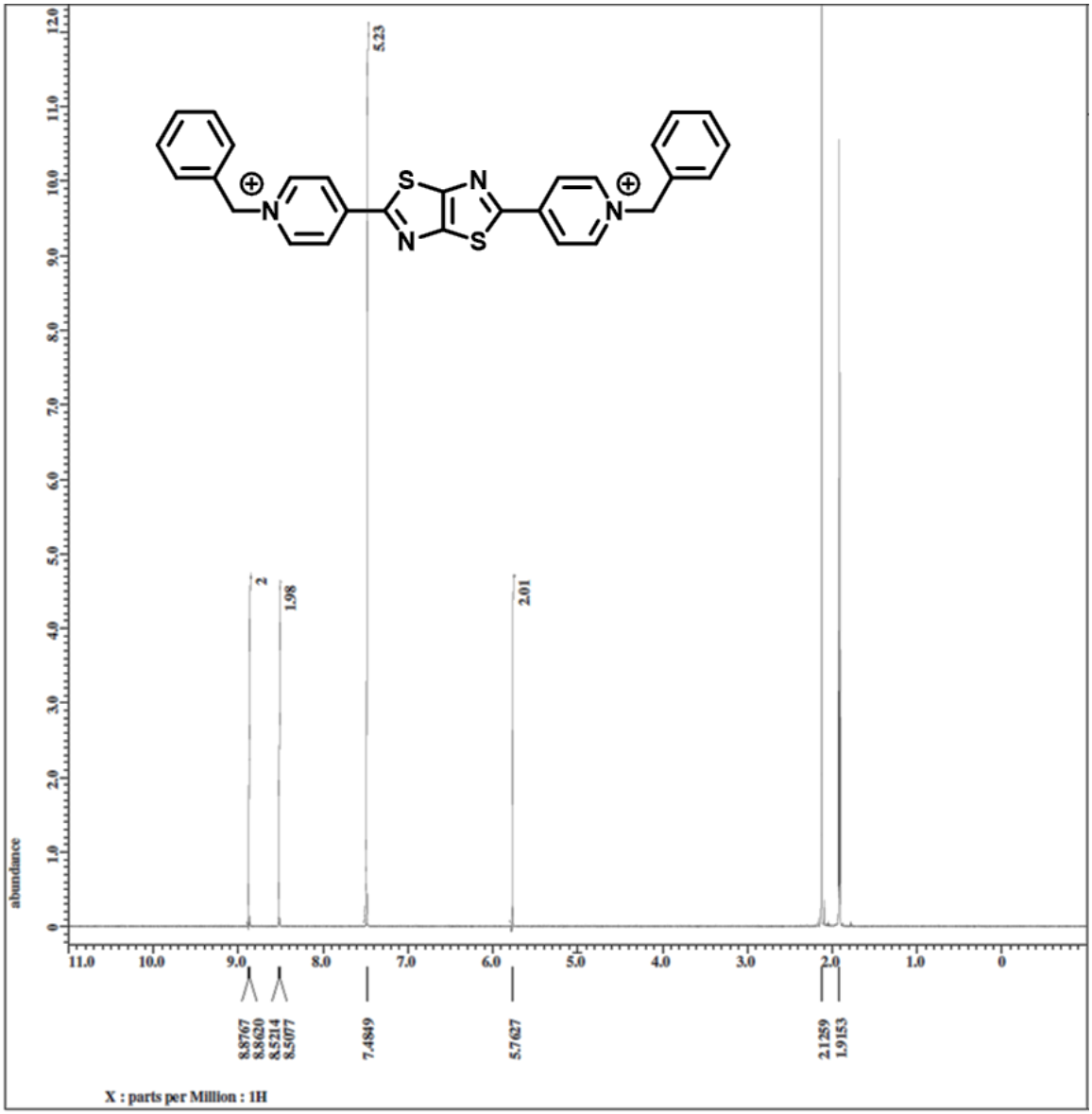
5.23
2
1.98
2.01
abundance
11.0
10.0
9.0
8.0
7.0
6.0
5.0
4.0
3.0
2.0
1.0
0
8.8767
8.8620
8.5214
8.5077
7.4849
5.7627
2.1259
1.9153
X : parts per Million : 1H

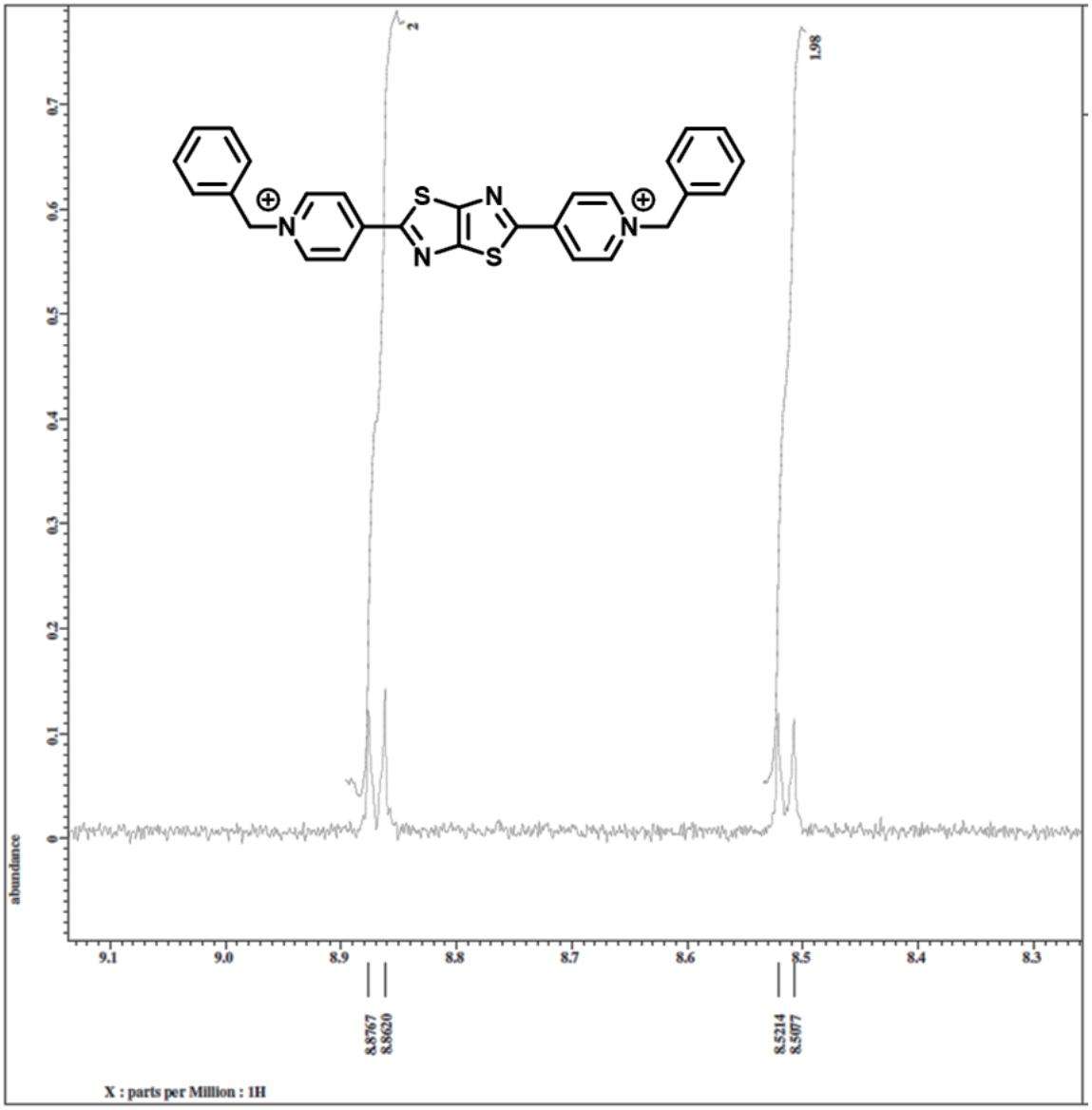

Supplementary Fig 26: ^{1}H-NMR of Bz_2TTz^{2+} in CD_3CN and aromatic region.

Chapter 3: Photochromic Films

3.1 Introduction

Photochromic materials are a popular research topic because of their potential applications in self-tinting smart windows,[26] eyeglasses,[1] displays,[17-18] and glucose sensors.[17-18] Some materials also exhibit photofluorochromism, where fluorescence intensity or wavelength changes with the light exposure, and can be used for displays, erasable memory devices,[27] or sensors.[3] Color changing oxygen sensing materials have a wide variety of uses for smart packaging,[43-44] medical bandages,[65] and wearable devices for confined spaces.[45] Organic materials are advantageous because of their high contrast, flexibility, easy processing, and inexpensive starting materials.[66]

There have been many materials used for photochromic and photofluorochromic devices and films. Organic dyes like Berry Red have been suspended in Paraloid B-72 and polyvinyl butyral polymeric films to yield high contrast photochromism that bleaches with heat.[67] One group targeted photofluorochromism by using cyanostilbene derivatives in poly(vinyl alcohol) nanowire films.[27] Ideally, the photochromic material would be organic, flexible, and cast out of water for fast roll-to-roll processing that is organic solvent-free, and environmentally-friendly. Many groups have pursued this, by coating indolinospirooxazine/ethylene-vinyl acetate copolymer in a two roll mill,[68] spirooxazine or spiropyran/disentangled ultrahigh molecular weight polyethylene via two roll mill,[69] and slot die coating spiropyran-based or spirooxazine-based photochromic compounds out of alcohols onto polyethylene terephthalate (PET) substrates.[70]

The absorbance of near infrared (NIR) light is advantageous for applications like photonics and telecommunications, since fiber optics use 1310 and 1550 nm light.[71] NIR

absorbing materials have also been studied for organic photovoltaics, since 52% of solar energy is in the NIR.[72] This is targeted for semi-transparent high efficiency window solar cells.[72] Materials that absorb NIR light can also be used as window glazing that rivals current low-e coatings for more energy efficient buildings by reducing solar heat gain.[73] Using molecular systems that absorb NIR light are useful for photothermal conversion and photothermal therapy, as NIR light, particularly 1000 – 1350 nm, can efficiently penetrate flesh.[74]

Oxygen sensing is advantageous for smart packaging of perishable items[43-44] or monitoring oxygen levels in confined work spaces.[45] Food is commonly packaged under nitrogen or carbon dioxide to reduce oxygen content to 0.5 to 2%, which decreases spoilage.[44] Oxygen induced spoilage occurs from aerobic microorganism growth, oxidation of oils or lipids, or enzymatic reactions that cause fruit/vegetable browning.[43-44] Packaging under inert atmospheres is also important for electronics, medical equipment, and pharmaceuticals to prohibit oxidation. Decataldo et al. used agarose hydrogel based organic electrochemical sensors made of PEDOT:PSS for flexible, wearable sensing in the tight range of 13-21% oxygen levels.[45] Quantitative color changes have been reported using platinum porphyrin and CdTe quantum dots.[46] Viologen containing MOF's have also been used for high contrast photochromism and oxygen sensing.[47] Material that not only senses the presence of oxygen, but also indicates the direction or location of a leak is advantageous to eliminate leaks or failure points.

Thiazolothiazole (TTz) viologens have gained interest because of their high fluorescence quantum yields,[15] strong electrochromic contrast,[15-16] and multifunctional properties.[16, 66] TTz viologens have been previously used for electrochromic,

electrofluorochromic, and photochromic devices[15-16] and have been incorporated into MOFs for photochromism and photofluorochromism,[75] or Hg sensing.[32] The TTz core has been incorporated into many studies for voltage sensitive dyes,[30] organic photovoltaics,[35] organic field effect transistors,[36-38] organic light-emitting diodes,[39] and redox flow batteries.[34] Dipyridyl TTz has also been attached to polymers for metal nanoparticle catalysis.[33] Poly(vinyl alcohol) (PVA) is an inexpensive, common polymer that is a "green polymer" because it can degrade over time and soluble in water. It can also be blended or copolymerized with other monomers to create copolymers for drug delivery, food packaging, and biomaterials.[76]

Previously, we achieved multifunctional chromogenic devices with dipyridinium TTz's in a PVA/Borax hydrogel that was reversibly electrochromic, electrofluorochromic, and photochromic.[16] Herein, dipyridinium TTz's and their photochromic, photofluorochromic, and oxygen sensing properties in PVA/Borax, agarose, and PMMA polymer films are reported and demonstrate the group's first TTz viologen fluorescing in solid state. **Figure 3.1 a** illustrates the reversible photochromism of the TTz molecule. When the yellow TTz^{2+} is excited by blue light, it photooxidizes the crosslinked PVA/borax and reduces to $TTz^{\bullet+}$ and reduces a second time via photooxidation of the PVA/borax to TTz^{0}. The TTz^{0} can be oxidized back to TTz^{2+} when exposed to oxygen in the dark. The flexible photochromic film is activated by blue light, changing from yellow to blue. By using a laser or a mask, a design can be made onto the film with high contrast (**figure 3.1 b-d**).

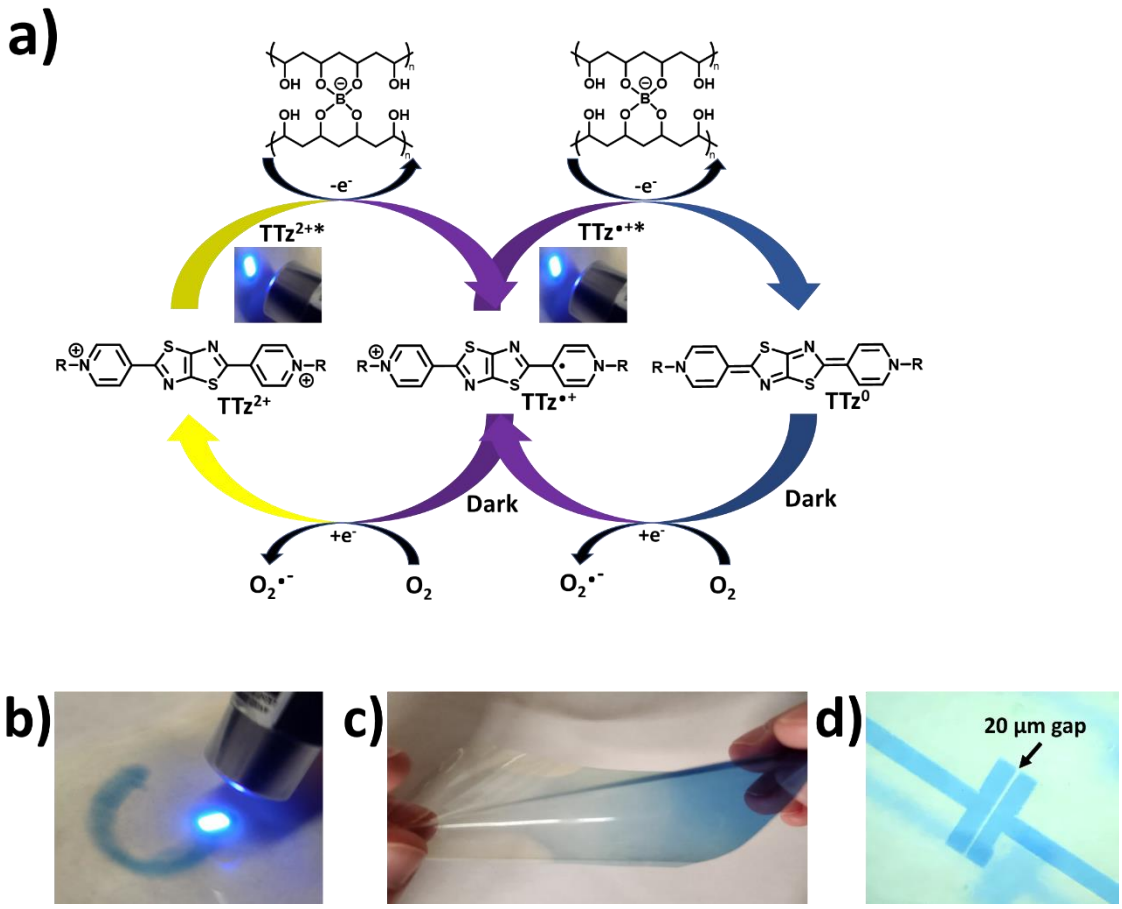

Figure 3.1: a) TTz reductions via photo-induced electron transfer and interaction with the crosslinked PVA/borax polymer matrix and oxidation due to exposure to oxygen in the dark, **b)** photochromic writing with a 405 nm laser pointer, **c)** the free-standing photochromic flexible film exhibiting illumination dependent color contrast, **d)** film photolithography with 20 µm gap mask.

3.2 Experimental

Materials and Instrumentation

Dithiooxamide, 4-pyridinecarboxaldehyde, (3-bromopropyl)-trimethylammonium bromide, poly(vinyl alcohol) (PVA) Mw 11000 – 31000, sodium tetraborate decahydrate

(Borax), Poly(methyl methacrylate-co-methacrylic acid) (PMMA) Mw 34,000, methyl p-tosylate, hexanes, and dimethyl formamide (DMF) were all purchased from Sigma-Aldrich and Baker Scientific. ^{1}H-NMR measurements were taken using a JEOL 500 MHz NMR and a JEOL 300 MHz NMR. Mass spectrometry measurements were obtained with a Perceptive Biosystems Voyager MALDI-TOF mass spectrometer.

A Varian Cary 50 Bio was used for UV-vis measurements and a Shimadzu RF-5301PC was used for fluorescence measurements. NIR measurements were collected with a Varian Cary 5000. A Gamry Reference 600 was used for cyclic voltammetry with a saturated calomel electrode reference, platinum foil counter electrode, and platinum button working electrode.

The 14 d low oxygen studies were conducted in an MBraun MB-20G glovebox, using an Ocean Optics QE65000 spectrophotometer and ecosmart 800 lumen multicolor LED light bulb selected to 630 nm red light (supplementary figure 3).

Film preparation

PVA/Borax films were made by dissolving [$((NPr)_2TTz^{4+})4Br^-$] in 4% PVA solution, then adding the appropriate amount of 4% borax solution. Depending on borax concentration, additional water was added for a thinner consistency for coating. The solutions were made as follows: 5% Borax: 60 mL 4% PVA solution, 10.4 mg [$((NPr)_2TTz^{4+})4Br^-$], 3 mL 4% Borax solution, 60 µm coater gap; 10% borax: 60 mL 4% PVA solution, 10.5 mg [$((NPr)_2TTz^{4+})4Br^-$], 7 mL 4% Borax solution, 5 mL DI water, 60 µm coater gap; 14% borax: 60 mL 4% PVA solution, 11.0 mg [$((NPr)_2TTz^{4+})4Br^-$], 10 mL 4% Borax solution, 10 mL DI water, 60 µm coater gap. PVA films were made by

dissolving 10.0 mg [$((NPr)_2TTz^{4+})4Br^-$] in 60 mL 4% PVA solution and coated at 60 µm. Agarose films were made by dissolving 1.0148 g agarose and 5.3 mg [$((NPr)_2TTz^{4+})4Br^-$] in 15 mL water, then coated (80 µm gap) while warm. The PMMA film was made by mixing 5.0003 g PMMA, 25 mg Me_2TTz^{2+} $2Tos^-$, and 10 mL dichloromethane and coating with a 50 µm coater gap. A LianDu six-inch adjustable film coating applicator was used to coat the films in a doctor blade like fashion. The films were coated onto mylar sheets (0.1 mm, 4 mil PET). Film thickness was measured with a digital micrometer, 20 – 30 µm film thickness.

For differing TTz concentrations, the solutions were made as follows: 0.4% [$((NPr)_2TTz^{4+})4Br^-$]: 60 mL 4% PVA solution, 11.0 mg [$((NPr)_2TTz^{4+})4Br^-$], 10 mL 4% Borax solution, 10 mL DI water, 60 µm coater gap; 1.7% [$((NPr)_2TTz^{4+})4Br^-$]: 60 mL 4% PVA solution, 51.8 mg [$((NPr)_2TTz^{4+})4Br^-$], 10 mL 4% Borax solution, 8 mL DI water, 60 µm coater gap; 3.4% [$((NPr)_2TTz^{4+})4Br^-$]: 60 mL 4% PVA solution, 102.6 mg [$((NPr)_2TTz^{4+})4Br^-$], 10 mL 4% Borax solution, 13 mL DI water, 60 µm coater gap; 5% [$((NPr)_2TTz^{4+})4Br^-$]: 60 mL 4% PVA solution, 150 mg [$((NPr)_2TTz^{4+})4Br^-$], 10 mL 4% Borax solution, 13 mL DI water, 60 µm coater gap.

The uvBeast V3 flashlight was held 11 cm from the film when conducting photochromic, photofluorochromic, and photomechanochromic testing. At this distance, the flashlight irradiates the film with 0.54 mW/cm^2 of 394 nm light (supplementary figure 4).

Synthesis

Please see Chapter 2 synthesis on page 12.

3.3 Results & Discussion

3.3.1 Borax Crosslinking Dependence

When coating the PVA/Borax, it was noted that without borax, the solution was watery and thinned out on the plastic backing, whereas inclusion of the borax thickened the solution and yielded better adhesion to the plastic backing. When comparing the PVA only film to the 14% borax film, the absorbance of the PVA only film showed much less reduced TTz^0 concentration than the 14% borax film. Two other borax concentration films were tested to determine if the 710 nm absorbance intensity was borax concentration dependent. With increasing borax concentration, the intensity of the 710 nm absorbance increases when comparing the max absorbance after 30 min of illumination and the rate of color change also increases, meaning the borax helps reduce more of the TTz and reduces the TTz faster (**figure 3.2 a-e**). Cyclic voltammetry of the PVA and borax shows the oxidation of the polymer becomes easier once crosslinked with the borate (**supplementary figure 1**). The onset potential for PVA alone is 1.18 V vs SCE, but decreases to 1.04 V vs SCE when borax is introduced and 1.00 V vs SCE upon crosslinking. This is shown and compared to the reduction potentials of TTz in **figure 3.2 g**. This decrease in oxidation level makes the photo-induced electron transfer more favorable and accelerated.

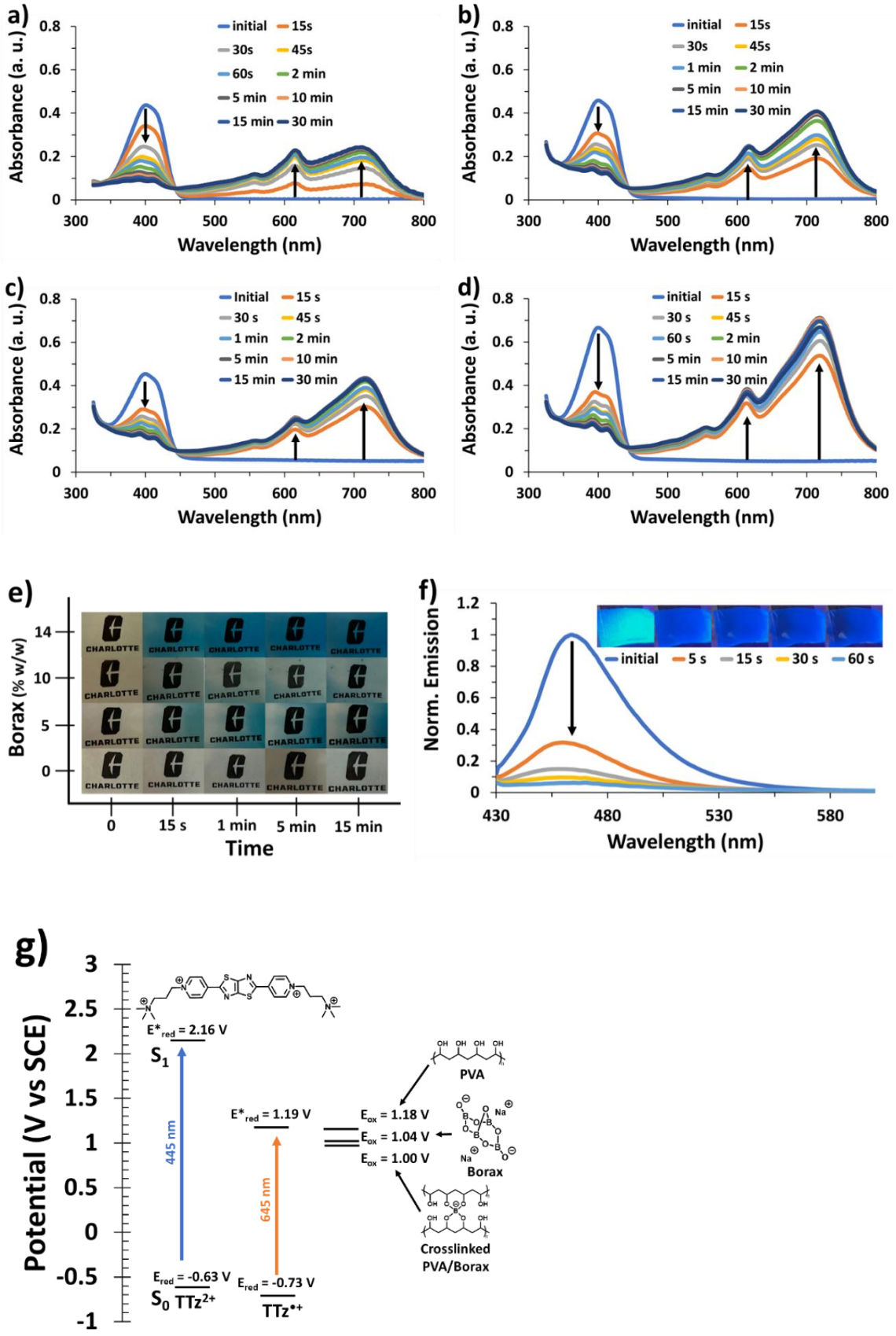
a)
Absorbance (a. u.)
Wavelength (nm)
initial
15s
30s
45s
60s
2 min
5 min
10 min
15 min
30 min
b)
Absorbance (a. u.)
Wavelength (nm)
initial
15s
30s
45s
1 min
2 min
5 min
10 min
15 min
30 min
c)
Absorbance (a. u.)
Wavelength (nm)
Initial
15 s
30 s
45 s
1 min
2 min
5 min
10 min
15 min
30 min
d)
Absorbance (a. u.)
Wavelength (nm)
initial
15 s
30 s
45 s
60 s
2 min
5 min
10 min
15 min
30 min
e)
Borax (% w/w)
Time
0
15 s
1 min
5 min
15 min
CHARLOTTE
f)
Norm. Emission
Wavelength (nm)
initial
5 s
15 s
30 s
60 s
g)
Potential (V vs SCE)
E*red = 2.16 V
S1
445 nm
Ered = -0.63 V
S0 TTz2+
E*red = 1.19 V
645 nm
Ered = -0.73 V
TTz•+
Eox = 1.18 V
Eox = 1.04 V
Eox = 1.00 V
PVA
Borax
Crosslinked
PVA/Borax

Figure 3.2: Photochromism of PVA/Borax films with different borax concentrations, **a)** 0% borax, **b)** 5% borax, **c)** 10% borax, **d)** 14% borax, **e)** visual representation of photochromism, **f)** photofluorochromism of 14% borax PVA/Borax film (420 nm excitation), with inset visual representation, **g)** band gap diagram of PVA, borax, PVA/borax mixture, and gelled crosslinked PVA/borax.

Although the TTz^{2+} state is highly fluorescent, the $TTz^{\bullet+}$ and TTz^{0} are non-emissive (in the visible range at 450 nm), causing the observed photofluorochromism. The photofluorochromism occurs quickly, starting with just 5 s of light exposure. After 1 min of illumination, the fluorescence drops 88%, 89%, 90%, and 94% for the 0%, 5%, 10% and 14% borax concentrations, respectively (**supplementary figure 2**). The addition of borax does not shift the excitation or emission wavelengths, as they stay around 420 nm and 465 nm, respectively. Representative fluorescence spectra and inset pictures are shown in **figure 3.2 f**.

3.3.2 The effects of TTz concentration

In the PVA/Borax films with 14% borax, different TTz concentrations were tested. The 0.4% TTz film showed an immediate double photoreduction to the TTz^{0} state, whereas the higher TTz concentration films show slower and stepwise reductions (**figure 3.3 a-d**). The 3.4% and 5% TTz films show the TTz^{2+} (400 nm absorbance) reduction to $TTz^{\bullet+}$ (610 nm absorbance) happens before reduction to the TTz^{0} state (710 nm). The rate of TTz reduction is shown in figure 3 e, which compares onset speed the 710 nm absorbance (TTz^{0}). The 0.4% TTz film takes only 5 min for full reduction whereas 5%

TTz takes 30 min. As expected, the higher concentrations yield much darker films when reduced (**figure 3.3 f**).

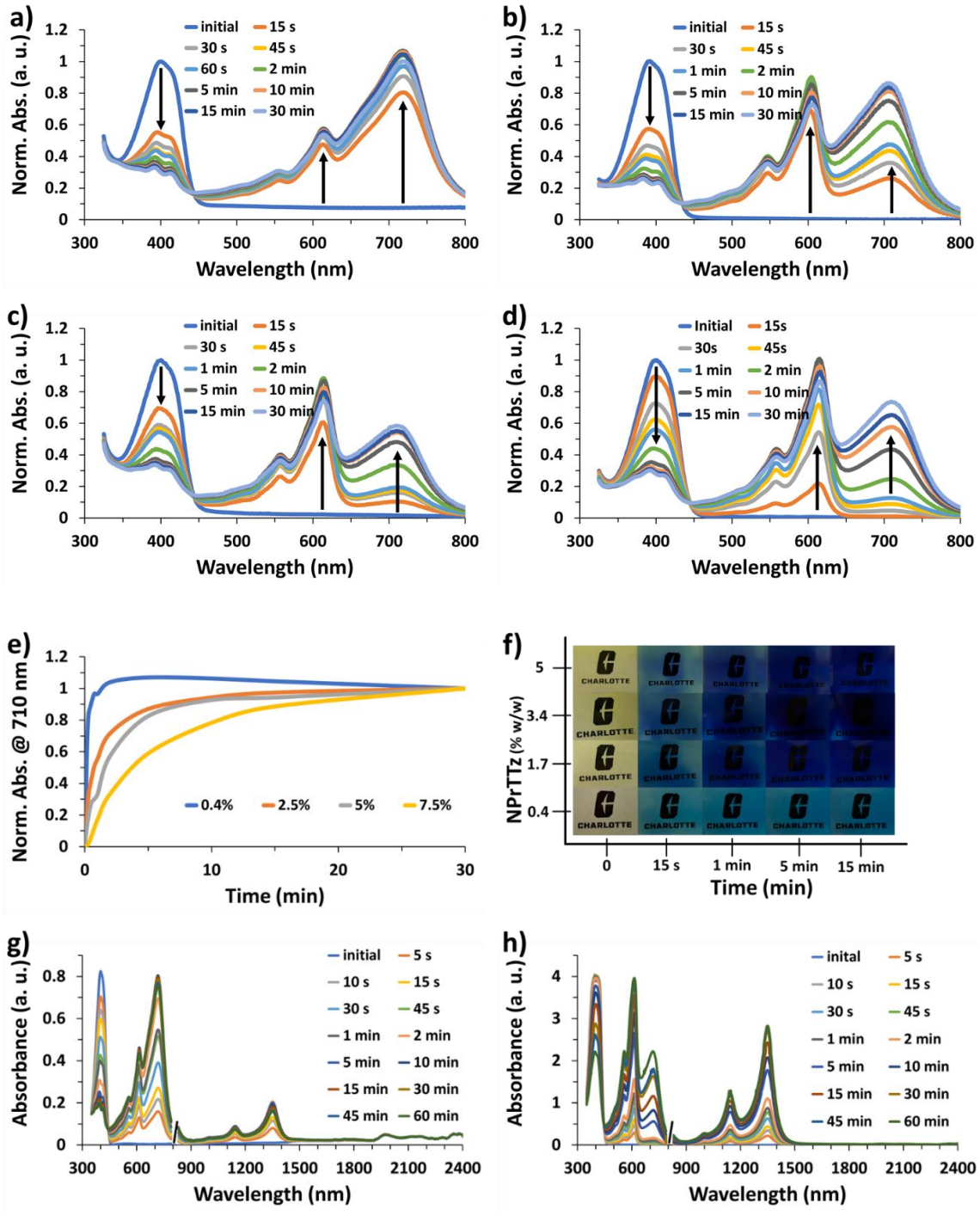

Figure 3.3: Photochromism of PVA/Borax films with different NPrTTz concentrations, **a)** 0.4%, **b)** 1.7%, **c)** 3.4%, **d)** 5%, **e)** change in 710 nm absorbance over photochromism

time, **f)** visual representation of photochromism, **g)** visible/NIR absorbance of 0.4% TTz film, **h)** visible/NIR absorbance of 5% TTz film.

When in the yellow TTz^{2+} state, the only absorbance is at 400 nm, with no other absorbance from 500 to 2500 nm. When the photochromism occurs and the $TTz^{\bullet+}$ is formed, in addition to the 610 nm absorbance, absorbances in the NIR at 1150 and 1350 nm occur. When analyzing the 0.4% TTz film (**figure 3.3 g**), both the first (610 nm) and second (710 nm) reductions occur quickly and the NIR absorbance (1150 and 1350 nm) increase steadily. However, after the 1350 nm peak maximizes at 2 min of illumination, the absorbance steadily decreases with further illumination, as the TTz^{0} 710 nm peak continues to increase until 10 min of light exposure. With the higher concentration 5% TTz film, the 1350 nm peak increased at a similar rate as the 610 nm TTz^{+} absorbance, before substantial 710 nm absorbance TTz^{0} was formed. With continued illumination, all absorbances increased. This may suggest that the NIR absorbances at 1150 and 1350 nm are caused by the radical cation $TTz^{\bullet+}$. The NIR absorbances overlap with the 1310 nm light used for fiber optic communications.

3.3.3 TTz/Film interactions

To get a better understanding of the mechanism behind the color change, a PVA/Borax film was submerged in liquid nitrogen and illuminated for 30 min. The absorbance and fluorescence spectra in **figure 3.4 a-b** show the reduction of the TTz is much slower in the liquid nitrogen, taking 30 min of illumination to achieve the same photofluorochromism that takes 5 s at room temperature. The reduction may be slower because the films components (TTz, PVA, Borax) cannot move freely enough to interact

and cause the photoreduction. The trend continued when a film was further dried under vacuum, as TTz reduction was also slower in the drier film, presumably as TTz could not move as much as with a slightly hydrated film (**figure 3.4 c-d**).

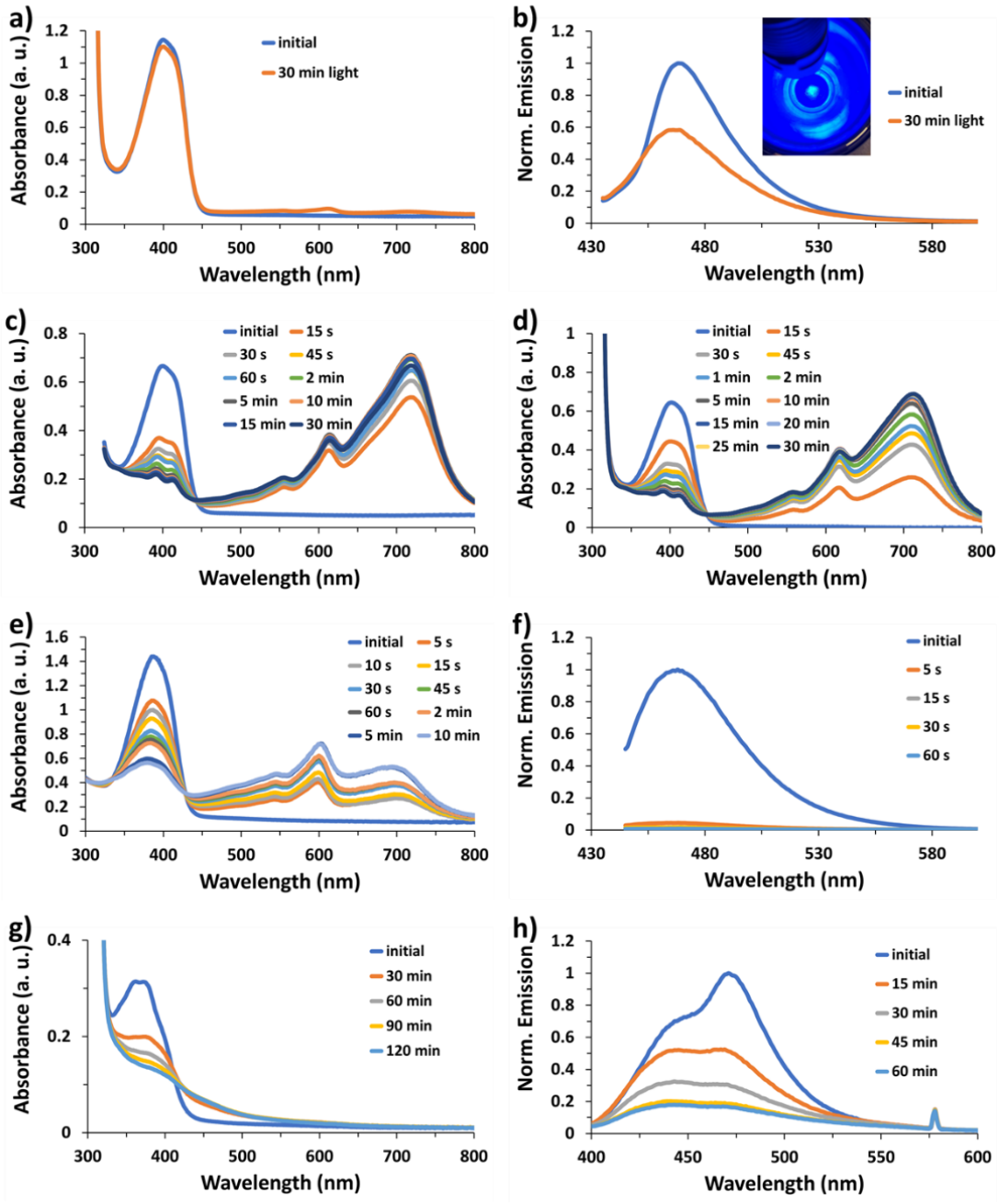

Figure 3.4: a) Absorbance and **b)** emission of 0.4% NPrTTz 14% Borax film before and after 30 min of illumination while in liquid nitrogen (-196 °C), **c)** photochromism of

0.4% NPrTTz 14% Borax film dried with normal conditions **d)** dried in vacuum oven for 72 h, **e)** photochromism and **f)** photofluorochromism of 0.5% NPrTTz agarose film. **g)** absorbance and **h)** fluorescence of NPrTTz photodegradation in a PMMA film.

In addition to PVA/borax, films were made using agarose and poly(methyl methacrylate) (PMMA). Agarose, like PVA/borax, is a hydrogel and contains many alcohol groups that could get oxidized by the photo-activated TTz. **Figure 4 e-f** shows how the agarose film is photochromic, showing the $TTz^{\bullet+}$ state at 600 nm and the TTz^{0} state at 710 nm, although the intensities are not as high as PVA/Borax films. The photofluorochromism however was nearly immediate, turning off fluorescence 95% within 5 s. The PMMA film that was cast out of dichloromethane, shown in **figure 3.4 g-h**, does not exhibit photochromism or photofluorochromism. The absorbance does not show any $TTz^{\bullet+}$ or TTz^{0} at the 610 nm or 710 nm regions, respectively. Instead, the TTz degrades with prolonged illumination, which is indicated by the loss of 372 nm absorbance and emission intensity.

When the PVA/Borax or agarose TTz films are exposed to light, they show photomechanochromism as they curl while they change from yellow TTz^{2+} to blue TTz^{0}. As films are illuminated, they curl towards the light, regardless of how they were originally coated. Films with increased TTz content curl faster, more drastically, and are more sensitive to light. As expected, the photomechanochromism is thickness dependent, where thinner films (approx. 20 – 30 μm) curled faster than thicker films (53 μm). The photomechanochromism is reversible, because the film uncurls and goes flat when light is taken away. This photomechanochromism is dependent upon TTz and illumination

because films without TTz do not curl and curling does not occur with the 2 ºC heat increase from the blue light.

3.3.4 Oxygen Sensing

The PVA/Borax films return to the yellow TTz^{2+} state from the blue TTz^{0} via interaction with oxygen, giving the films the ability to sense oxygen and give a visual indication. **Figure 3.5 a** shows initial high absorbance of 710 nm light after 1 min of illumination and how the film's absorbance changes depending on its environment. When in an open container, the film returns to yellow within 12 h, meanwhile if the film is put in a low (sub 100 ppm) oxygen sealed cuvette, it takes over 72 h to return to yellow. If the cuvette is purged with nitrogen gas to ensure minimal oxygen, the film stays consistently blue, which suggests that testing in the sealed cuvette, oxygen was slowly leaking in. Pictures of the film in the cuvette indicate that the film nearest to the cap was yellow while the bottom was still blue, suggesting the TTz film also indicates the direction of oxygen leakage. To verify the sensitivity, a similar experiment was conducted, monitoring the absorbance change from TTz^{0} to TTz^{2+} while in a ~100 ppm O_2 nitrogen atmosphere glovebox (**figure 3.5 b**). The absorbance did not decrease to show the return to TTz^{2+}, instead the overall absorbance at 630 nm increased over the 14 days. Although the measurement was shielded from light, small amounts of ambient light may have further reduced the TTz film. To visually monitor longer term color change, two films were kept in the glovebox atmosphere for 6 weeks and show little visible color change since being activated (**figure 3.5 c & d**).

In the food packaging industry, a vast number of products are sealed under nitrogen. To mimic this, a film was placed in a nitrogen flushed, zipper-closed food storage bag to show long term oxygen leakage (**figure 3.5 e**). Not only did it indicate the presence of oxygen after 2 weeks, but also showed what direction the leak was coming from, in this case the zipper corner of the bag. These results show the TTz films are sensitive to oxygen exposure and yield clear, high contrast visual indication which can be used for smart packaging and other oxygen susceptible applications.

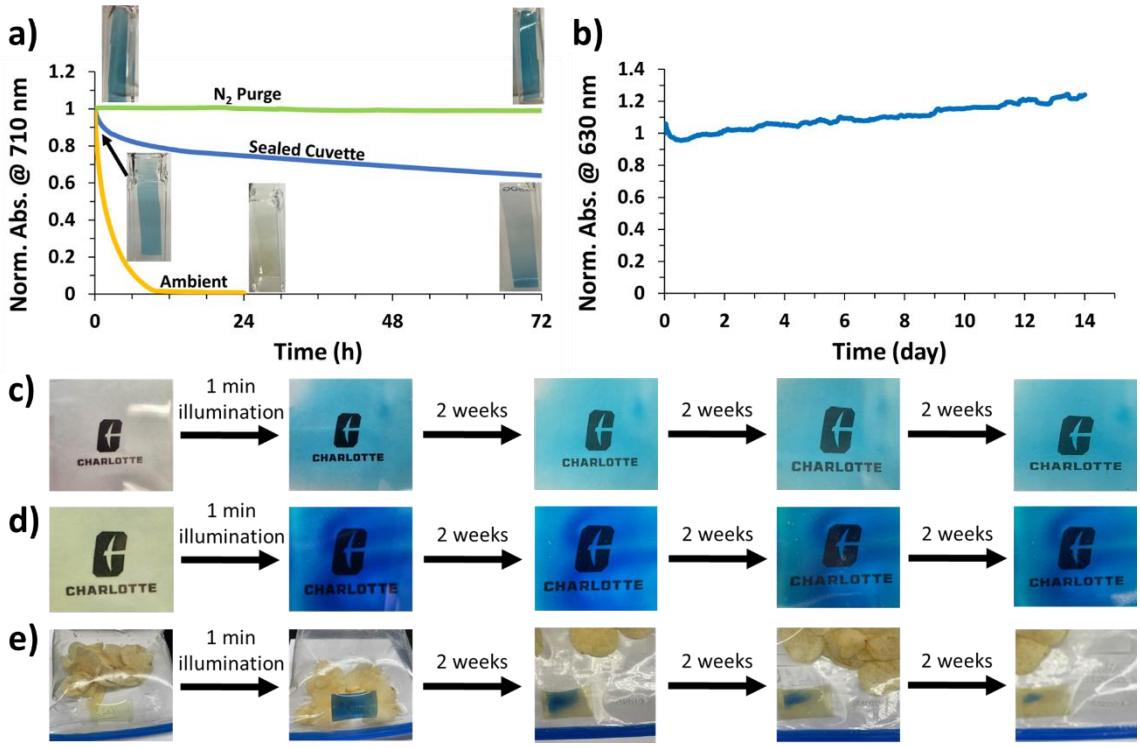

Figure 3.5: a) Change in 710 nm absorbance over time at low ppm O_2 levels and ambient conditions showing oxygen sensitivity, with corresponding pictures inset, **b)** film absorbance change at 630 nm over 14 d in the glovebox ~100 ppm O_2, **c)** pictures of 0.4% TTz film in glovebox atmosphere, **d)** pictures of 5% TTz film in glovebox atmosphere, **e)** oxygen sensing TTz film in nitrogen flushed zipper closed bag.

3.4 Conclusion

Water soluble dipyridinium thiazolothiazole compounds incorporated into inexpensive PVA/borax films and exhibit fast and high contrast photochromism, photofluorochromism, and oxygen sensing. When exposed to light, the films change color from yellow TTz^{2+} to purple $TTz^{\bullet+}$, then blue TTz^{0}. The contrast and speed of the photochromism is dependent upon the polymer matrix and how easily it can be oxidized and the concentration of photoactive TTz. In addition to visible light absorbance, the films also absorb near infrared. The blue film returns to yellow via oxidation of the TTz when exposed to O_2, making the films light activated oxygen sensors that can also sense leak direction for smart packaging. These films show potential to be used in self-tinting smart windows, eyeglasses, displays, erasable memory devices, fiber optic communication, and oxygen sensing.

3.5 Appendix II: Supplementary Information

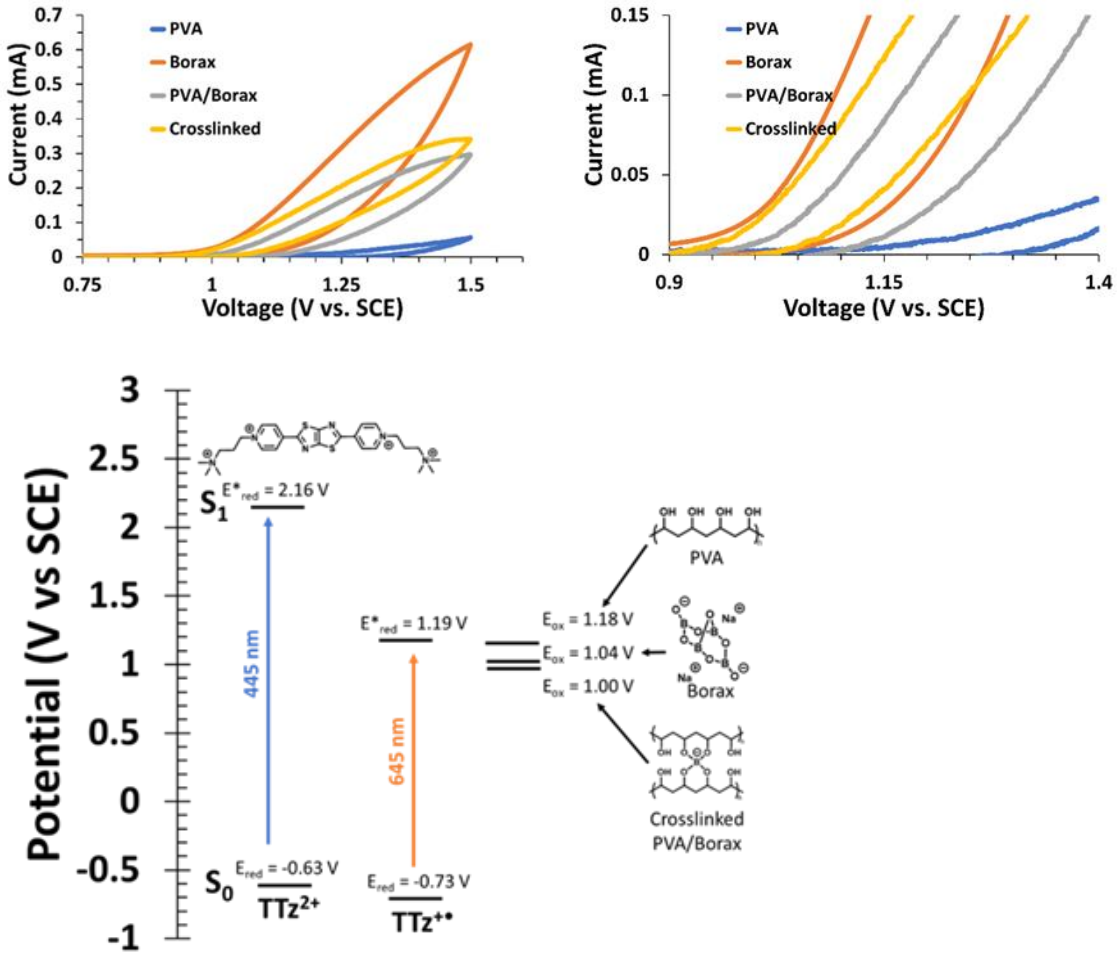

Supplementary figure 1: Cyclic voltammetry and corresponding band gap diagram of PVA, borax, PVA/borax mixture, and gelled crosslinked PVA/borax.

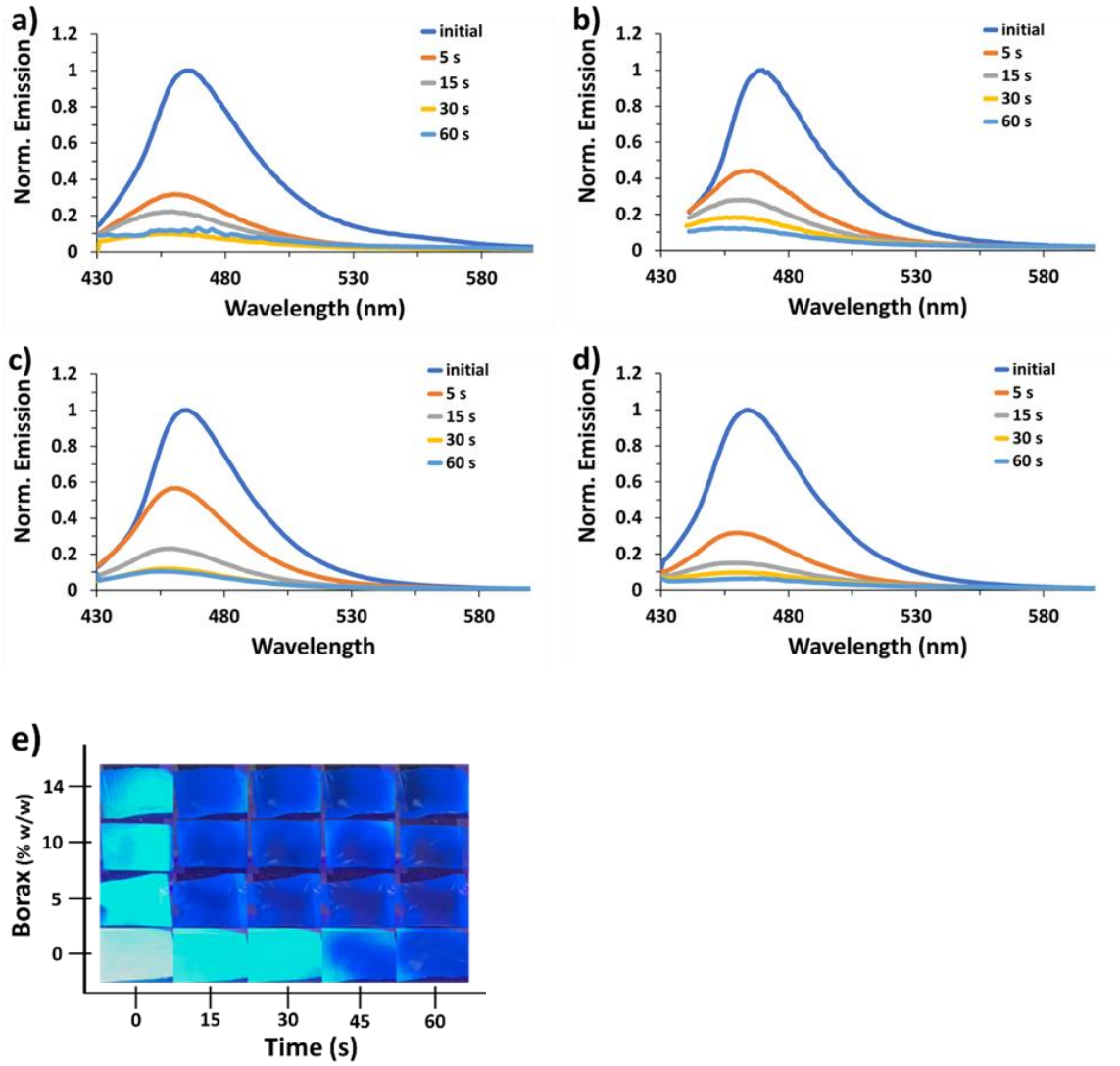

Supplementary figure 2: Photofluorochromism of PVA/Borax films with different borax concentrations (excitation/emission), **a)** 0% borax (418 nm/465 nm), **b)** 5% borax (425 nm/470 nm), **c)** 10% borax (415 nm/465 nm), **d)** 14% borax (420 nm/464 nm), **e)** visual representation of photofluorochromism.

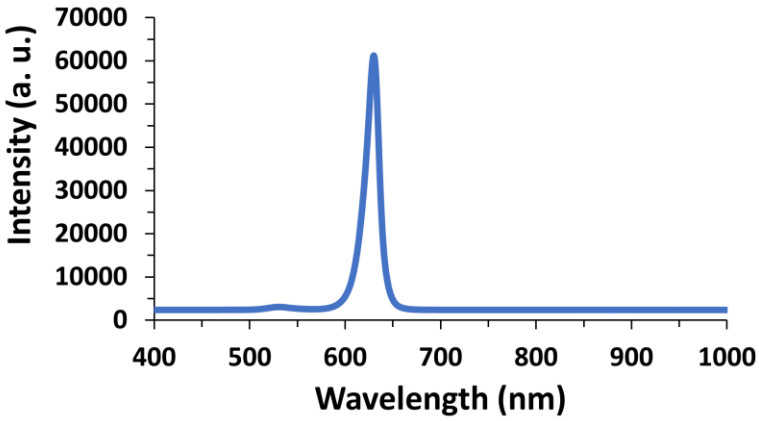

Supplementary figure 3: Irradiance spectrum of the red light bulb for glovebox atmosphere measurements.

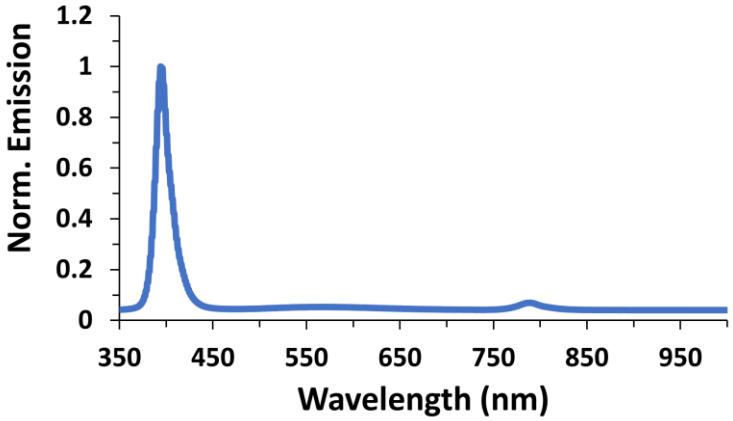

Supplementary figure 4: Irradiance spectrum of the uvBeast handheld flashlight used for photochromic, photofluorochromic, and photomechanochromic measurements.

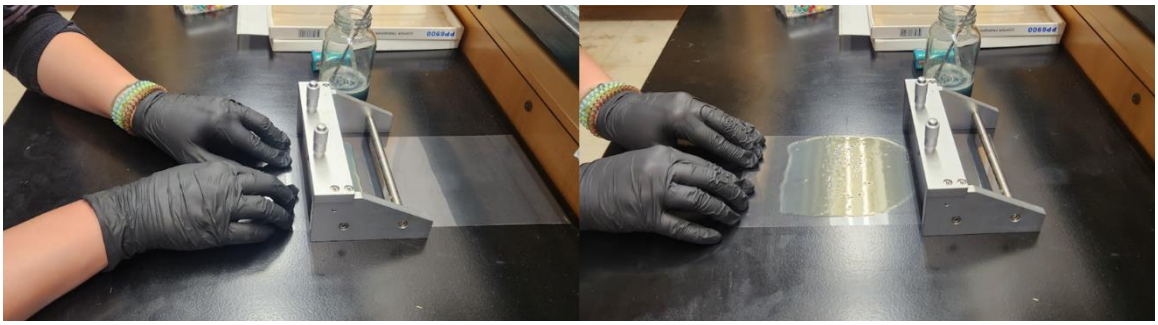

Supplementary figure 5: Pictures of coater and coating the gel onto plastic backing.

Chapter 4: Applications of Combined Photoactive and Electroactive TTz Materials

4.1 Introduction

With the increasing need for renewable energy and efficiency, there needs to be effective energy storage. This is particularly important for solar or wind energy production, where they are weather dependent and have inconsistent output.[40-41, 48] Lithium ion batteries are difficult to scale up for grid use because of expense and limited earth abundance.[48] Redox flow batteries (RFBs) store charge in the electrolyte solution tanks, rather than the electrodes like traditional batteries.[48] Power can be tuned based upon size of the electrodes and number of cells in the stack, and storage capacity is dictated by concentration and volume of the electrolyte, which also makes modular design available.[48] RFBs consist of two storage tanks that separately contain the two redox couples with electrolyte which are connected to an electrode chamber, consisting of the anode and cathode, with flowing solution and a semi-permeable membrane for supporting electrolyte to transfer between solutions (**figure 4.1**).[48-49] When charging, the catholyte oxidizes, while the anolyte reduces, causing a change in charges and moving electrolyte ions. When discharged, the opposite occurs, causing ions to move and create electrical current.

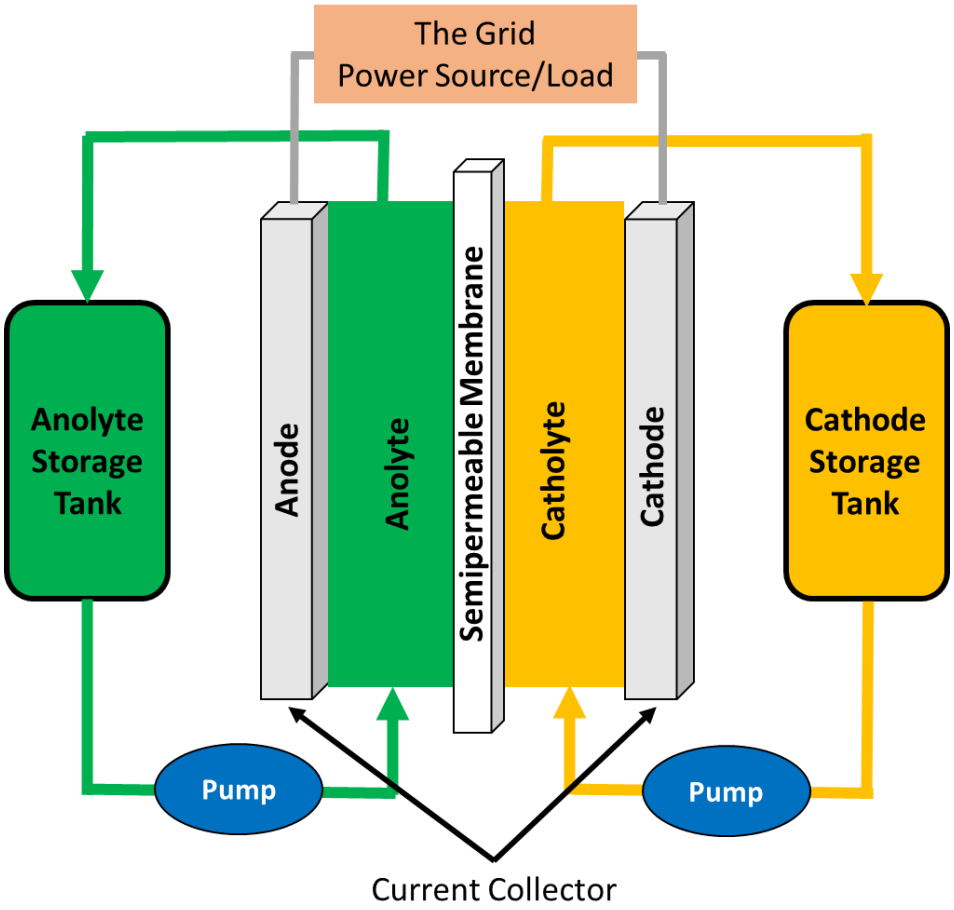

Figure 4.1: Schematic of redox flow batteries.

Vanadium RFBs take advantage of vanadium's four oxidation states, using VO_2^+ to VO^{2+} as the catholyte and V^{2+} to V^{3+} for the anolyte to afford a cell voltage of 1.26 V when discharging.[48] Vanadium RFBs have been implemented at large scale, up to 6 MWh at wind farms, however, sulfuric acid is used as an electrolyte.[48] At the necessary high concentrations, the vanadium and sulfuric acid solution is toxic and corrosive. Traditional RFBs, like those employing vanadium or Zn – Br_2, that use transition metals are highly reported, but have difficulty with large scale implementation due to low energy density, low materials abundance, mining practices, high cost, and corrosive electrolytes.[50-51]

Aqueous organic redox flow batteries (AORFBSs) use water soluble electroactive organic molecules and electrolytes, which is more economically and environmentally friendly, while obtaining high energy density.[50] A very common organic compound used as the anolyte, which reduces during charging, is methyl viologen.[40-41] Methyl viologen has two reductions at -0.45 V and -0.76 V vs NHE, however, after the second reduction, it becomes insoluble and irreversible.[34] By adding an extended conjugation bridge, like thiazolothiazole, the reductions are lower and closer, (-0.38 V and -0.50 V vs NHE) which helps with more consistent battery voltages and stability.[34] Dipyridinium thiazolothiazole is often paired with derivatives of TEMPO for AORFBs and affords reversible and efficient charging/discharging, with a battery voltage above 1.1 V.[34, 77]

Some groups have targeted bipolar molecules that achieve both the reduction and oxidation, to eliminate possible cross-contamination, commonly using TEMPO or viologen derivatives.[50, 78-80] For example, 1-[3-(trimethylammonio)propyl]-4-(4-pyridyl)pyridinium diiodide has been reported as trifunctional in an AORFB, as the pyridinium is the anolyte, the iodide is the catholyte, and since all are charged, they're also the supporting electrolyte.[50]

Rather than having a solar cell charge the RFB, some progress has been made to combine the two and create photo-rechargeable or photo-assisted rechargeable RFBs, occasionally called solar redox flow batteries (SRFBs). Originally called a photoelectrochemical cell, the first SRFB was reported in 1976 using polycrystalline chalcogenide electrodes to convert the solar energy into chemical energy storage.[81] Since then, most SRFBs rely on photoelectrodes like n^+ pp^+ -Si photoanode,[82] CdS photoanode,[83] TiO_2,[84] and $BiVO_4$ on TiO_2/SnO_2.[85] These photoelectrode SRFBs can

achieve solar-to-chemical conversion efficiencies of 9.4% using silicon photoelectrodes[86] or 15.4% using GaAs photoelectrodes.[87] Instead of using photoelectrodes, the anolyte/catholyte solutions themselves may be able to absorb light and become charged, which could be called a photoanolyte/catholyte-driven, solar redox energy storage device. By implementing photocatholytes and/or photoanolytes, solar-to-chemical conversion efficiencies similar to photoelectrodes can be expected while eliminating the need for additional photoelectrode materials, which lowers material and charging costs of the overall device. However, the use of photoactive catholytes or analytes to charge such a battery has not yet been reported.

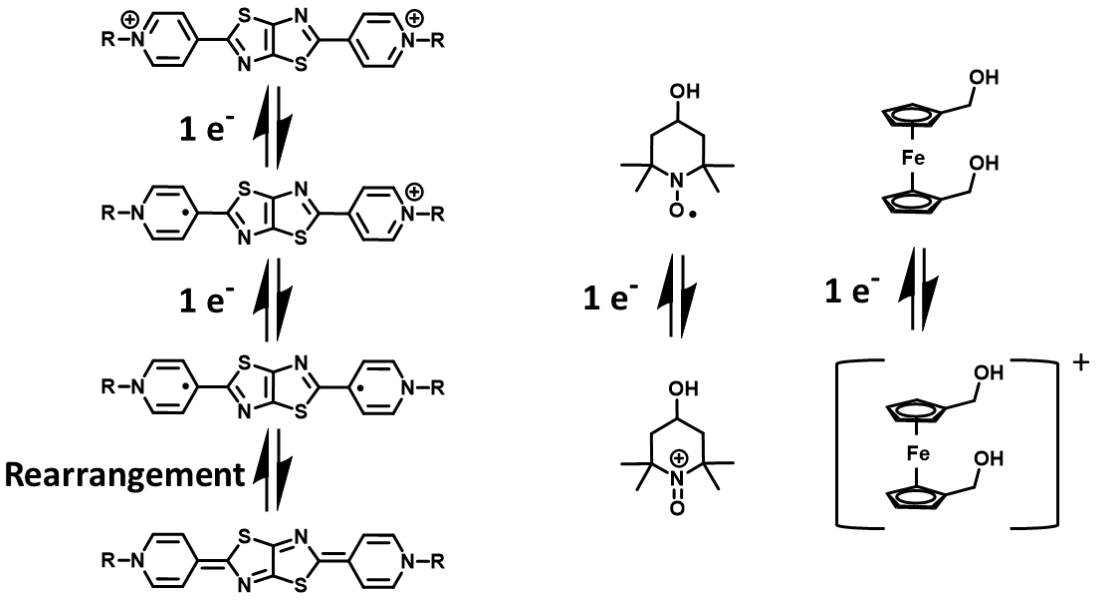

Figure 4.2: The two single electron reductions of TTz and the single electron oxidation of OH-TEMPO and 1,1'-ferrocenedimethanol.

Herein, photo-charging hydrogel, H-cell, and thin film devices are studied using photoactive chromogenic dipyridinium thiazolothiazole and well known catholytes. The two single electron reductions of TTz and the catholytes used are shown in **figure 4.2**.

Although dipyridinium thiazolothiazole molecules have been reported before for use in AORFBs, the effects of light illumination have not been.[34] At the present time, the term "photoanalyte" has not been reported, making it difficult to create a standard method of measuring photoanalyte properties as voltage, current, and light effects need to be fully probed.

4.2 Experimental

Materials

Dithiooxamide, 4-pyridinecarboxaldehyde, (3-bromopropyl)-trimethylammonium bromide, poly(vinyl alcohol) (PVA) Mw 11000 – 31000, sodium tetraborate decahydrate (Borax), ammonium hexafluorophosphate, 4-hydroxy-2,2,6,6-tetramethylpiperidine 1-oxyl (OH-TEMPO), tetrabutylammonium hexafluorophosphate ($TBAPF_6$), ferrocene, 1,1'-ferrocenedimethanol, acetonitrile, and dimethyl formamide (DMF) were all purchased from Sigma-Aldrich, Acros Organics, and Baker Scientific. 1H-NMR measurements were taken using a JEOL 500 MHz NMR and a JEOL 300 MHz NMR. Mass spectrometry measurements were obtained with a Perceptive Biosystems Voyager MALDI-TOF mass spectrometer.

Synthesis

Please refer to Ch. 2 synthesis page 12.

Device Fabrication

A PVA/borax-based CG gel was obtained following a similar procedure as previously reported.[6, 16] The TTz PVA/borax gel was prepared using 5 mM [$((NPr)_2TTz^{4+})4Br^-$] added to a 0.6 mL aqueous PVA solution (4% by mass) and 10 mM concentrations of 1,1'-ferrocenedimethanol ($Fc(CH_2OH)_2$). After the solution was homogeneous via sonication or vortex, 0.1 mL of borax aqueous solution (4% by mass) was added and mixed vigorously with a spatula until the gel formed. The prepared CG gel was coated onto one FTO glass and another FTO-coated glass was quickly placed on top of the gel, giving FTO/CG gel/FTO device configuration. Similarly, devices incorporating the anion exchange membrane were made by putting the [$((NPr)_2TTz^{4+})4Br^-$] gel on one piece of FTO and the $Fc(CH_2OH)_2$ gel on another piece of FTO, then adding the membrane on top of the TTz gel and quickly flipping the $Fc(CH_2OH)_2$ gel FTO on top. The FTO glass was cleaned via sonication with water, acetone, and isopropyl alcohol in 15-min iterations and dried with N_2. Double sided scotch tape was used as a spacer (60 μm) with the FTO glass giving the active CG gel an area of 3 to 4 cm^2.

Cyclic Voltammetry

The CV collected in figure 4.4 a uses 0.1 M $TBAPF_6$ as the electrolyte in acetonitrile with platinum flag and glassy carbon electrodes with a silver wire reference. The Scan rate was 100 mV/s. The aqueous CV of [$((NPr)_2TTz^{4+})4Br^-$] and 1,1'-ferrocenedimethanol was collected in 0.5 M Na_2SO_4 using a Pt flag and glassy carbon electrodes and a SCE reference. It was scanned at a rate of 20 mV/s.

H-Cell Testing

The H-cell using organic solvent in figure 4.4 b utilizes 5 mM [$((NPr)_2TTz^{4+})4PF_6^-$] solution and a 10 mM ferrocene solution, both with 1 M $TBAPF_6$ electrolyte in anhydrous air-free acetonitrile. The H-cell was assembled in the nitrogen atmosphere glovebox and contained carbon felt electrodes and a Celgard 2400 porous membrane. This setup has an 80% SOC theoretical capacity of 12.9 mAh. The H-cell was charged at 645 µA for 2 h and discharged at -430 µA for 3 h.

The AORFB shown in figure 4.5 was tested using a 10 mM [$((NPr)_2TTz^{4+})4Br^-$] solution and a 20 mM OH-TEMPO solution, both with 2 M NaCl electrolyte. The 80% SOC theoretical capacity of this system is 2.14 mAh. The setup was assembled using carbon felt electrodes and Selemion AMV anion exchange membrane (AEM). After a 1 h Ar purge, cyclic charge discharge was performed on the H-cell, by charging at 6 mA for 2 h or until 1.8 V and discharging at 1 mA for 2 h or until 0.2 V.

Film Device Assembly

FTO glass was cleaned via sonication with water, acetone, and isopropyl alcohol in 15-min iterations and dried with N_2. The 3.4% by weight [$((NPr)_2TTz^{4+})4Br^-$] film and 6.7% by weight OH-TEMPO film were cut to approximately 2.8 cm x 2.8 cm and laid onto the FTO glass, ensuring conductive side is in contact with the films. The AEM was laid on top of the TTz film and the OH-TEMPO film and FTO glass was laid on top. Small binder clips are attached to keep this FTO/TTz Film/AEM/OH-TEMPO Film/FTO structure together. Films were made by mixing the following: 3.4% NPrTTz: 60 mL 4%

PVA solution, 101.7 mg [$((NPr)_2TTz^{4+})4Br^-$], 10 mL 4% Borax solution, 10 mL DI water, 60 µm coater gap; 6.7% OH-TEMPO: 60 mL 4% PVA solution, 204.4 mg OH-TEMPO, 10 mL 4% Borax solution, 10 mL DI water, 60 µm coater gap.

Film Device Testing

The chronopotentiometry of the film devices testing light effects was performed via open circuit (0 A) conditions and exposure to AM 1.5 (1 sun) light at a 6-inch distance. Figure 4.9 a comparing the charge and discharge of the device in the dark vs in light uses 3 mA for 20 s and -0.2 mA for 100 s of applied current for 10 cycles. Similarly, the device in figure 4.9 b had 30 µA for 40 s and -2 µA for 140 s for 10 cycles of charge/discharge.

4.3 Results and Discussion

4.3.1 Hydrogel devices

Although it's clear that there is a connection between the electroactive and photoactive properties of the TTz hydrogel devices based upon the electrochromic, photochromic, and voltage-assisted photochromism, it was not expected to show photovoltaic characteristics.[16] One of the first indications that the TTz hydrogel devices are photovoltaic was simply noticing a small voltage change when exposed to high power light. The original chromogenic device, (**figure 4.3 a**) was tested with chronoamperometry and chronopotentiometry under open circuit (0 V) and short circuit (0 A) conditions, respectively, to measure the change in current or voltage when the device was exposed to light (**figure 4.3 b & c**). Both tests indicate an immediate response

showing a photocurrent or photovoltage, however these responses are small (2 µA and 0.03 V) and show odd charging characteristics. This is likely due to the lack of directionality in the device because electrons are free to move in any direction.

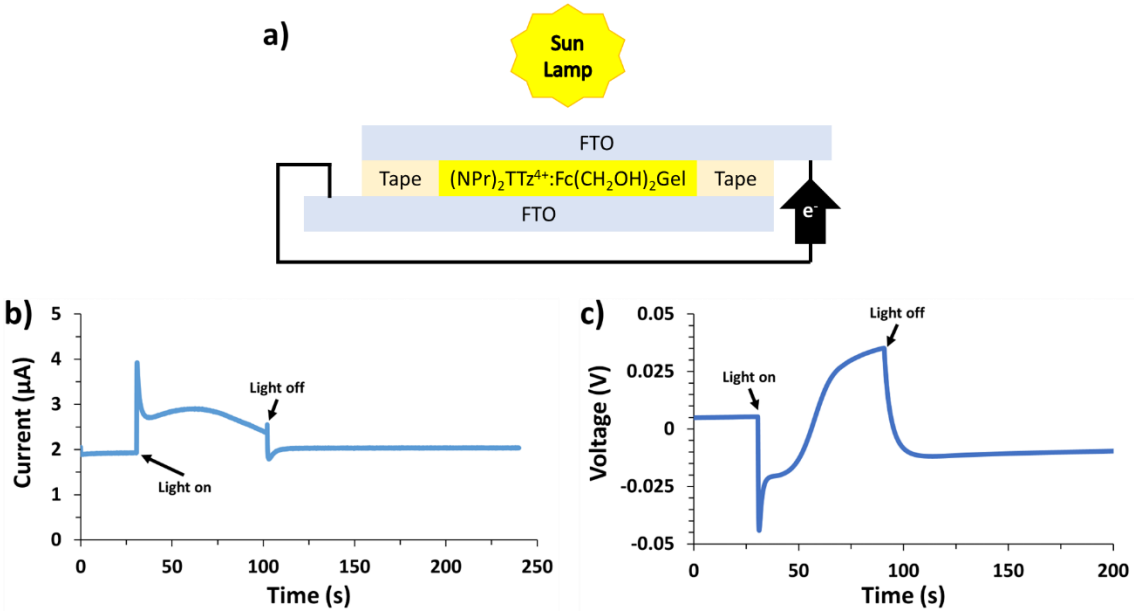

Figure 4.3: a) Chromogenic device structure with 1:2 [$((NPr)_2TTz^{4+})4Br^-$]: $Fc(CH_2OH)_2$ PVA/borax hydrogel for preliminary photo-charging tests, **b)** chronoamperometry under open circuit conditions, and **c)** chronopotentiometry under short circuit conditions.

To make these voltage changes more evident and promote electron movement directionality, an anion exchange membrane was included between TTz and 1,1'-ferrocenedimethanol ($Fc(CH_2OH)_2$) hydrogels while sandwiched between FTO glass electrodes (**figure 4.4 a**). The chronopotentiometry and chronoamperometry (**figure 4.4 b & c**) show the immediate effect of light exposure. When testing the chronopotentiometry, 0 A is maintained when the device is exposed to light and shows 0.4 V charging change, then discharge when light is taken away. Similarly, with chronoamperometry, 0 V is maintained as the current is monitored, which shows a 6.3 µA difference between dark

and light environments. Although the change in current is small, current is area and concentration dependent, and the current can be increased if a larger or more concentrated device is made. To verify these results, a silver wire reference electrode was included in the device by laying the wire in the $Fc(CH_2OH)_2$ hydrogel. With the silver reference, a 20 µA change in photocurrent and 0.2 V change in voltage is shown. Including the $Fc(CH_2OH)_2$ yields higher device voltage than devices without $Fc(CH_2OH)_2$ (**supplementary figure 4.1**). To ensure these materials can be charged and discharged, H-cell tests need to be analyzed.

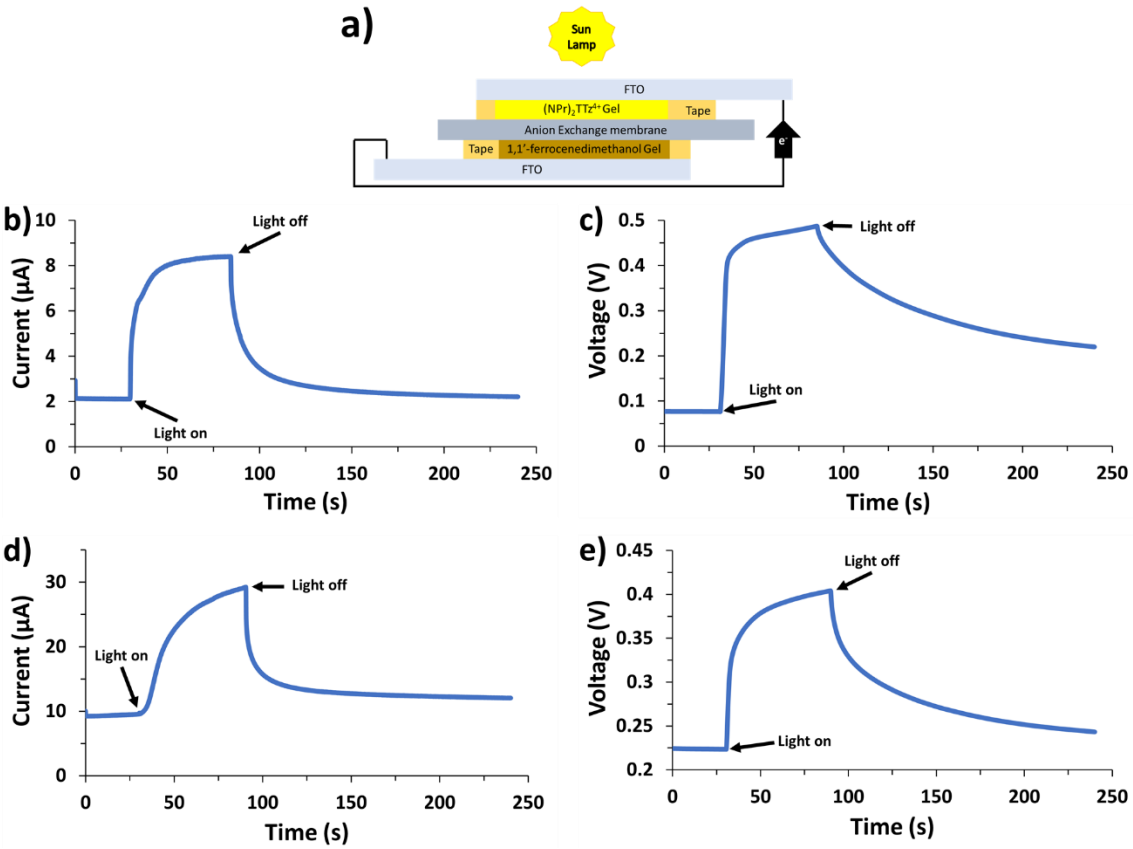

Figure 4.4: a) Photo-charging hydrogel device setup, **b)** change in current in response to light exposure (0 V applied), **c)** change in voltage in response to light exposure (0 A

applied), **d)** chronoamperometry with Ag reference (0 V), **e)** chronopotentiometry with Ag reference (0 A).

4.3.2 H-Cells

H-cells are a common method of testing materials for RFBs because they mimic a flow battery, but only require approximately 6 mL of solution. Like large scale RFBs, H-cells are solution phase with supporting electrolytes with a catholyte and cathode on one side and anolyte with an anode on the other side, separated by a membrane. Instead of a pump to keep the solutions moving, stir bars are employed. By measuring the volumes and concentrations of the redox active solutions, the theoretical capacity can be calculated by using the equation in **figure 4.5**. An 80% state of charge (SOC) is applied to this number as batteries typically only use 80% of the total catholyte/anolyte. The resulting capacity is necessary for effective charging and discharging currents and times.

$$C_p = \frac{V(L) * Concentration\left(\frac{mol}{L}\right) * \#e^- * Faraday\ Constant\ \left(\frac{A\,s}{mol}\right)}{3600\left(\frac{s}{h}\right)}$$

Figure 4.5: Capacity equation for H-cell systems, resulting in theoretical capacity in Ah.

When translating the photo-charging devices into H-cells, $[((NPr)_2TTz^{4+})4PF_6^-]$ was used as the anolyte with ferrocene as the catholyte. Ferrocene is desirable as a catholyte because of its highly investigated oxidation potentials and possible use as a pseudo-reference. To satisfy the solubility of ferrocene and reduce oxygen exposure, the H-cell testing was performed in acetonitrile in the nitrogen atmosphere glovebox. Additionally, the $[((NPr)_2TTz^{4+})4Br^-]$ salt was anion exchanged to the PF_6 salt for solubility in organic solvents. Organic solvents also require a different membrane, so

instead of an AEM, a porous membrane was employed. The porous membrane has 43 nm diameter pores that lets small ions through, but not the larger ferrocene or $[((NPr)_2TTz^{4+})4PF_6^-]$ molecules. Cyclic voltammetry of $[((NPr)_2TTz^{4+})4PF_6^-]$ and ferrocene show a battery voltage of 0.81 V and the redox process is reversible (**figure 4.6 a**). Repeating chronopotentiometry of the H-cell shows the battery can charge and discharge with applied current up to 2.7 V and down to -2.2 V.

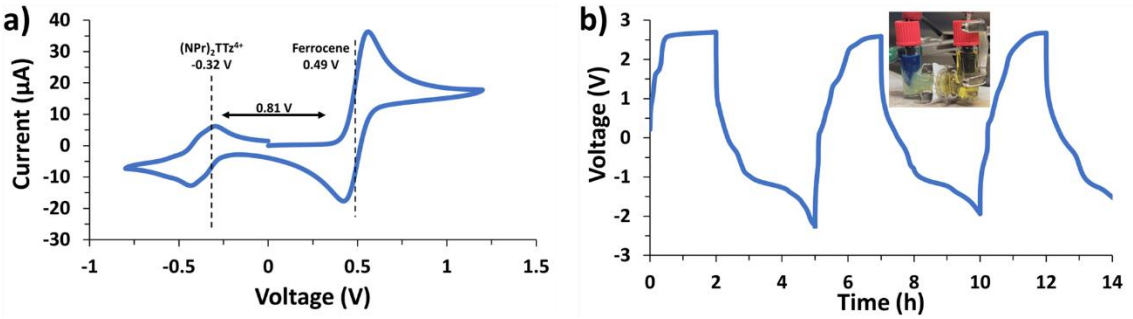

Figure 4.6: a) Cyclic voltammetry and **b)** repeating chronopotentiometry in H-cell of $[((NPr)_2TTz^{4+})4PF_6^-]$ and ferrocene in acetonitrile, picture of H-cell inset.

An aqueous organic H-cell was also tested to verify correct settings as it closely resembles work previously done by Luo et al.[34] In a flow cell, they reported the use of $[((NPr)_2TTz^{4+})4Cl^-]$ with trimethylammonium TEMPO which had a battery voltage of 1.44 V and showed reversible and efficient charge discharge capacity. The H-cell test in **figure 4.7** shows the charge, discharge, and capacity of the $[((NPr)_2TTz^{4+})4Br^-]$ and OH-TEMPO battery. OH-TEMPO was used instead of the previously used $Fc(CH_2OH)_2$, because the $Fc(CH_2OH)_2$ is only sparingly soluble in water. After 3 cycles, the battery has consistent charge and discharge peaks that have a difference of 1.5 V, which is the calculated battery voltage. The capacity graph shows the capacity efficiency is low at first because the charge capacity is high and discharge capacity is near zero. However, as the

charges and discharges become more consistent, the charge and discharge capacities are much closer together and more efficient. This system shows the battery can be charged and discharged electrically, but needs improvement, which could need better stirring, different electrodes, or deleterious exposure to oxygen.

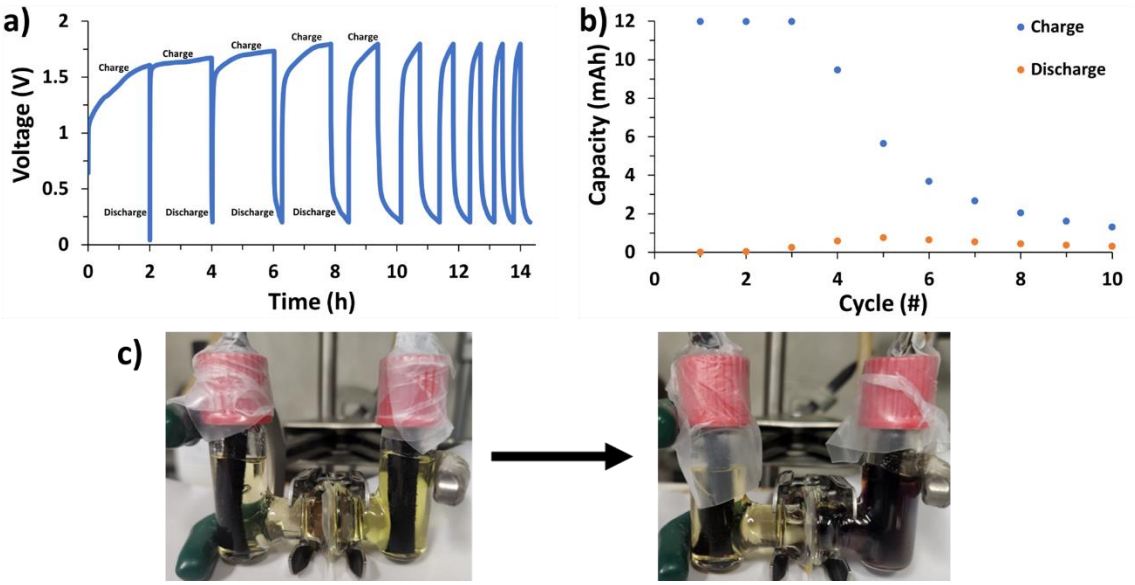

Figure 4.7: a) Cyclic charge discharge graph and **b)** charge and discharge capacities of the **c)** $[((NPr)_2TTz^{4+})4Br^-]$ and OH-TEMPO aqueous H-cell.

4.3.3 Film devices

Film devices consist of a 3.4 % by weight $[((NPr)_2TTz^{4+})4Br^-]$ PVA/Borax film, anion exchange membrane (AEM), and 6.7% by weight OH-TEMPO PVA/Borax film sandwiched between two pieces of FTO glass shown in **figure 4.8 a**. This system is much like the hydrogel devices, but in solid state rather than hydrated gel and using OH-TEMPO rather than $Fc(CH_2OH)_2$ because $Fc(CH_2OH)_2$ does not fully dissolve in water and yields poor films. Without the water, the film devices are still able to show changes in voltage when exposed to light (**figure 4.8 b-d**). The increase in voltage can be up to

0.35 V in difference and the device slowly discharges when the light is turned off. **Figure 4.8 d** shows this can be done multiple times with near identical response and the charging plateaus upon long illumination time.

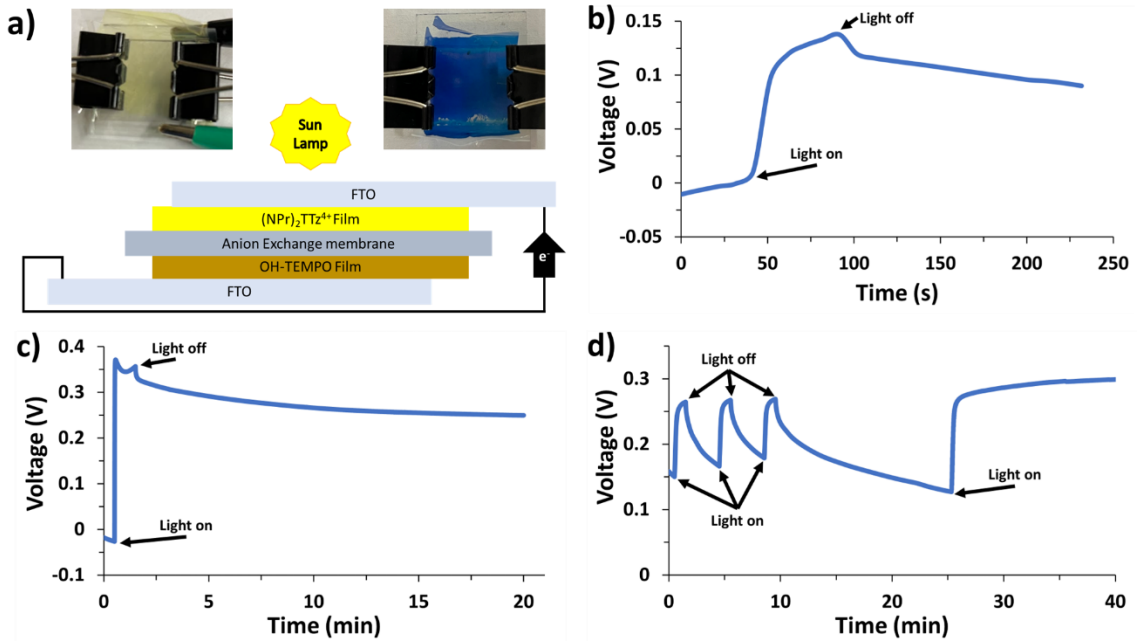

Figure 4.8: a) Film device assembly using PVA/borax films with [$((NPr)_2TTz^{4+})4Br^-$] and OH-TEMPO, with pictures before/after charging, **b)** open circuit chronopotentiometry of the film device as its exposed to 60 s of light, **c)** open circuit chronopotentiometry of the film device as its exposed to 60 s of light, **d)** open circuit chronopotentiometry of the film device as its exposed to light.

The film devices can also be charged and discharged with electrical current, however light exposure can make a large difference in the device voltage and storage (figure 4.9). In figure 4.9 a, the devices charge and discharge well in the dark, but the discharge is short as it goes from 4 V to -2.5 V almost immediately. When exposed to light, the voltage stays at -1 V for a longer amount of time before dropping to -2.5 V, suggesting a boost in charge storage with light exposure. More impressively, in figure 4.9

b, the dark curve shows charging to 0.9 V and discharging to -1.3 V, while the light curve shows charging to 1.1 V and discharges to 0.07 V. This suggests that light boosts the battery voltage by 0.2 V and keeps electrons moving in one direction for an always positive voltage.

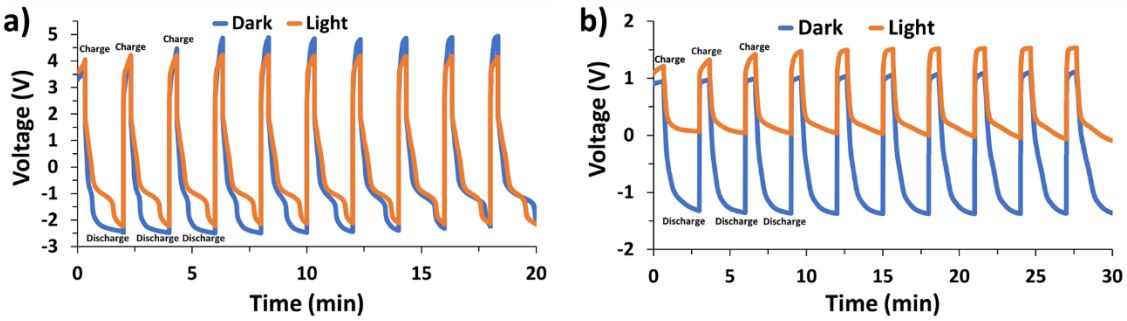

Figure 4.9: a) Repeating chronopotentiometry of the film device in dark and light conditions (3 mA 20 s charge, -0.2 mA 100 s discharge), **b)** repeating chronopotentiometry of the film device in dark and light conditions (30 µA 40 s charge, -2 µA 140 s discharge).

4.4 Conclusion

A range of devices and setups were developed that show charging and discharging battery properties as well as strong photo-charging. Simple FTO/hydrogel/FTO devices first showed current and voltage changes with light exposure, which increased with the implementation of an anion exchange membrane to improve directionality of electron movement. These devices showed 0.4 V and 6.3 µA photovoltage and photocurrent, confirming the possibility of creating a photo-charging battery. H-cells were used to further demonstrate the use of $[((NPr)_2TTz^{4+})4Br^-]$ as an anolyte, however, H-cells did not have enough consistency to full probe the effects of light. Lastly, film devices were

made to show battery properties in solid state devices. Not only do they create a photovoltage, but they can also be traditionally electrically charged/discharged with light giving boosted 0.2 V voltage and capacity to the battery. These devices using TTz to charge and maintain capacity with light exposure may be one of the first examples of photoanalytes for battery devices or redox flow batteries.

4.5 Appendix: Supplementary information

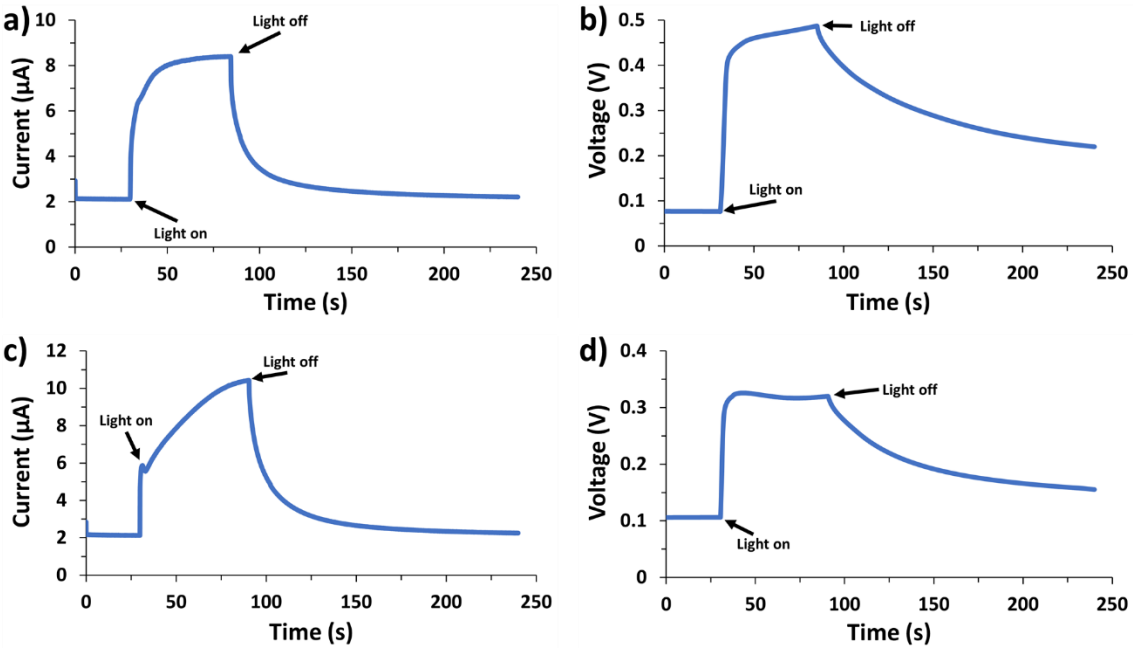

Supplementary Fig 1: Comparison of gel devices with and without 1,1'-ferrocenedimethanol: **a)** chronoamperometry and **b)** chronopotentiometry response to light exposure of $[((NPr)_2TTz^{4+})4Br^-]$ gel/AEM/Ferrocenedimethanol gel devices compared to **c)** chronoamperometry and **d)** chronopotentiometry response to light exposure of $[((NPr)_2TTz^{4+})4Br^-]$ gel/AEM/PVA/Borax gel without 1,1'-ferrocenedimethanol.

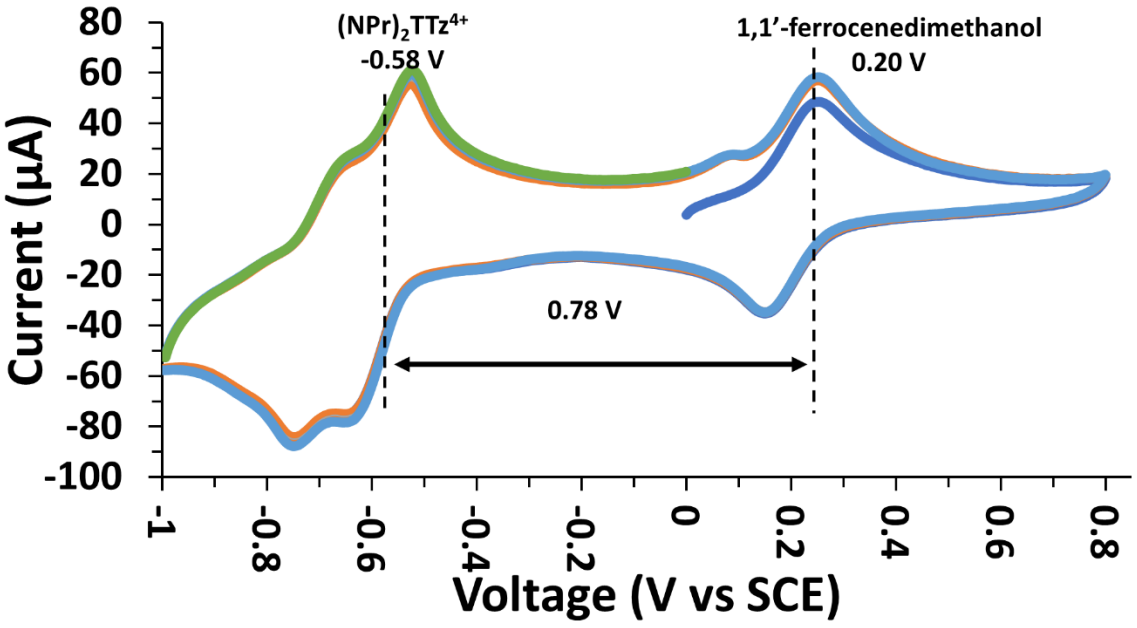

Supplementary Fig 2: Cyclic voltammetry of [((NPr)$_2$TTz^{4+})4Br$^-$] and Fc(CH$_2$OH)$_2$ in 0.5 M Na_2SO_4 aqueous solution.

Chapter 5: Conclusion

This work has fully characterized the electrochromism, electrofluorochromism, and photochromism of four dipyridinium TTz derivatives in PVA/borax hydrogels, photochromism of [$((NPr)_2TTz^{4+})4Br^-$] solid state films and explored the new topic of using a photoanolyte for photo-charging batteries. Dipyridinium TTz molecules specifically have gained interest because the rigid, planar, electron deficient core improves electrochemical reversibility and lowers the reduction potential when compared to methyl viologen. Methyl viologen has been utilized for many applications but suffers from instability and irreversible reductions leading to degradation. The inclusion of the TTz bridge improves many properties of viologen, including sensing, electrochromism, and photochromism, improving efficiency for numerous applications previously dominated by 4,4'-bipyridinium moieties.

The multifunctional chromogenic hydrogel devices show high contrast electrochromism with activation voltages less than 2 V. Several of the devices were able to achieve 75% transmittance contrast with a driving voltage or a contrast of 50%, with illumination. The cyclability and reversibility of the TTz CGDs is excellent, losing only 6% transmittance contrast after 250 on/off cycles or 1% transmittance loss in contrast after an hour of applied voltage. In addition, it is notable that these devices operate under ambient, aqueous conditions and still achieve reversible color change that barely fades. In the case of electrofluorochromism, > 90% of the fluorescence can be turned off with the application of 2.5 V. After reporting this work on the multifunctional chromogenic properties of dipyridinium TTz molecules, TTz has increased momentum and has gained a reputation for exceptionally high contrast electrochromism and electrofluorochromism.

By adjusting concentrations and water content of the PVA/borax TTz hydrogels used in chapter 2, the hydrogel can be coated and dried into films that retain the typical yellow color and more importantly the multifunctional properties. The films are highly fluorescent and show photochromism and photofluorochromism with 15 s of light illumination. The yellow TTz^{2+} to blue TTz^{0} contrast and color change speed can be tuned by adjusting the concentration of $[((NPr)_2TTz^{4+})4Br^-]$ or borax in the films. The return to yellow from blue is caused by interaction with ambient oxygen. Depending on the environment, like ambient conditions, the film will turn back to yellow in 12 h, but in lower oxygen environments it will take days or weeks, while environments under nitrogen like a glovebox or continuous N_2 purge shows constant blue color. This can be used for smart packaging of food, pharmaceuticals, or electronics, and the photochromism can be used for displays, erasable memory devices, or smart windows to decrease solar heat gain. Because they are flexible and solid state, they can be applied to nearly any surface. Due to the flexibility of the films, they can be easily adhered to window surfaces, incorporated into packaging materials, or assembled as part of a device.

In chapter 2, voltage assisted photochromism is reported, showing a clear connection between the electroactive and photoactive properties of the TTz hydrogel devices, however this connection becomes more evident with the chronopotentiometry and chronoamperometry data collected. When illuminating the devices, a current or voltage jump is started and charges the device until the light is turned off and the device slowly charges. Because the TTz anolyte is photoactive and causes charging, it creates a new subject of photoanolytes. Chapter 4 proves the chemistry needed for photo-charging battery devices and RFBs exists and works, however the engineering needs improvement

before large scale implementation. Typical RFB setups will likely be incompatible because of the need for light to penetrate into the solution to activate the photoanolyte.

This work shows that small molecule dipyridinium TTz's have truly multifunctional chromogenic properties and yield high contrast electrochromism, electrofluorochromism, photochromism, and photofluorochromism. These abilities make the TTz able to be used in a variety of applications, like sensors, smart windows, batteries, and displays while also being able to be implemented in solution, hydrogels, or films.

References

1. Österholm, A. M.; Shen, D. E.; Kerszulis, J. A.; Bulloch, R. H.; Kuepfert, M.; Dyer, A. L.; Reynolds, J. R., Four Shades of Brown: Tuning of Electrochromic Polymer Blends Toward High-Contrast Eyewear. *ACS Applied Materials & Interfaces* **2015,** *7* (3), 1413-1421.
2. Wang, W.-H.; Chang, J.-C.; Wu, T.-Y., 4-(Furan-2-yl)phenyl-containing polydithienylpyrroles as promising electrodes for high contrast and coloration efficiency electrochromic devices. *Organic Electronics* **2019,** *74*, 23-32.
3. Corrente, G. A.; Beneduci, A., Overview on the Recent Progress on Electrofluorochromic Materials and Devices: A Critical Synopsis. *Adv. Opt. Mater.*, 19.
4. Beaujuge, P. M.; Ellinger, S.; Reynolds, J. R., The donor–acceptor approach allows a black-to-transmissive switching polymeric electrochrome. *Nat. Mater.* **2008,** *7* (10), 795-799.
5. Zhao, S.; Huang, W.; Guan, Z.; Jin, B.; Xiao, D., A novel bis(dihydroxypropyl) viologen-based all-in-one electrochromic device with high cycling stability and coloration efficiency. *Electrochimica Acta* **2019,** *298*, 533-540.
6. Alesanco, Y.; Palenzuela, J.; Vinuales, A.; Cabanero, G.; Grande, H. J.; Odriozola, I., Polyvinyl Alcohol-Borax Slime as Promising Polyelectrolyte for High-Performance, Easy-to-Make Electrochromic Devices. *ChemElectroChem* **2015,** *2* (2), 218-223.
7. Andersson, P.; Forchheimer, R.; Tehrani, P.; Berggren, M., Printable All-Organic Electrochromic Active-Matrix Displays. *Advanced Functional Materials* **2007,** *17* (16), 3074-3082.
8. Tang, Q.; He, L. H.; Yang, Y. H.; Long, J. F.; Fu, X. K.; Gong, C. B., Effects of substitution position on electrochemical, electrochromic, optical, and photoresponsive properties of azobenzenecarboxylic acid alkyl ester derivatives. *Organic Electronics* **2016,** *30*, 200-206.
9. Dmitrieva, E.; Rosenkranz, M.; Alesanco, Y.; Vinuales, A., The reduction mechanism of p-cyanophenylviologen in PVA-borax gel polyelectrolyte-based bicolor electrochromic devices. *Electrochimica Acta* **2018,** *292*, 81-87.
10. Dmitrieva, E.; Rosenkranz, M.; Alesanco, Y.; Vinuales, A., Spectroelectrochemical study of alkyl-aryl asymmetric viologens in poly(vinyl alcohol) (PVA) - borax electrolyte. *Electrochimica Acta* **2019,** *323*, 7.
11. Pan, M.; Ke, Y.; Ma, L.; Zhao, S.; Wu, N.; Xiao, D., Single-layer electrochromic device based on hydroxyalkyl viologens with large contrast and high coloration efficiency. *Electrochimica Acta* **2018,** *266*, 395-403.
12. Pande, G. K.; Kim, N.; Choi, J. H.; Balamurugan, G.; Moon, H. C.; Park, J. S., Effects of counter ions on electrochromic behaviors of asymmetrically substituted viologens. *Sol. Energy Mater. Sol. Cells* **2019,** *197*, 25-31.
13. Striepe, L.; Baumgartner, T., Viologens and Their Application as Functional Materials. *Chem.-Eur. J.* **2017,** *23* (67), 16924-+.
14. Xiao, S. X.; Zhang, Y. J.; Ma, L.; Zhao, S.; Wu, N.; Xiao, D. B., Easy-to-make sulfonatoalkyl viologen/sodium carboxymethylcellulose hydrogel-based electrochromic devices with high coloration efficiency, fast response and excellent cycling stability. *Dyes Pigment.* **2020,** *174*, 8.

15. Woodward, A. N.; Kolesar, J. M.; Hall, S. R.; Saleh, N.-A.; Jones, D. S.; Walter, M. G., Thiazolothiazole Fluorophores Exhibiting Strong Fluorescence and Viologen-Like Reversible Electrochromism. *Journal of the American Chemical Society* **2017,** *139* (25), 8467-8473.
16. Adams, T. J., Brotherton, A. R., Molai, J. A., Parmar, N., Palmer, J. R., Sandor, K. A., Walter, M.G., Obtaining Reversible, High Contrast Electrochromism, Electrofluorochromism, and Photochromism in an Aquesous Hydrogel Device Using Chromogenic Thiazolothiazoles. *Advanced Functional Materials* **2021**.
17. Soylemez, S.; Kaya, H. Z.; Udum, Y. A.; Toppare, L., A thiazolothiazole containing multichromic polymer for glucose detection. *Express Polym. Lett.* **2019,** *13* (10), 845-857.
18. Soylemez, S.; Kaya, H. Z.; Udum, Y. A.; Toppare, L., A multipurpose conjugated polymer: Electrochromic device and biosensor construction for glucose detection. *Organic Electronics* **2019,** *65*, 327-333.
19. Akpinar, H. Z.; Udum, Y. A.; Toppare, L., Multichromic and soluble conjugated polymers containing thiazolothiazole unit for electrochromic applications. *Eur. Polym. J.* **2015,** *63*, 255-261.
20. Shi, Y.; Chen, Q.; Zheng, J.; Xu, C., Electrochromism of substituted phthalate derivatives and outstanding performance of corresponding multicolor electrochromic devices. *Electrochimica Acta* **2020,** *341*, 136023.
21. Wu, J.-H.; Liou, G.-S., High-Performance Electrofluorochromic Devices Based on Electrochromism and Photoluminescence-Active Novel Poly(4-Cyanotriphenylamine). *Advanced Functional Materials* **2014,** *24* (41), 6422-6429.
22. Beneduci, A.; Cospito, S.; La Deda, M.; Veltri, L.; Chidichimo, G., Electrofluorochromism in π-conjugated ionic liquid crystals. *Nature Communications* **2014,** *5* (1).
23. Corrente, G. A.; Fabiano, E.; La Deda, M.; Manni, F.; Gigli, G.; Chidichimo, G.; Capodilupo, A. L.; Beneduci, A., High-Performance Electrofluorochromic Switching Devices Using a Novel Arylamine-Fluorene Redox-Active Fluorophore. *Acs Applied Materials & Interfaces* **2019,** *11* (13), 12202-12208.
24. Sentanin, F. C.; Ponez, L.; Pawlicka, A., Electrochromic Windows with PVB Electrolytes. *Mol. Cryst. Liquid Cryst.* **2014,** *604* (1), 107-116.
25. Li, K.; Xiang, Y.; Wang, X. Y.; Li, J.; Hu, R. R.; Tong, A. J.; Tang, B. Z., Reversible Photochromic System Based on Rhodamine B Salicylaldehyde Hydrazone Metal Complex. *Journal of the American Chemical Society* **2014,** *136* (4), 1643-1649.
26. Li, X.-N.; Xu, H.; Huang, L.; Shen, Y.; Li, M.-J.; Zhang, H., A multifunctional coordination polymer for photochromic films, smart windows, inkless and erasable prints and anti-counterfeiting. *Dyes Pigment.* **2023,** *213*, 111151.
27. Gao, R.; Cao, D.; Guan, Y.; Yan, D., Flexible Self-Supporting Nanofibers Thin Films Showing Reversible Photochromic Fluorescence. *ACS Applied Materials & Interfaces* **2015,** *7* (18), 9904-9910.
28. Reginato, G.; Mordini, A.; Zani, L.; Calamante, M.; Dessì, A., Photoactive Compounds Based on the Thiazolo[5,4-d]thiazole Core and Their Application in Organic and Hybrid Photovoltaics. *European Journal of Organic Chemistry* **2016,** *2016* (2), 233-251.

29. Johnson, J. R.; Ketcham, R., Thiazolothiazoles. I. The Reaction of Aromatic Aldehydes with Dithioöxamide1. *Journal of the American Chemical Society* **1960,** *82* (11), 2719-2724.
30. Sayresmith, N. A.; Saminathan, A.; Sailer, J. K.; Patberg, S. M.; Sandor, K.; Krishnan, Y.; Walter, M. G., Photostable Voltage-Sensitive Dyes Based on Simple, Solvatofluorochromic, Asymmetric Thiazolothiazoles. *Journal of the American Chemical Society* **2019,** *141* (47), 18780-18790.
31. Brotherton, A. R.; Shibu, A.; Meadows, J. C.; Sayresmith, N. A.; Brown, C. E.; Ledezma, A. M.; Schmedake, T. A.; Walter, M. G., Leveraging Coupled Solvatofluorochromism and Fluorescence Quenching in Nitrophenyl-Containing Thiazolothiazoles for Efficient Organic Vapor Sensing. *Advanced Science* **2023,** *10* (18), 2205729.
32. Khatun, A.; Panda, D. K.; Sayresmith, N.; Walter, M. G.; Saha, S., Thiazolothiazole-Based Luminescent Metal-Organic Frameworks with Ligand-to-Ligand Energy Transfer and Hg2+-Sensing Capabilities. *Inorg. Chem.* **2019,** *58* (19), 12707-12715.
33. Dikmen, Z.; Isık, M.; Turhan, O.; Akbari, M.; Tuncer, C.; Javanifar, R.; Bütün, V., Thiazolo[5, 4-d]thiazole based dye modified microspheres as metal nanoparticle reactor template and hybrid catalyst. *Eur. Polym. J.* **2022,** *175*, 111391.
34. Luo, J.; Hu, B.; Debruler, C.; Liu, T. L., A π-Conjugation Extended Viologen as a Two-Electron Storage Anolyte for Total Organic Aqueous Redox Flow Batteries. *Angewandte Chemie International Edition* **2018,** *57* (1), 231-235.
35. Cao, Z. X.; Chen, J. L.; Liu, S. J.; Qin, M. C.; Jia, T.; Zhao, J. J.; Li, Q. D.; Ying, L.; Cai, Y. P.; Lu, X. H.; Huang, F.; Gao, Y., Understanding of Imine Substitution in Wide-Bandgap Polymer Donor-Induced Efficiency Enhancement in All-Polymer Solar Cells. *Chem. Mat.* **2019,** *31* (20), 8533-8542.
36. Ando, S.; Nishida, J.-i.; Inoue, Y.; Tokito, S.; Yamashita, Y., Synthesis, physical properties, and field-effect transistors of novel thiophene/thiazolothiazole co-oligomers. *Journal of Materials Chemistry* **2004,** *14* (12), 1787-1790.
37. Osaka, I.; Sauvé, G.; Zhang, R.; Kowalewski, T.; McCullough, R. D., Novel Thiophene-Thiazolothiazole Copolymers for Organic Field-Effect Transistors. *Advanced Materials* **2007,** *19* (23), 4160-4165.
38. Cheng, C.; Yu, C.; Guo, Y.; Chen, H.; Fang, Y.; Yu, G.; Liu, Y., A diketopyrrolopyrrole–thiazolothiazole copolymer for high performance organic field-effect transistors. **2013,** *49* (20), 1998.
39. Peng, Q.; Lu, Z.-Y.; Huang, Y.; Xie, M.-G.; Han, S.-H.; Peng, J.-B.; Cao, Y., Synthesis and Characterization of New Red-Emitting Polyfluorene Derivatives Containing Electron-Deficient 2-Pyran-4-ylidene−Malononitrile Moieties. *Macromolecules* **2004,** *37* (2), 260-266.
40. Freeman, M. B.; Wang, L.; Jones, D. S.; Bejger, Christopher M., A cobalt sulfide cluster-based catholyte for aqueous flow battery applications. *Journal of Materials Chemistry A* **2018,** *6* (44), 21927-21932.
41. Turner, N. A.; Freeman, M. B.; Pratt, H. D.; Crockett, A. E.; Jones, D. S.; Anstey, M. R.; Anderson, T. M.; Bejger, C. M., Desymmetrized hexasubstituted [3]radialene anions as aqueous organic catholytes for redox flow batteries. *Chemical Communications* **2020,** *56* (18), 2739-2742.

42. Cook, S. K.; Horrocks, B. R., Heterogeneous Electron-Transfer Rates for the Reduction of Viologen Derivatives at Platinum and Bismuth Electrodes in Acetonitrile. *ChemElectroChem* **2017,** *4* (2), 320-331.
43. Won, S.; Won, K., Self-powered flexible oxygen sensors for intelligent food packaging. *Food Packaging and Shelf Life* **2021,** *29*, 100713.
44. Mills, A., Oxygen indicators and intelligent inks for packaging food. *Chemical Society Reviews* **2005,** *34* (12), 1003-1011.
45. Decataldo, F.; Bonafè, F.; Mariani, F.; Serafini, M.; Tessarolo, M.; Gualandi, I.; Scavetta, E.; Fraboni, B., Oxygen Gas Sensing Using a Hydrogel-Based Organic Electrochemical Transistor for Work Safety Applications. *Polymers* **2022,** *14* (5), 1022.
46. Wang, X.-d.; Chen, X.; Xie, Z.-x.; Wang, X.-r., Reversible Optical Sensor Strip for Oxygen. *Angewandte Chemie International Edition* **2008,** *47* (39), 7450-7453.
47. Gong, Y.-N.; Lu, T.-B., Fast detection of oxygen by the naked eye using a stable metal–organic framework containing methyl viologen cations. *Chemical Communications* **2013,** *49* (70), 7711-7713.
48. Yang, Z.; Zhang, J.; Kintner-Meyer, M. C. W.; Lu, X.; Choi, D.; Lemmon, J. P.; Liu, J., Electrochemical Energy Storage for Green Grid. *Chemical Reviews* **2011,** *111* (5), 3577-3613.
49. Yuan, J.; Pan, Z.-Z.; Jin, Y.; Qiu, Q.; Zhang, C.; Zhao, Y.; Li, Y., Membranes in non-aqueous redox flow battery: A review. *Journal of Power Sources* **2021,** *500*, 229983.
50. Liu, B.; Tang, C. W.; Jiang, H.; Jia, G.; Zhao, T., An aqueous organic redox flow battery employing a trifunctional electroactive compound as anolyte, catholyte and supporting electrolyte. *Journal of Power Sources* **2020,** *477*, 228985.
51. Song, Z.; Zhou, H., Towards sustainable and versatile energy storage devices: an overview of organic electrode materials. *Energy & Environmental Science* **2013,** *6* (8), 2280-2301.
52. Yun, T. G.; Park, M.; Kim, D. H.; Kim, D.; Cheong, J. Y.; Bae, J. G.; Han, S. M.; Kim, I. D., All-Transparent Stretchable Electrochromic Supercapacitor Wearable Patch Device. *ACS Nano* **2019,** *13* (3), 3141-3150.
53. Lin, X. C.; Li, N.; Zhang, W. J.; Huang, Z. J.; Tang, Q.; Gong, C. B.; Fu, X. K., Synthesis and electrochromic properties of benzonitriles with various chemical structures. *Dyes Pigment.* **2019,** *171*, 8.
54. Ma, D.-M.; Wang, J.; Guo, H.; Qian, D.-J., Photophysical and electrochemical properties of newly synthesized thioxathone–viologen binary derivatives and their photo-/electrochromic displays in ionic liquids and polymer gels. *New Journal of Chemistry* **2020,** *44* (9), 3654-3663.
55. Beaujuge, P. M.; Ellinger, S.; Reynolds, J. R., The donor-acceptor approach allows a black-to-transmissive switching polymeric electrochrome. *Nat. Mater.* **2008,** *7* (10), 795-799.
56. Beneduci, A.; Corrente, G. A.; Chidichimo, G., Chapter 9 Electrochromic and Electrofluorescence Liquid Crystals. In *Electrochromic Smart Materials: Fabrication and Applications*, The Royal Society of Chemistry: 2019; pp 261-292.
57. Corrente, G. A.; Fabiano, E.; Manni, F.; Chidichimo, G.; Gigli, G.; Beneduci, A.; Capodilupo, A. L., Colorless to All-Black Full-NIR High-Contrast Switching in Solid Electrochromic Films Prepared with Organic Mixed Valence Systems Based on Dibenzofulvene Derivatives. *Chem. Mat.* **2018,** *30* (16), 5610-5620.

58. Beneduci, A.; Cospito, S.; La Deda, M.; Chidichimo, G., Highly Fluorescent Thienoviologen-Based Polymer Gels for Single Layer Electrofluorochromic Devices. *Advanced Functional Materials* **2015,** *25* (8), 1240-1247.
59. Jin, H. Y.; Tian, J. H.; Wang, S. R.; Tan, T. F.; Xiao, Y.; Li, X. G., Novel photochromic and electrochromic diarylethenes bearing triphenylamine units. *RSC Adv.* **2014,** *4* (32), 16839-16848.
60. Yamamoto, K.; Mutoh, K.; Abe, J., Photo- and Electro-Driven Molecular Switching System of Aryl-Bridged Photochromic Radical Complexes. *J. Phys. Chem. A* **2019,** *123* (10), 1945-1952.
61. Safaei, S.; Wang, J.; Junk, P. C., Incorporation of thiazolothiazole fluorophores into a MOF structure: A highly luminescent Zn(II)-based MOF as a selective and reversible sensor for Cr2O72- and MnO4- anions. *J. Solid State Chem.* **2021,** *294*, 7.
62. Li, P.; Guo, M. Y.; Yin, X. M.; Gao, L. L.; Yang, S. L.; Bu, R.; Gong, T.; Gao, E. Q., Interpenetration-Enabled Photochromism and Fluorescence Photomodulation in a Metal-Organic Framework with the Thiazolothiazole Extended Viologen Fluorophore. *Inorg. Chem.* **2019,** *58* (20), 14167-14174.
63. Biswal, B. P.; Vignolo-González, H. A.; Banerjee, T.; Grunenberg, L.; Savasci, G.; Gottschling, K.; Nuss, J.; Ochsenfeld, C.; Lotsch, B. V., Sustained Solar H2 Evolution from a Thiazolo[5,4-d]thiazole-Bridged Covalent Organic Framework and Nickel-Thiolate Cluster in Water. *Journal of the American Chemical Society* **2019,** *141* (28), 11082-11092.
64. Wang, J., *Analytical electrochemistry*. Wiley-VCH: Hoboken, N.J., 2006.
65. Ji, S.; Zhou, S.; Zhang, X.; Li, C.; Chen, W.; Jiang, X., Oxygen-Sensing Probes and Bandage for Optical Detection of Inflammation. *ACS Applied Bio Materials* **2019,** *2* (11), 5110-5117.
66. Rathod, P. V.; Puguan, J. M. C.; Kim, H., Multi-Stimuli Responsive Thiazolothiazole Viologen-Containing Poly(2-Isopropyl-2-Oxazoline) and Its Multi-Modal Thermochromism, Photochromism, Electrochromism, and Solvatofluorochromism Applications. *Advanced Materials Interfaces* **2022,** *n/a* (n/a), 2201227.
67. Favaro, G.; Ortica, F.; Romani, A.; Smimmo, P., Photochromic behaviour of Berry Red studied in solution and polymer films. *Journal of Photochemistry and Photobiology A: Chemistry* **2008,** *196* (2), 190-196.
68. Xu, S.; Qi, Y.; Zhang, J., Incorporation of indolinospirooxazine on ethylene-vinyl acetate copolymer to produce a intelligently temperature-regulated nonwhite cool material. *Journal of Applied Polymer Science* **2020,** *137* (29), 48887.
69. Saha, S.; Bonda, S.; Tripathi, S. N.; Shukla, D. K.; Srivastava, V. K.; Srinivasa Rao, G. S.; Jasra, R. V., Photochromic films prepared by solid state processing of disentangled ultrahigh molecular weight polyethylene and photochromic dyes composites. *Journal of Applied Polymer Science* **2021,** *138* (15), 50188.
70. Farahat, M. E.; Welch, G. C., Slot-Die Coated Organic UV Indicators and Filters Processed from Green Solvents. *Advanced Sustainable Systems* **2022,** *6* (2), 2100055.
71. Wang, Z. Y.; Zhang, J.; Wu, X.; Birau, M.; Yu, G.; Yu, H.; Qi, Y.; Desjardins, P.; Meng, X.; Gao, J. P.; Todd, E.; Song, N.; Bai, Y.; Beaudin, A. M. R.; LeClair, G., Near-infrared absorbing organic materials. *Pure and Applied Chemistry* **2004,** *76* (7-8), 1435-1443.

72. Meng, D.; Zheng, R.; Zhao, Y.; Zhang, E.; Dou, L.; Yang, Y., Near-Infrared Materials: The Turning Point of Organic Photovoltaics. *Advanced Materials* **2022,** *34* (10), 2107330.
73. Pu, J.; Shen, C.; Wang, J.; Zhang, Y.; Zhang, C.; Kalogirou, S. A., Near-infrared absorbing glazing for energy-efficient windows: A critical review and performance assessments from the building requirements. *Nano Energy* **2023,** *110*, 108334.
74. Tang, B.; Li, W.-L.; Chang, Y.; Yuan, B.; Wu, Y.; Zhang, M.-T.; Xu, J.-F.; Li, J.; Zhang, X., A Supramolecular Radical Dimer: High-Efficiency NIR-II Photothermal Conversion and Therapy. *Angewandte Chemie International Edition* **2019,** *58* (43), 15526-15531.
75. Li, P.; Guo, M.-Y.; Yin, X.-M.; Gao, L. L.; Yang, S.-L.; Bu, R.; Gong, T.; Gao, E.-Q., Interpenetration-Enabled Photochromism and Fluorescence Photomodulation in a Metal–Organic Framework with the Thiazolothiazole Extended Viologen Fluorophore. *Inorg. Chem.* **2019,** *58* (20), 14167-14174.
76. Yang, S. B.; Karim, M. R.; Lee, J.; Yeum, J. H.; Yeasmin, S., Alkaline Treatment Variables to Characterize Poly(Vinyl Alcohol)/Poly(Vinyl Butyral/Vinyl Alcohol) Blend Films. *Polymers* **2022,** *14* (18), 3916.
77. Janoschka, T.; Morgenstern, S.; Hiller, H.; Friebe, C.; Wolkersdörfer, K.; Häupler, B.; Hager, M. D.; Schubert, U. S., Synthesis and characterization of TEMPO- and viologen-polymers for water-based redox-flow batteries. *Polymer Chemistry* **2015,** *6* (45), 7801-7811.
78. Winsberg, J.; Stolze, C.; Muench, S.; Liedl, F.; Hager, M. D.; Schubert, U. S., TEMPO/Phenazine Combi-Molecule: A Redox-Active Material for Symmetric Aqueous Redox-Flow Batteries. *ACS Energy Letters* **2016,** *1* (5), 976-980.
79. Janoschka, T.; Friebe, C.; Hager, M. D.; Martin, N.; Schubert, U. S., An Approach Toward Replacing Vanadium: A Single Organic Molecule for the Anode and Cathode of an Aqueous Redox-Flow Battery. *ChemistryOpen* **2017,** *6* (2), 216-220.
80. Zhu, Y.; Yang, F.; Niu, Z.; Wu, H.; He, Y.; Zhu, H.; Ye, J.; Zhao, Y.; Zhang, X., Enhanced cyclability of organic redox flow batteries enabled by an artificial bipolar molecule in neutral aqueous electrolyte. *Journal of Power Sources* **2019,** *417*, 83-89.
81. Hodes, G.; Manassen, J.; Cahen, D., Photoelectrochemical energy conversion and storage using polycrystalline chalcogenide electrodes. *Nature* **1976,** *261* (5559), 403-404.
82. Liu, F.; Ma, Z.; Liu, Q.; Wang, Z.; He, C., An integrated solar redox flow battery using a single Si photoanode and near-neutral electrolytes. *Journal of Power Sources* **2022,** *549*, 231987.
83. Azevedo, J.; Seipp, T.; Burfeind, J.; Sousa, C.; Bentien, A.; Araújo, J. P.; Mendes, A., Unbiased solar energy storage: Photoelectrochemical redox flow battery. *Nano Energy* **2016,** *22*, 396-405.
84. Man, Y.; Hao, Q.; Chen, F.; Chen, X.; Wang, Y.; Liu, T.; Liu, F.; Li, N., A Photo-Assisted Chargeable Aqueous Zinc-Iodine Battery. *ChemElectroChem* **2019,** *6* (23), 5872-5875.
85. Dong, M.; Wang, Y.; Li, A.; Cheng, C., Three-dimensional BiVO4-based semiconductor photocathode for high efficiency photo-assisted Zn-iodine redox flow batteries. *Nanotechnology* **2022,** *33* (26), 265401.

86. Bae, D.; Kanellos, G.; Faasse, G. M.; Dražević, E.; Venugopal, A.; Smith, W. A., Design principles for efficient photoelectrodes in solar rechargeable redox flow cell applications. *Communications Materials* **2020,** *1* (1), 17.
87. Fu, H.-C.; Li, W.; Yang, Y.; Lin, C.-H.; Veyssal, A.; He, J.-H.; Jin, S., An efficient and stable solar flow battery enabled by a single-junction GaAs photoelectrode. *Nature Communications* **2021,** *12* (1), 156.